AEROTEST RADIOGRAPHY AND RESEARCH REACTOR
LICENSE NO. R-98
DOCKET NO. 50-228

AEROJET-GENERAL NUCLEONICS INDUSTRIAL REACTOR
HAZARDS SUMMARY REPORT
SEPTEMBER 1964

REDACTED VERSION*

SECURITY-RELATED INFORMATION REMOVED

*REDACTED TEXT AND FIGURES BLACKED OUR OR DENOTED BY BRACKETS

AGN

AEROJET-GENERAL NUCLEONICS INDUSTRIAL REACTOR

Hazards Summary Report

AN-1193 September 1964

GENERAL TIRE

AEROJET-GENERAL NUCLEONICS
SAN RAMON, CALIFORNIA

AGN

AEROJET-GENERAL NUCLEONICS INDUSTRIAL REACTOR

HAZARDS SUMMARY REPORT

by

R. L. Newacheck, Project Engineer

H. Montgomery
R. E. Quilici
I. E. Lamb
F. W. Boone

Report No. AN-1193 September 1964

AEROJET-GENERAL NUCLEONICS
A SUBSIDIARY OF AEROJET-GENERAL CORPORATION

GENERAL TIRE

ABSTRACT

Aerojet-General Nucleonics proposes to build the Aerojet-General Nucleonics Industrial Reactor (AGNIR), a 250-kw research reactor, at its plant site near San Ramon, California. This report describes the location and characteristics of the reactor site and the principal characteristics of the AGNIR and its associated facilities and equipment. Initial tests and operating procedures are outlined, together with the administrative and procedural safeguards to be provided. Potential hazards associated with operation of the AGNIR are analyzed. Details of the meteorological and seismic characteristics of the San Ramon area are presented in appendixes.

CONTENTS

(Continued)

CONTENTS - Continued

TABLES

(Continued)

CONTENTS - Continued

FIGURES

(Continued)

CONTENTS - Continued

I. INTRODUCTION AND SUMMARY

A. LOCATION

The proposed Aerojet-General Nucleonics Industrial Reactor (AGNIR) is to be built by Aerojet-General Nucleonics at San Ramon, California. It will be used for industrial research, primarily the determination of radiation effects.

The reactor and associated equipment will be housed in a steel building in an exclusion area at the AGN plant near San Ramon, about 25 miles east of San Francisco. The reactor tank will be set into the ground in the main section of the facility. The control room will house the operating console and peripheral equipment. A storage facility for radioactive material and hot fuel elements will be located in the same building. The design also includes areas for a hot cell, a change room, and a laboratory area.

The AGNIR will be the twenty-second reactor designed and built by Aerojet-General Nucleonics. The company's comprehensive experience in this field includes design and production of the AGN-201 research reactors, 15 of which are now in operation, and of four AGN-211 pool type reactors. In addition, AGN designed, built, and operated the GCRE-I reactor and the ML-1 mobile nuclear power plant for the AEC and the US Army. AGN has also conducted extensive in-pile irradiation experiments in various reactors, including the BRR, MTR, GETR, and LPTR.

B. PRINCIPAL CHARACTERISTICS OF THE AGNIR

The AGNIR will be a pool type reactor with the core emplaced in a tank of water 22 ft deep. The reactor is designed to operate at a maximum

thermal power of 250 kw, but initial operation will be at about 50 kw. Shielding will be provided by 17 ft of water above the core and by water, concrete, and soil around it. The principal characteristics of the AGNIR are briefly summarized in Table 1 below. A more comprehensive tabulation appears in Section V.

TABLE 1

SUMMARY OF REACTOR CHARACTERISTICS

Reactor power (thermal)	250 kw
Fuel elements	TRIGA pin
Fuel loading per element	[redacted]
Critical mass, nominal	[redacted]
Moderator	ZrH and H_2O
Reflector, coolant	Demineralized H_2O
Reactivity coefficients	
Temperature	-1.2×10^{-4} $\Delta k/k$ per ^{o}C
Void	-2.0×10^{-3} $\Delta k/k$ per % void
Total worth of control rods	$\sim 6\% \Delta k/k$

C. SAFETY

Zirconium hydride fuel elements have been used in TRIGA reactors for many years, and no safety problems have been encountered. These elements are inherently safe because of the large negative prompt temperature coefficient. This safety feature has repeatedly been proven by pulsing these cores to peak powers of 2000 Mw and more.

An additional safety factor is the fact that no radioactive effluents will be produced in the course of normal AGNIR operations. Therefore, no special safety or disposal problems caused by effluents need be anticipated in this facility or in its vicinity.

II. REACTOR SITE

A. DESCRIPTION

1. Geographic Location

Aerojet-General Nucleonics' facilities for nuclear research, development, and production are located on a 498-acre tract about one-half mile east of the town of San Ramon in Contra Costa County, California. San Ramon lies at the southern (upper) end of the San Ramon Valley, about 25 miles due east of San Francisco and 15 miles east of Oakland (see Figure 1). It is separated from the East Bay urban complex by a series of ridges and hills up to 1600 ft high.

The town and the AGN plant site are bordered on the east and west by sparsely settled areas which are still predominantly agricultural. To the north are the towns of Danville (about 3 miles) and Walnut Creek (about 9 miles) and to the south are San Ramon Village (about 3 miles) and Dublin (about 4 miles). The nearest "uncontrolled habitat" is a farmhouse located on neighboring land about 1000 ft from the proposed reactor facility. The AGN site is intersected by a single Southern Pacific Railroad track which is not presently used except for storage of old cars to the south and occasional inspections. The roadbed lies 500 ft from the proposed reactor facility at the nearest point. State Highway Route 21 passes through the town one-half mile west of the plant. Construction of a new freeway section along the east side of this highway will be initiated in 1965.

The geographical relationship of the AGN plant site to nearby inhabited areas is shown in Figure 2, and a plan of the site showing the location of the proposed AGNIR facility is shown in Figure 3.

8539-64-1912

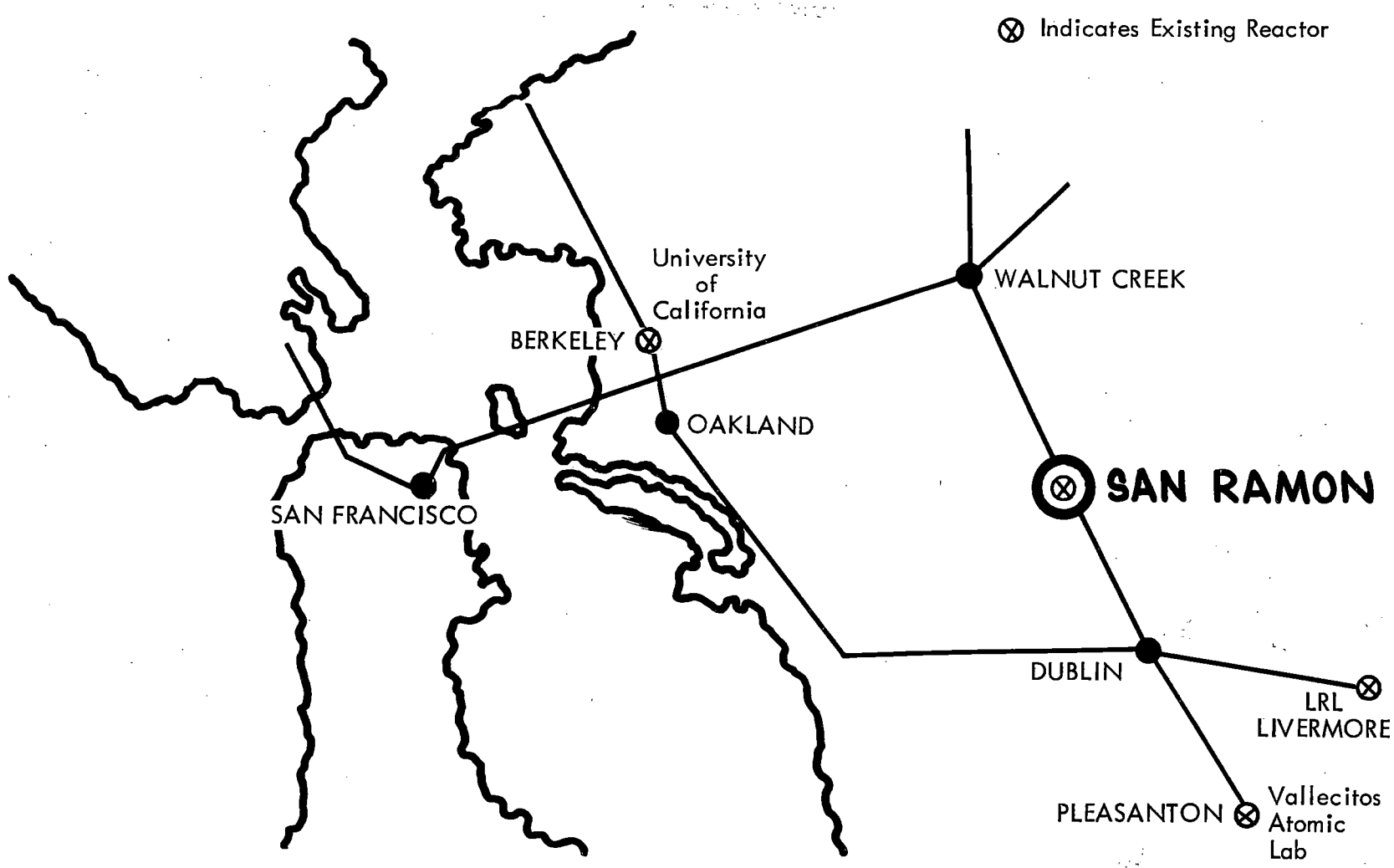

FIGURE 1. MAP OF SAN FRANCISCO BAY AREA

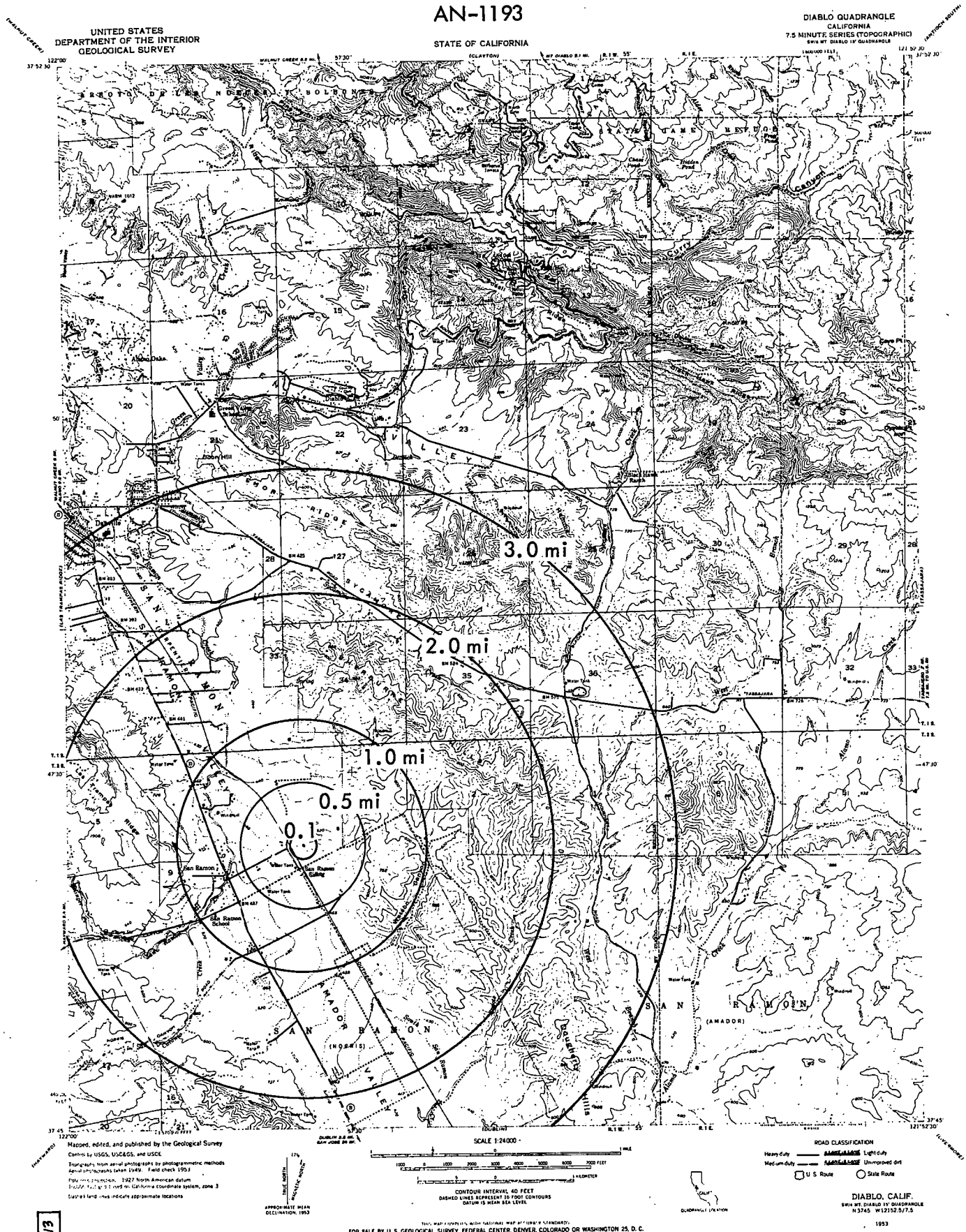

FIGURE 2. MAP OF SAN RAMON AREA

85.30-64-1914

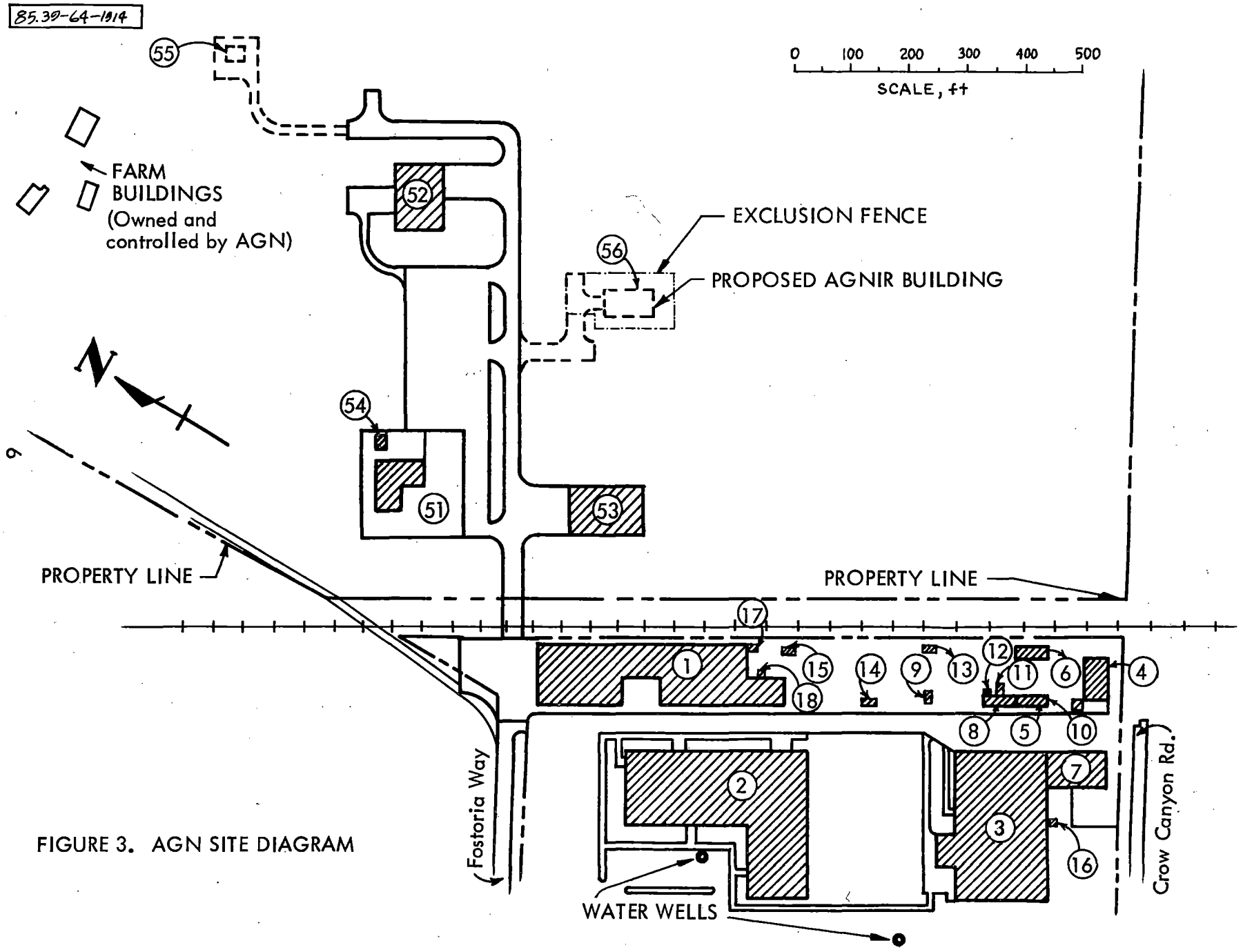

FIGURE 3. AGN SITE DIAGRAM

2. Population Density in Surrounding Area

The greater San Francisco area, to the west of San Ramon, has a population approaching 3.5 million people, including the East Bay cities. Population estimates for the communities in the San Ramon Valley and Contra Costa County in 1960 and 1963 are shown in Table 3. Population estimates for nearby communities in adjacent Alameda County are: Dublin (including San Ramon Village), 10,000 (1964); Pleasanton, 4,203 (1960); Livermore, 20,000 (1964); Hayward, 72,700 (1960). An analysis of the population within a three-mile radius of the AGNIR site (Figure 2) is presented below in Table 2.

Table 2

POPULATION WITHIN THREE-MILE RADIUS OF REACTOR SITE

Radial Distance from Site	Est. Number of People (Daytime)
0.1 mile	500*
0.5 mile	600
2.0 miles	1000
3.0 miles	3000

* AGN employees, during working hours only

3. Land Uses in Surrounding Area

The AGN plant is located on AGN property zoned for Light Industrial use. Land uses in the surrounding areas are still principally agricultural, involving walnut orchards, pear orchards, and cattle grazing lands. However, in the western half of the 1.0 mile circle on Figure 2, there are presently, in addition to AGN, 8 retail uses, 2 commercial, 4 controlled manufacturing, and 1 engineering office. Many agricultural parcels are for sale. An effective master plan is currently being developed with the County which will provide for orderly development of the San Ramon Valley and prevent conflicting uses.

4. Other Nuclear Facilities

An AGN 201 research reactor is currently in use at the AGN plant. This reactor is located in Building 1 (Figure 3), about 550 ft from the planned location of the AGNIR installation. With this distance between the two reactors, no operational problems are anticipated.

TABLE 3

POPULATION

1960 U. S. CENSUS

Total, Contra Costa County: 409,030

Alamo-Danville Division	12,692
Alamo (U)	1,791
Danville (U)	3,585
Diablo (U)	2,096
Ambrose Division	8,569
Pittsburg West (U)	5,188
Shore Acres (U)	3,093
Antioch Division	19,175
Antioch City	17,305
Brentwood-Byron Division	6,620
Brentwood City	2,186
Briones Division	919
Clayton-Tassajara Division	2,263
Concord Division	49,309
Concord City	36,208
El Monte (U)	4,186
Pleasant Hill (U) (Part)	11
Crockett Division	3,907
El Cerrito Division	25,437
El Cerrito City	25,437
Kensington Division	6,161
Lafayette Division	17,800
Lafayette (U)	7,114
Martinez Division	20,967
Martinez City	9,604
Martinez East (U)	3,958
Pacheco (U)	1,518
Oakley-Bethel Division	4,998
Orinda-Moraga Division	16,686
Orinda (U)	4,712
Orinda Village (U)	5,568
Pinole-Hercules Division	6,477
Hercules Town	310
Pinole City	6,064
Pittsburg Division	21,190
Pittsburg City	19,062
Pittsburg East (U)	1,977
Pleasant Hill Division	22,287
Pleasant Hill (U) (Part)	21,376
Port Chicago Division	2,432
Port Chicago (U)	1,746
Richmond Division	100,872
Richmond City	71,854
Rodeo Division	6,697
San Pablo Division	19,693
San Pablo City	19,687
Walnut Creek Division	33,879
Pleasant Hill (U) (Part)	2,457
Saranap (U)	6,450
Walnut Creek City	9,903
Walnut Heights (U)	5,080

(U denotes an unincorporated Place)
Boundaries determined by the Bureau of the Census

POPULATION — CONTRA COSTA COUNTY

POSTMASTER'S ESTIMATES

MAY 1, 1963

Alamo	5,012
Antioch	22,292
Berkeley Park and Kensington	6,636
Bethel Island	884
Brentwood	6,490
Byron	1,267
Canyon	200
Clayton	625
Concord	75,787
Cowell	229
Crockett	3,800
Danville	2,698
Diablo	585
El Cerrito	26,500
El Sobrante	11,450
Hercules	350
Knightsen	850
Lafayette	24,538
Martinez (Includes Mt. View, Vine Hill, Pacheco and Alhambra Valley)	25,750
Moraga	3,300
Oakley	5,500
Orinda	17,000
Pinole	8,250
Pittsburg (Includes West Pittsburg)	31,717
Pleasant Hill	22,827
Port Chicago	2,300
Port Costa	240
Richmond (Includes Rollingwood, Giant, East and North Richmond)	92,947
Rodeo	7,800
Saint Mary's College	1,025
San Pablo	22,925
San Ramon	400
Selby	250
Walnut Creek	44,076
TOTAL	476,500

Other nuclear reactors are located at Pleasanton (General Electric Vallecitos Atomic Laboratory), about 13 air miles south of San Ramon, at Livermore (University of California Lawrence Radiation Laboratory), about 16 air miles southeast of San Ramon, and at the University of California in Berkeley, about 25 miles to the northwest.

5. Control of AGN Site

Access to the AGN plant is fully controlled by the Plant Protection force and is limited to AGN personnel and to authorized visitors, who are escorted at all times when in exclusion areas. The main group of offices, laboratories, and shops (see Figure 3) is enclosed by a steel exclusion fence. [redacted] Facilities to the east of the main plant occupy separate, fenced exclusion areas, connected by paved private roadways. The proposed AGNIR facility (described in Section IV) will be enclosed by an exclusion fence with a single locked gate controlled by the supervisor on duty.

B. SITE CHARACTERISTICS

1. Topography

The elevation of the AGN plant site is about 460 ft above sea level. The basic subsoil structure is sandstone over 200 ft thick. The loam-like surface soil varies from 15 to 30 ft in depth and is sufficiently porous to allow percolation to the highly absorbent subsoil structure. According to local well drillers, the true water table is reached at a depth of approximately 200 ft. A topographical map of the area is shown in Figure 2.

2. Hydrology

San Ramon lies at the southern end of the San Ramon Valley, which drains into the mouth of the Sacramento River (Suisun Bay) and eventually into the Pacific Ocean. San Ramon is bordered on the south by the Amador Valley, on the east by the Sherburne Hills, and on the west by Las Trampas Ridge. The principal watercourse is San Ramon Creek. Any run-off from the AGN plant during the wet season would enter San Ramon Creek and would proceed northward into Walnut Creek and thence to Suisun Bay. During the dry season, which comprises nearly two-thirds of the average year, any foreseeable release of water from the AGN plant would percolate underground.

3. Geology

San Ramon is located in the Southern Coast Range, to the southwest of Mount Diablo. The area is underlain by a basement of Franciscan rocks belonging to the Northern Franciscan Area. This structure is characterized by the ability to yield under deforming forces even when covered by sedimentary rocks, as is the case in the area under consideration. This characteristic tends to cause extreme complexity of the geological structure.

The surface in the vicinity shows evidence of several ages varying from Franciscan to the most recent alluvium. The Franciscan is many thousands of feet thick, consisting of arkosic sandstones, arenaceous shales, and cherts. A few thin conglomeritic lenses occur as well as glaucophase lawsonite schists.

The evidence found in the calera limestone near San Francisco, as well as in the marine cherts and in grain and bedding characteristics, etc., suggests a marine origin. It has been suggested that the Franciscan sediments were derived from a large land mass in what is now the Pacific Ocean.

4. Climatology

A survey for meteorological data has been made of the reactor site by Aerojet-General Nucleonics and Universal Weather Services. Few records are available for the San Ramon area at the present time; however, meteorological instrumentation has recently been installed at AGN for this purpose. The general climatological characteristics of the area may be expected to be quite similar to those of the Bay Area and the Livermore Valley which have been studied in some detail. The climate is mild; high winds and severe storms are abnormal and infrequent. Appendix A includes the available weather data for the San Ramon area and the survey by Universal Weather Services.

5. Seismology

A study of the area with regard to the hazards due to earthquake is enclosed as Appendix B. Slight tremors are fairly common in the San Ramon area. However, severe quakes in this area are uncommon; by careful engineering, hazards from this cause have been kept at a minimum. The reactor design provides for automatic scramming in the event of an earthquake.

III. AGN PLANT FACILITIES

Aerojet-General Nucleonics is principally engaged in nuclear research and development work. Its main facilities are located on the western portion of its 498-acre site near San Ramon and at present cover approximately 189,000 sq ft of floor space. These facilities include offices, laboratories, assembly facilities and testing areas for power conversion equipment, fabrication facilities for cores and refractory materials, experimental test loop areas, and production shops. The location of these facilities in relation to the proposed site of the AGNIR facility is shown in Figure 3. The uses of the various buildings are briefly described below. Numbers in parentheses, e.g., (1), refer to corresponding numbers on Figure 3.

The composite laboratory building (1) contains the following facilities:

1) An AGN-201 reactor, currently operating at 20 w, used for instrument and dosimeter calibrations and for research work in connection with AGN's fissiochemistry development programs.

2) A hot cell with high-density concrete walls 20 in. thick and high-density glass viewing windows, also 20 in. thick, designed to handle specimens up to 300 curies at 1 Mev

3) Chemistry laboratories, including two radiochemical laboratories, two wet chemical laboratories, a sample preparation laboratory, and storerooms

4) A specialized experimental laboratory for AGN's fissiochemistry programs, used for UO_2 slurry circulation, sample vessel assembly, loading, and unloading, safety tests, and sample analysis

5) A metallurgical and materials laboratory for evaluation of high-temperature materials and nuclear applications of both fueled and unfueled materials

6) A liquid metals laboratory, including two liquid metal capsule corrosion test facilities, a boiling and condensing heat transfer test facility for space system radiators and boilers, and a dynamic liquid metal corrosion loop test facility

7) An electronics development laboratory

8) A nuclear measurements laboratory with equipment for precision alpha, beta, and gamma counting

The main office building (2) contains engineering and administrative offices, drafting rooms, computer facilities, a document control center, and printing, photographic, and other supporting services. It includes special AEC and DOD restricted areas for work on classified projects.

The shops building (3) includes a general machine shop, a separate bay of 3000 sq ft for welding operations, specialized machine tool areas for the handling of radioactive materials, facilities for the fabrication, assembly, maintenance, and calibration of instrumentation and electronic equipment, and supporting shop services.

The nuclear fuel fabrication facility (7) is used for ceramic fuel production, sealing and assembly of wire-spaced pins for elements, and preparation of fuel-loaded parts. It is equipped with dust-free assembly rooms, glove boxes, and special equipment for inspection, testing, analysis, and leak detection. Fireproof vaults are provided for storage of plutonium and uranium. The entire facility is a restricted area, and appropriate accountability and health physics services are provided.

Other installations on the western side of the railroad tracks include a special radionuclide laboratory (14), cleaning and decontamination facilities, housing for pumps, generators, and air compressors, and special storage facilities for inflammable (5) and hazardous (9) materials.

To the east of the tracks, a new facility (51) for testing power conversion equipment and other rotating machinery was completed this year. The

facility includes a high-bay assembly area, control room, test room, and special power sources and testing machinery. The concrete floor slab extends outside the building to provide a base for testing fully-assembled power conversion units for nuclear power plants.

A new physics laboratory (52) was recently completed to accommodate AGN's expanding research in plasma physics and related fields. The laboratory houses various large magnetic-field power supplies, capacitor banks, vacuum chambers, von Ardenne and other ion sources, an energetic arc, microwave diagnostic equipment, and other special equipment for experimentation and analysis. The building is 300 ft from the site of the proposed AGNIR facility.

A new building (55) for a pulse power research facility is now under construction northeast of the new physics laboratory. The building will provide 650 sq ft of floor space for research and experimentation in the field of pulsed power production.

The location of the building site for the proposed AGNIR facility is shown (56) in Figure 3. The facility is described in Section IV below.

Plant Utilities

1) The AGN plant now obtains water from two wells on AGN property (see Figure 3) supplying 100 gpm with a line pressure of 80 psi. AGN has contracted to receive future water supplies from a new line presently being laid by the East Bay Municipal Utility District. This service is expected to begin in July 1965.

2) Electrical power (120/240 v, 3-phase, 60-cycle) is obtained through a Pacific Gas & Electric Company transformer.

3) Natural gas is also supplied to the plant by Pacific Gas & Electric.

4) Wastes (other than storm run-off) are removed from the plant site through a public sewer owned by the Contra Costa County Sanitary District.

IV. REACTOR BUILDING

The Aerojet-General Nucleonics Industrial Reactor will be housed in a steel building to be constructed on AGN property about 700 ft east of the main office building. The building will be a high-bay, fabricated-steel shell with interior walls of gypsum board on a wooden framework. It is designed to contain the main reactor room, the control room, a hot cell, a laboratory area, and the other areas shown in Figure 4. The building is designed to meet local building codes for earthquake-resistant buildings.

A 3-ton bridge crane will serve most of the work area, including the hot-storage holes under the southeast portion of the building. The bridge crane will be used for general work, including the handling of heavy shields.

[redacted]

A criticality monitor (Eberline Instrument Company Model RM-1 or equivalent) will be mounted on the wall separating the reactor and the control console. In the event of an unanticipated rise in the radiation level, this unit will sound an evacuation alarm (oscillating siren) in the reactor building,

[redacted]

Although the possibility of a fire in this facility is extremely remote, portable fire extinguishers will be strategically located throughout the building. A fire evacuation alarm (claxon horn) will be installed. This

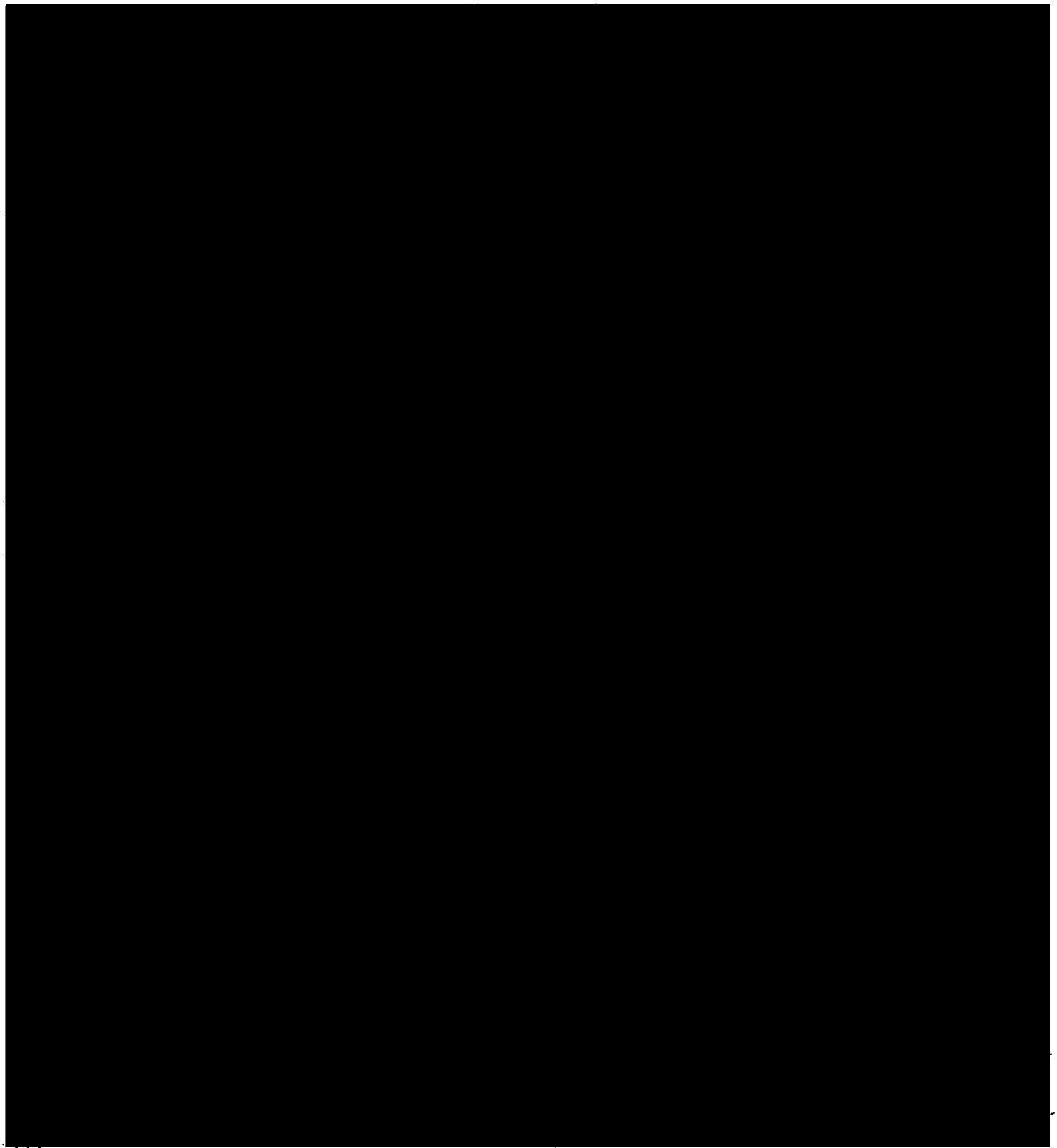

FIGURE 4. GENERAL ARRANGEMENT OF AGNIR BUILDING

alarm will be interconnected with the main plant fire alarm system, [redacted]

Access to the AGNIR facility will be restricted by means of a steel perimeter fence with a locked gate. The lock can be disengaged only by keys, which will be issued only to authorized personnel, or electrically by means of a switch in the reactor control room. The operator on duty in the AGNIR facility will identify the person requiring access by means of an intercom system between the gate and the reactor control room.

V. REACTOR

A. STRUCTURE

1. Core Tank

The reactor tank will be 10 ft in diameter by 23 ft deep and will extend 22 ft below the floor level of the building (see Figure 5). The water level in the tank will be maintained approximately at floor level, 17 ft above the top of the core. The aluminum tank, with walls 1/4 in. thick, will be set in concrete, which will add greatly to mechanical integrity. The exterior of the tank will be treated to minimize corrosion. The tank will be of all-welded construction, with no openings below the water surface. One 24-in. OD pipe about 13 ft long will butt up against the outside of the tank opposite the center of the core. However, the tank wall will not initially be cut open at this location. The pipe sleeve is provided so that a horizontal beam port may be installed at a later date, if desired, without having to break through the concrete around the tank. An amendment of the AGNIR operating license would be obtained before installation of the beam port.

The top edge of the tank will end in a flange which will support the reactor bridge (Fig. 6) and add stiffening to the tank wall. At each point where the bridge structure rests on the top flange, a vertical structural member welded to the tank wall will extend into the concrete liner. The load of the bridge will thus be transmitted directly into the concrete liner rather than being supported by the tank wall.

The tank will be surrounded by a concrete-lined trench, approximately 2 ft wide by 2 ft deep, to permit experimental and control cables and pipes to be located under the floor and thus protected from

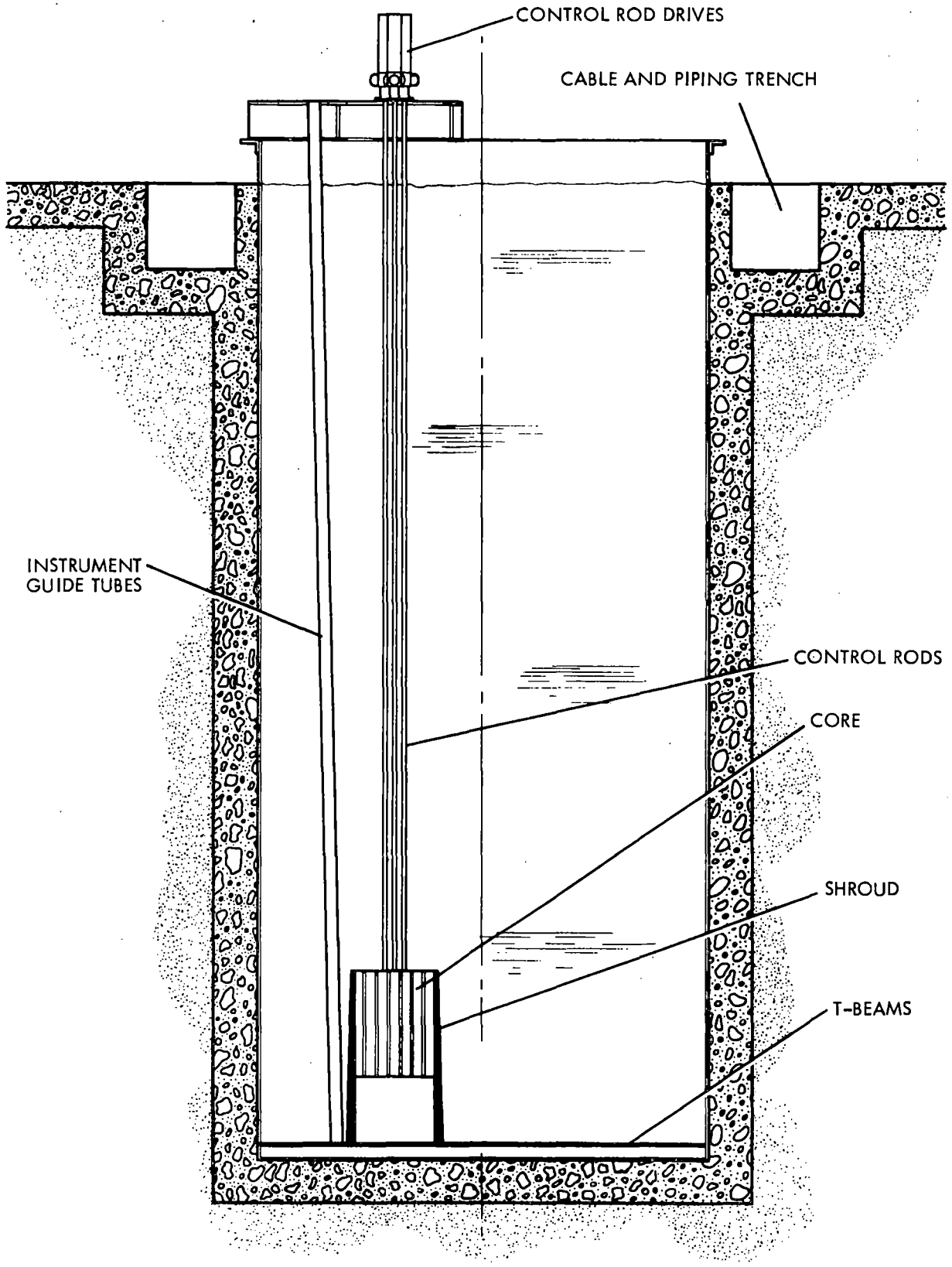

FIGURE 5. REACTOR CROSS SECTION

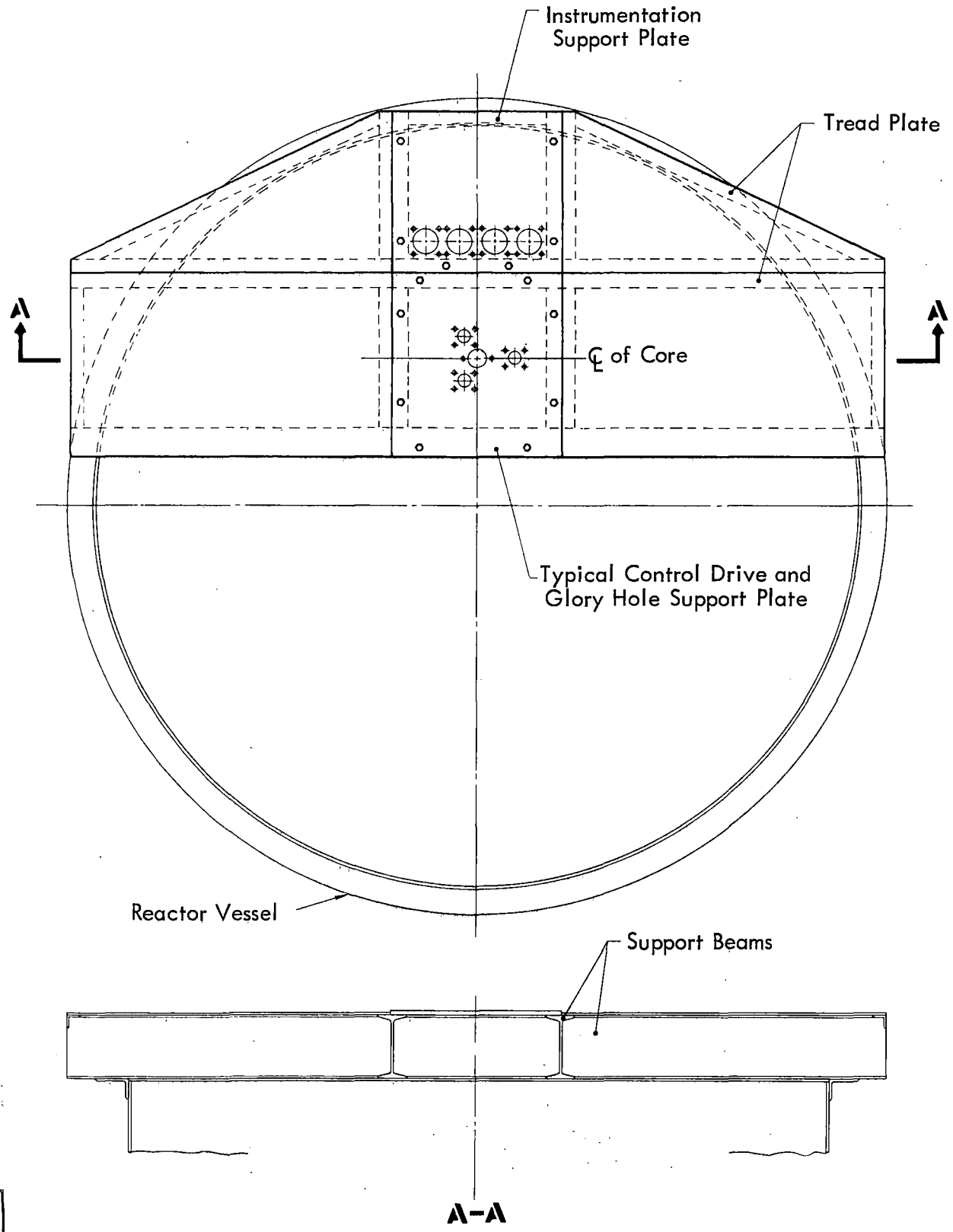

FIGURE 6. AGNIR BRIDGE ASSEMBLY

physical damage. The trench will be covered by steel cover-plates. Radial trenches will extend from the reactor tank in four directions. One radial trench will extend into the control room to house the reactor control cabling. A second trench will extend to the rear of the building to provide underfloor routing of the demineralizer and cooling water loops. The two additional radial trenches, one extending into the laboratory room, will be used for experimental apparatus as required. Drains will be provided in the trenches and, in addition, moisture-sensitive cables and equipment will be mounted on shelves to hold them above the trench floor.

2. Support Bridge

The reactor bridge will be a support structure of 10 in. structural steel I-beams. Two of these beams will support a 3/4 in.-thick aluminum control rod drive mounting plate. This plate will locate the control rods and glory hole. Different plates will be used to relocate control rods or the glory hole. A loading of 400 lb in addition to the normal weight of the control rods and equipment would result in a maximum I-beam deflection of 0.0025 in.

The area above the bridge structural members that is not covered by the mounting plate will be covered with closed-tread plate. This plate will provide a working platform giving access to the control rods and instrument tubes for maintenance. The tread plate is designed so that it can be removed with a minimum possibility of being dropped into the pool. All retaining screws will be of the captive type so that they will not be free to drop into the pool.

The reactor bridge will be secured at one position on the tank flange. Leveling shims will be used to provide accurate alignment between the bridge and the core support (grid) plate.

3. Core and Support Structures

The core structure design (Figure 7) consists of a cylindrical shroud and top and bottom grid plates. The base of the structure is bolted to T-beams emplaced on the bottom of the tank. The shroud, an aluminum right circular cylinder, is about 4 ft high and has an inside diameter of about 22 in. Cooling water enters the core region through large access holes cut through the shroud between the grid plates, and through holes in the bottom grid plate. The region below the core is accessible through large openings in the lower portion of the shroud. The grid plates are bolted to the shroud. The weight of the fuel is supported by a bottom grid plate (Figure 8) of 3/4-in.-thick aluminum. The fuel elements and control rods are positioned laterally by holes approximately 1½ in. in diameter in the aluminum top grid plate (Figure 9). A total of 127 grid positions (126 in six concentric rings around a central hole) are available for core components (Figure 10). Each position is identified by a letter and number combination. Sixty-eight of the positions are typically occupied by fuel elements and control rods, as shown in Figure 10. Unused positions, except in the outer ring, are occupied by dummy elements which contain only graphite. The center of the active fuel region is approximately 3 ft above the bottom of the reactor pool.

Triangular spacer blocks on the upper ends of the fuel elements are positioned in the upper grid plate holes in a way that allows water to flow out of the core through the top grid plate. This plate has a thickness of 5/8 in. Small holes at various positions in the top and bottom grid plates permit insertion of wires into the core to obtain flux measurements.

A hexagonal section can be removed from the center of the upper grid plate for the insertion of specimens about 4.4 in. in diameter into the region of highest flux. This requires prior relocation of the central fuel element and the six elements from the B-ring to the outer portion of the core.

Two triangular sections, each of which encompasses one D-ring and two E-ring holes, are cut out of the upper grid plate. When fuel elements are placed in these locations, their lateral support is provided by special aluminum pieces. With the fuel elements removed, there is room for inserting specimens about 2.4 in. in diameter.

AN-1193

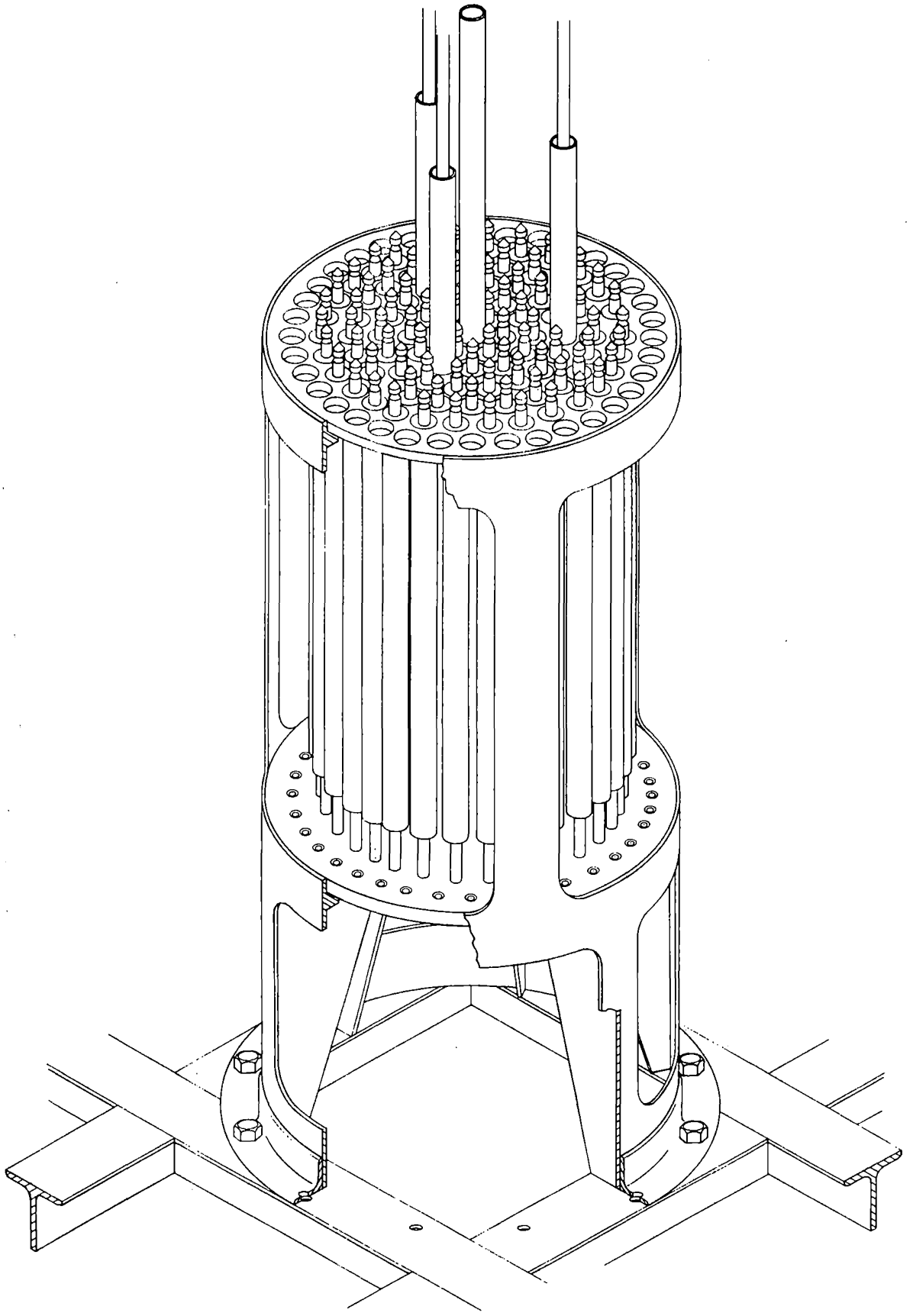

BS-39-64-1018

FIGURE 7. AGNIR CORE AND SUPPORT STRUCTURE

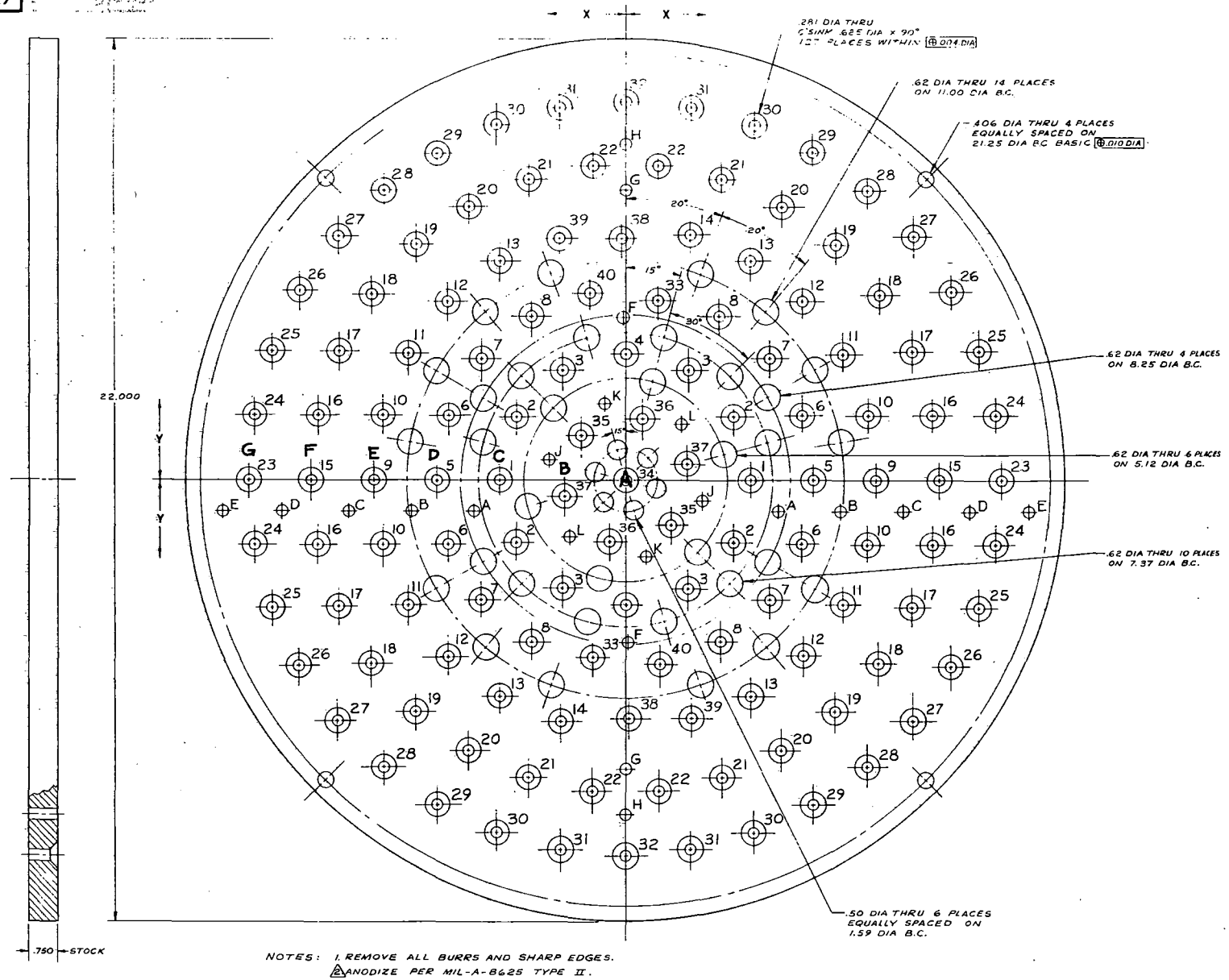

FIGURE 8. BOTTOM GRID PLATE

85.30-64-1920

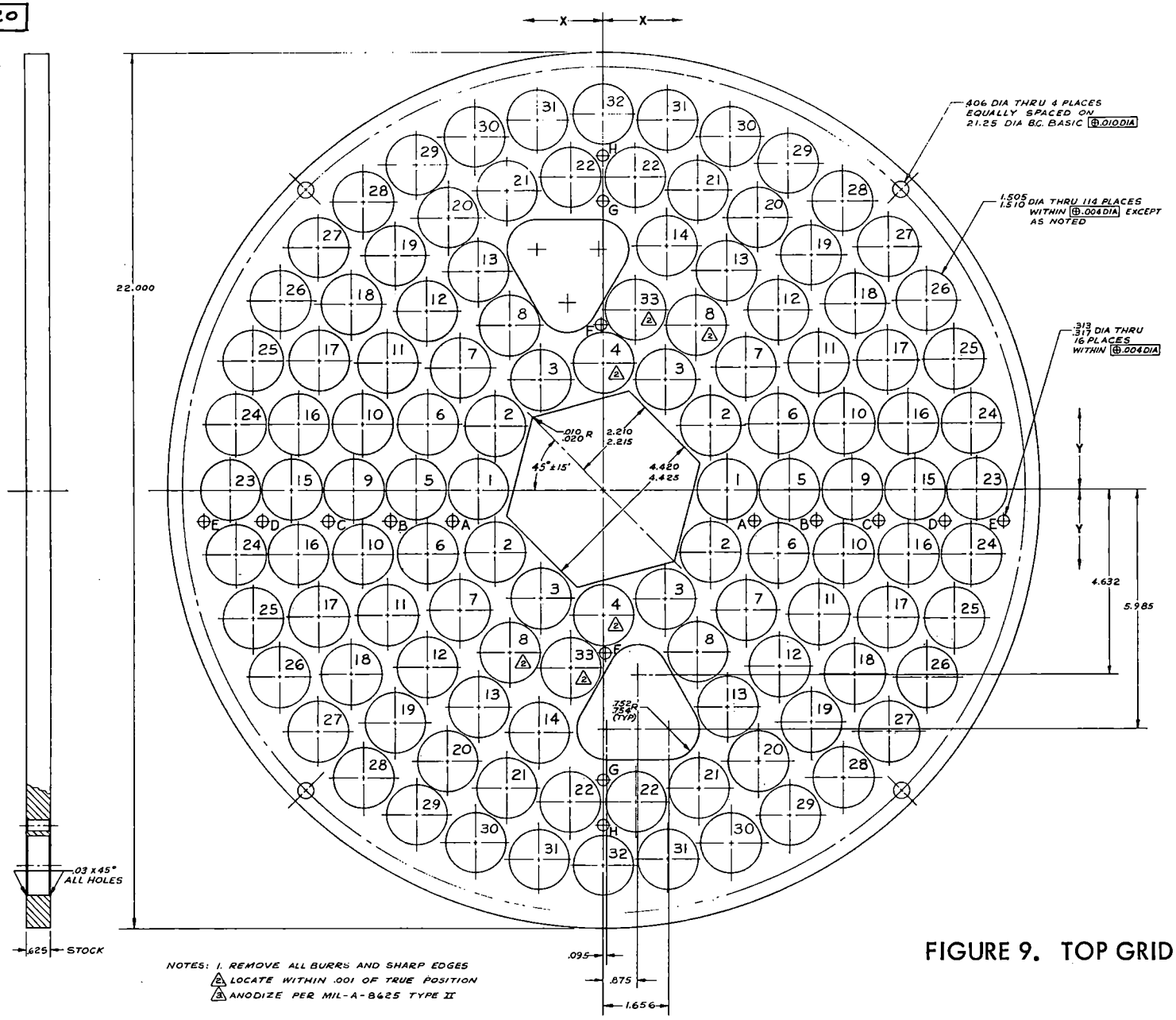

FIGURE 9. TOP GRID PLATE

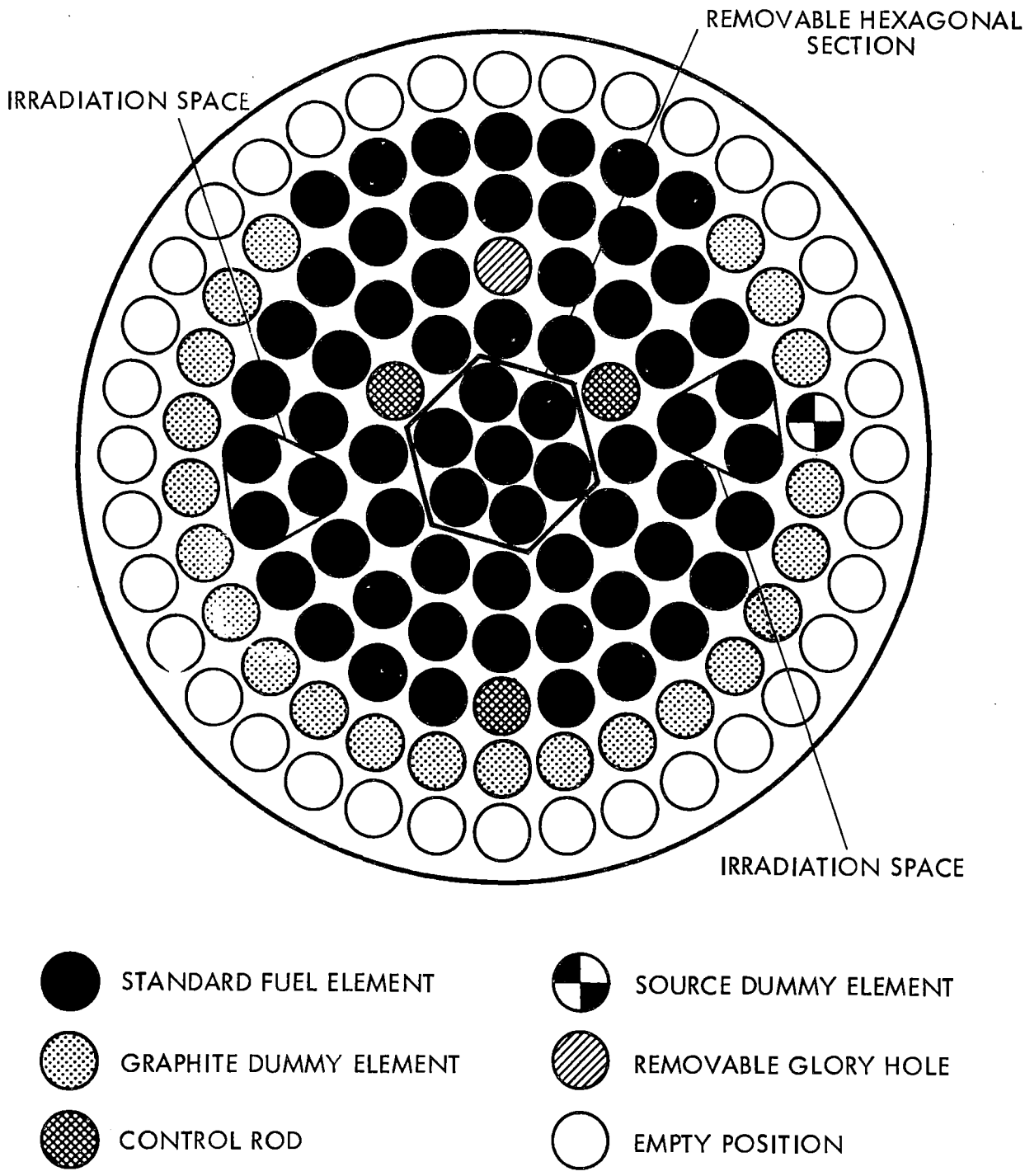

Note: Rings of element positions are identified by letters A to G, as shown in Figure 8.

FIGURE 10. TYPICAL GRID ARRAY

4. Instrument Guide Tubes

Four instrument guide tubes are provided for the four channels of instrumentation. These are held in place at the top by the support bridge and at the bottom by the T beam.

5. Fuel Element Storage Racks

A fuel element storage rack [redacted] will be located on the wall of the reactor tank. Elements will be centered about 6 feet above the floor.

B. REACTOR CHARACTERISTICS

The principal characteristics of the Aerojet-General Nucleonics Industrial Reactor design are summarized in Table 4.

It should be noted that the reactivity worth of all rods is dependent on the core configuration. The values shown in Table 4 are nominal. Under no circumstances will the reactor be operated when the shim rod is worth less than 2.25% Δk/k. The total worth of all rods will be about 5% Δk/k during operation. Thus, if the shim rod should stick, the safety rod will shut the core down.

TABLE 4

SUMMARY OF REACTOR DATA

Responsible Organization	Aerojet-General Nucleonics
Location	San Ramon, California
Purpose of Reactor	Industrial Research
Reactor Materials	
Fuel	20% enriched U-235
Moderator	Zirconium hydride and water
Reflector	Demineralized water or graphite
Coolant	Demineralized water
Control	1 shim rod, 1 regulating rod, 1 safety rod, all boron carbide
Structural material	Aluminum
Shield	Demineralized water
Dimensions	
Core (active)	19.44 in. dia. by 14 in. high (nominal)

Reflector	
Water	∞
Graphite	1.5 in. (side), 4 in. (top and bottom)
Thermal Characteristics	
Operating power	250 kw
Maximum heat flux	50,000 Btu/hr-ft^2
Maximum water temperature	130°F
Specific power (water reflected core)	108 w/gm U-235
Reactor Physics	
Core loading (graphite reflected crit.)	[redacted]
Average thermal flux	4.0 x 10^{12} nv
Average fast flux	~6.7 x 10^{12} nv
Reactivity in control system	~6% Δk/k
Temperature coefficient (50°C)	-1.2 x 10^{-4} Δk/k per °C
Void coefficient (average over core)	-0.2% Δk/k per % void
Prompt neutron lifetime	65 μsec
Equilibrium Reactivity Requirements (at 250 kw)	
Equilibrium xenon	~2.0% Δk/k
Temperature	~1.3% Δk/k
Experiments (typical)	0.7% Δk/k
Total equilibrium requirements*	~4.0% Δk/k
Total Reactivity Available (license limit)	2.25% Δk/k (cold, clean)
Fuel Elements	
Type	TRIGA pin
Enrichment	20 wt% U-235 nominal
Fuel alloy	Uranium-zirconium hydride
Fuel loading per pin	[redacted]
Cladding material	Aluminum, anodized
Cladding thickness	0.030 in.
Control Rods	
Number	3 (1 shim, 1 safety, 1 regulating)
Containment material	Aluminum
Neutron poison	Boron carbide, powdered
Worth (shim and safety rods)	~2.6% Δk/k each
(regulating rod)	~0.75% Δk/k

*Operation at 250 kw limited to approximately 5 hr

C. FUEL-MODERATOR ELEMENTS

The AGNIR will use TRIGA type fuel elements developed by General Atomic. As shown in Figure 11, each fuel element consists of a central rod of fuel-moderator material, burnable poison wafers, and graphite end reflectors, all encased in aluminum cladding.

The fuel is a solid homogeneous mixture of uranium and zirconium hydride containing 8% by weight of uranium enriched to 20% in U-235. The hydrogen-to-zirconium ratio is approximately 1.

A wafer 0.05 in. (1.3 mm) thick at each end of the active fuel section contains a burnable poison. Thus, an appropriate amount of burnable neutron-absorbing material is incorporated in each fuel element to minimize the reactivity effect due to the fission product poisoning and the fuel burnup.

The fuel elements are clad with a heliarc-welded, aluminum can 0.030 in. (0.76 mm) thick. Two 4-in. (10.2 cm) sections of graphite are inserted in the can above and below the active fuel region, but are separated from it by the burnable-poison aluminum wafers. When the fuel elements are loaded into the core, the graphite sections form the top and bottom core reflectors. Aluminum end fixtures are attached to each end of the can. The bottom end fixture locates and supports the element in the bottom grid plate; the top end fixture is designed for convenient handling of the fuel element. The fuel element cladding is anodized to retard wear and corrosion.

Each standard fuel element contains approximately [redacted]

Graphite dummy elements occupy all grid positions (except those in the "G" ring) not filled by the fuel-moderator elements or other core components. They are of the same dimensions and construction as the fuel-moderator elements, but are filled entirely with graphite.

D. SOURCE

1. Neutron Source Holder

The neutron source holder (Figure 12) is made of aluminum, is cylindrical in shape, and has a cavity to contain the source. The source holder can be installed in any vacant fuel or graphite element location. A shoulder at the upper end of the holder supports the assembly on the upper

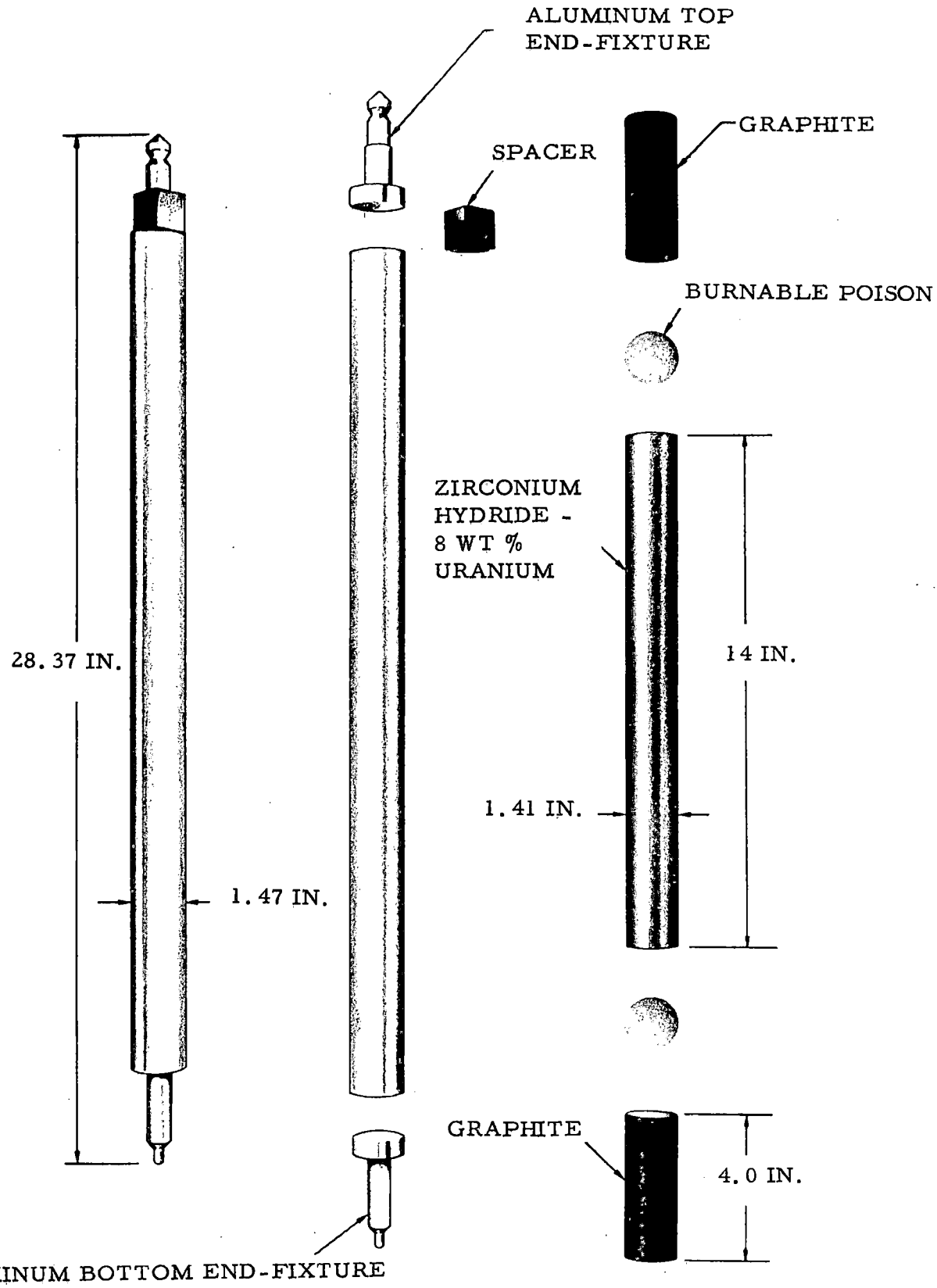

FIGURE 11. FUEL-MODERATOR ELEMENT

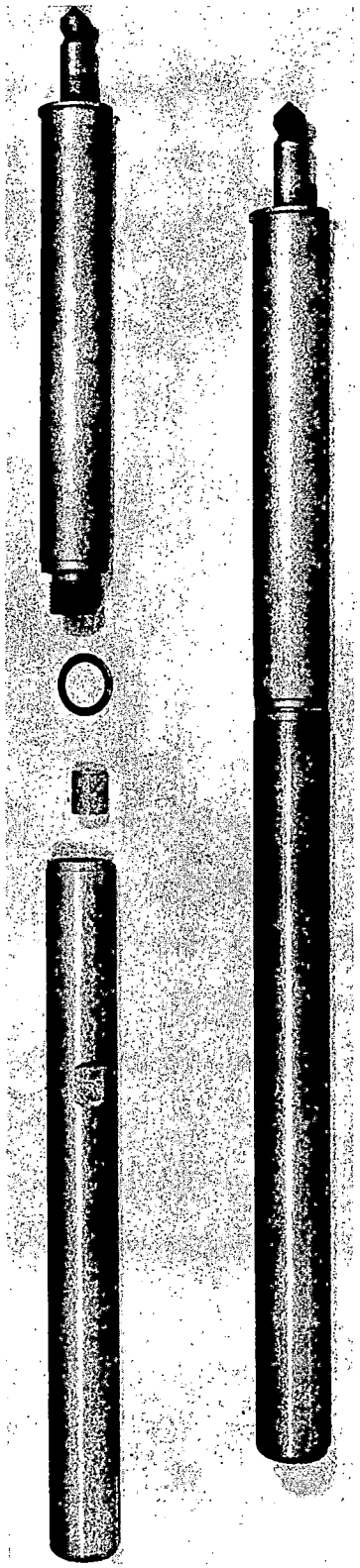

FIGURE 12. NEUTRON SOURCE HOLDER

grid plate, the rod itself extending down into the core region. The neutron source is contained in a cavity in the lower portion of the rod assembly at the horizontal centerline of the core. This cylindrical cavity is 0.981 in. (2.49 cm) in diameter and 3 in. (7.60 cm) deep. The upper and lower portions are screwed together. A soft aluminum ring provides sealing against water leakage into the cavity. Since the upper end fixture of the source holder is similar to that of the fuel element, the source holder can be installed or removed with the fuel handling tool. In addition, the upper end fixture has a small hole through which one end of a stainless steel wire may be inserted to facilitate handling from the top of the tank.

2. Neutron Source (Polonium-Beryllium)

The initial neutron source will consist of a mixture of polonium and beryllium; it will have a nominal required strength of 2 curies for achieving the necessary count rate during initial reactor startup. Cylindrical in shape, the source will have a nominal outside diameter of approximately 0.7 in. (1.8 cm) and a height of 0.7 in.

The source will be double-encapsulated to ensure leaktightness, the polonium-beryllium mixture being contained in an inner capsule of platinum, stainless steel, or a similar material, with an outside capsule of stainless steel sealed by heliarc welding.

E. CONTROL RODS

1. Control Rod Guide Tubes

The three control rod guide tubes can be inserted into any of the 137 fuel element positions. The guide tube assembly, shown in Figure 13, is made of aluminum, anodized to increase resistance to wear and corrosion. The outside diameter of the tube is 1.495 in. (3.80 cm). The tube receives its support from the lower grid plate. It is fixed in place in the lower grid plate by a locking pin in the lower end fixture. Water passage through the tube is provided by a large number of holes evenly distributed over the entire length of the tube.

2. Control Rods

Three boron carbide control rods - safety, shim, and regulating - operate in perforated aluminum guide tubes (Figure 13). Each control rod is a sealed aluminum tube containing powdered boron carbide as a neutron poison (Figure 14). The upper end of the control rod screws into the control rod drive assembly extension tube. The control rods are approximately 20 in. (51 cm) long. The outside diameter of the regulating rod is 7/8 in. (2.22 cm), and the shim and safety rods are each 1.25 in. (3.2 cm) in diameter. The vertical travel of the control rods is approximately 15 in.

The shim and safety rods are each worth about 2.6% $\Delta k/k$, and the regulating rod is worth about 0.75% $\Delta k/k$. The total rod worth is thus about 6.0% $\Delta k/k$.

3. Control Rod Drive Assemblies

The control rod drive assembly is shown in the photographs in Figure 15. The drive assemblies for the three control rods are mounted on the I-beam bridge assembly; each consists of a motor and reduction gear driving a rack and pinion. A helipot connected to the pinion generates the position indication. Each control rod has an extension tube that extends to a dashpot below the surface of the water. The dashpot and control rod assembly are connected to the rack through an electromagnet and armature. In the event of a power failure or scram signal, the control rod magnets are de-energized and the rods fall into the core. The rod-drive motor is nonsynchronous, single-phase, and instantly reversible, and will insert or withdraw the control rod at a rate of approximately 12 in. per minute. Electrical dynamic and static braking on the motor are used for fast stops.

Limit switches mounted on the drive assembly indicate the following:

1) The up and down positions of the magnet
2) The down position of the rod
3) The magnet contact with the rod

The complete drive assembly is enclosed in an aluminum can.

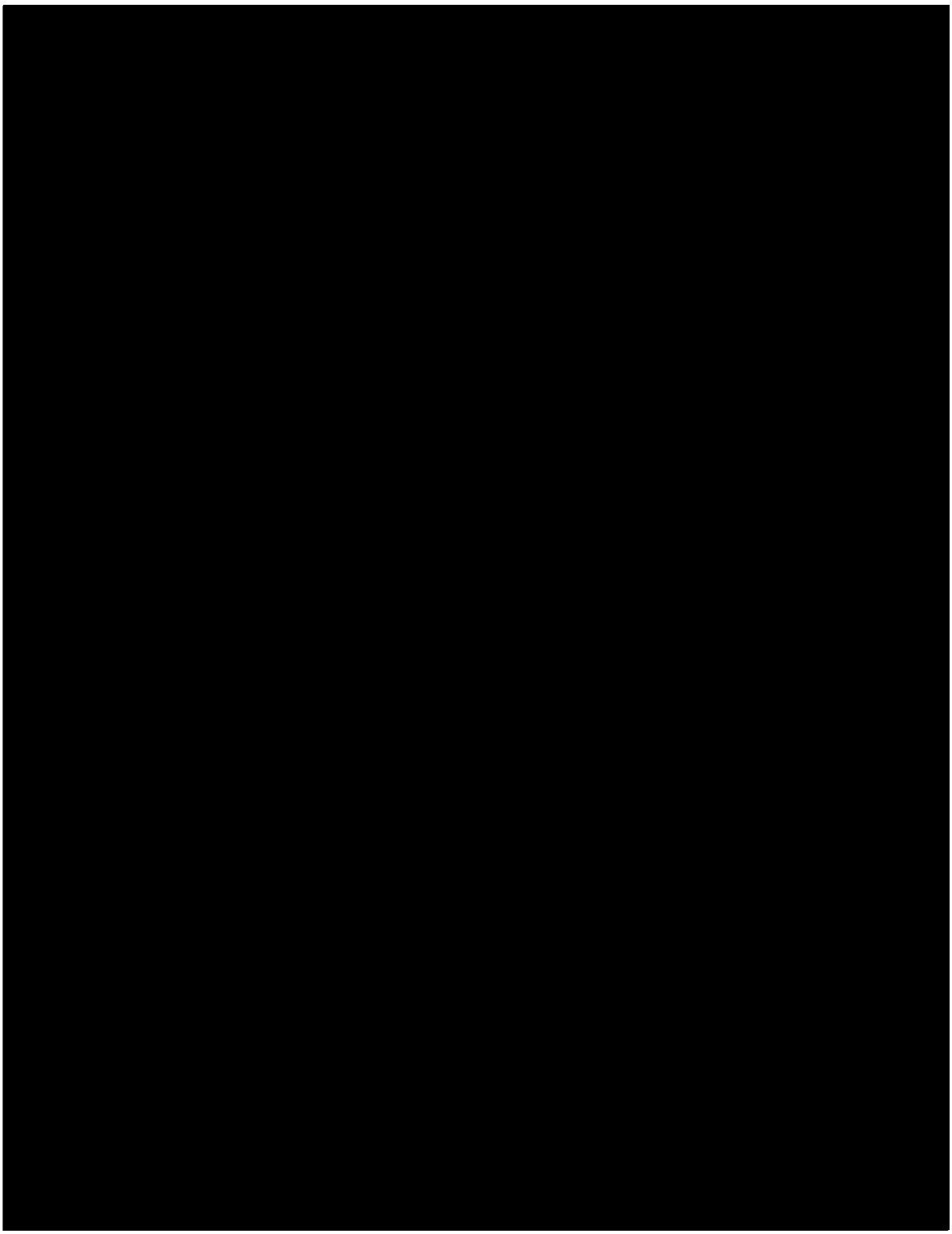

FIGURE 13. CONTROL ROD GUIDE TUBE AND REMOVAL TOOL

FIGURE 14. CONTROL ROD (POISON CONTAINER)

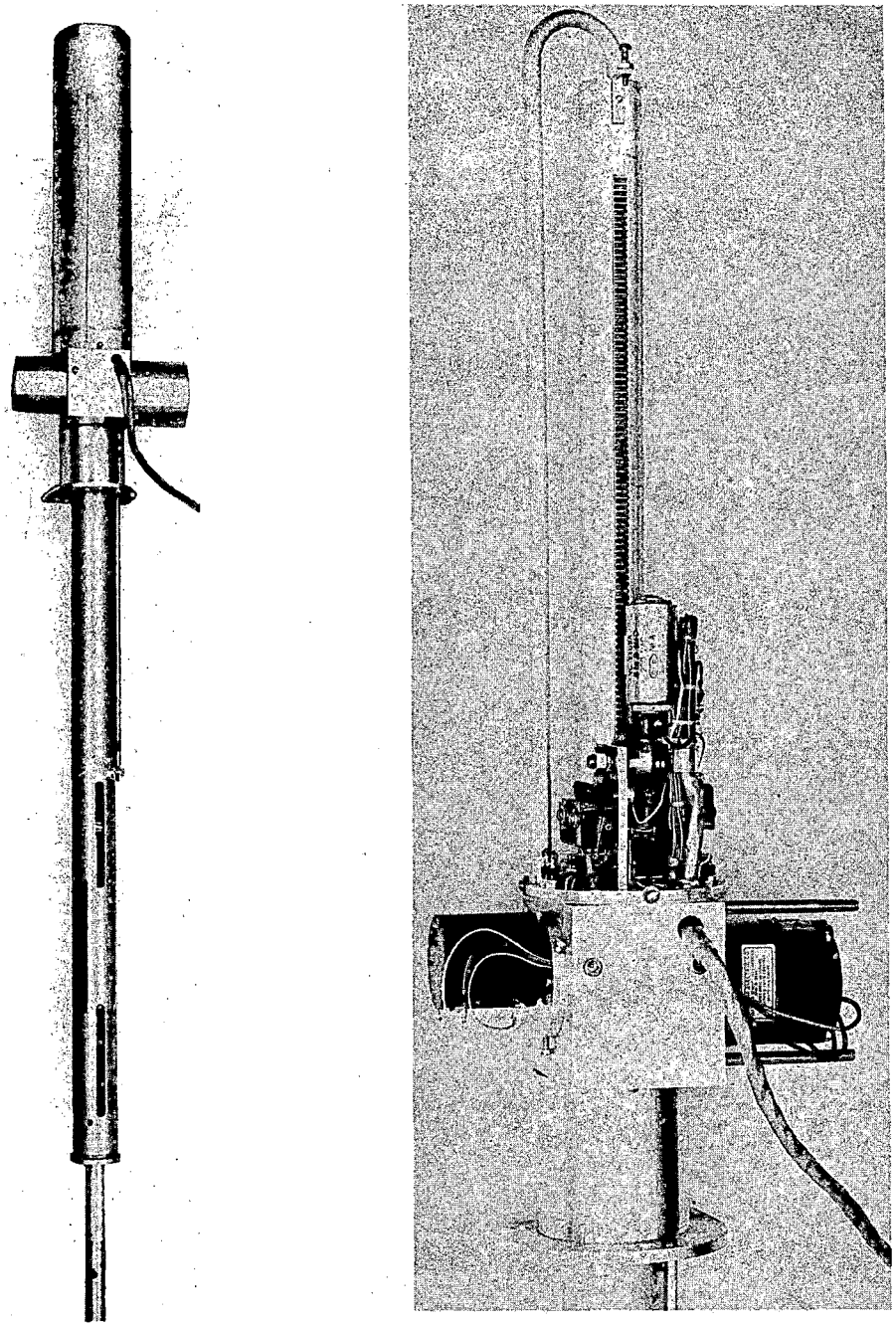

FIGURE 15. CONTROL ROD DRIVE ASSEMBLY

F. AUXILIARY SYSTEMS

1. Demineralizer

A mixed-bed demineralizer will be provided to maintain the resistivity of the pool water at 1 megohm/cm. This demineralizer will have a capacity of 10 gal/min. It will be located outside the reactor building and will be adequately shielded. Water will be pumped to the demineralizer from the reactor tank through pipes in the channels under the floor.

2. Storage Facilities

[redacted]

3. Heat Transfer Equipment

A tubular-type heat exchanger is used to remove heat from the reactor tank water. This heat exchanger has a steel shell containing stainless steel tubes through which the reactor water flows. Secondary cooling water flows around the tubes to remove the heat from the primary water. The heat exchanger is rated at 875,000 Btu/hr.

Piping and valving will be installed as required.

VI. EXPERIMENTAL FACILITIES

Facilities for two methods of irradiating experimental samples are provided in the AGNIR design: a glory hole giving access to the interior of the core, and an irradiation box for exposures outside the core.

A. GLORY HOLE

The glory hole, extending from the reactor bridge to the lower grid plate, will be an aluminum tube of 1.5 in. outside diameter which will fit into any fuel element hole. It will be both positioned and supported by the lower grid plate. Material to be irradiated will be lowered through the tube into the core region. A shield plug will be placed in the top of the tube to reduce gamma streaming to acceptable levels.

B. IRRADIATION BOX

An aluminum box with a face covering a 90° section of the core will be used for irradiation of experimental materials outside the core. A typical box design is shown in Figure 16. Samples to be irradiated will be placed inside the box, and the box will be weighted sufficiently to overcome buoyancy. It will then be lowered into the reactor pool and rigidly fastened to the T beams on the bottom of the tank.

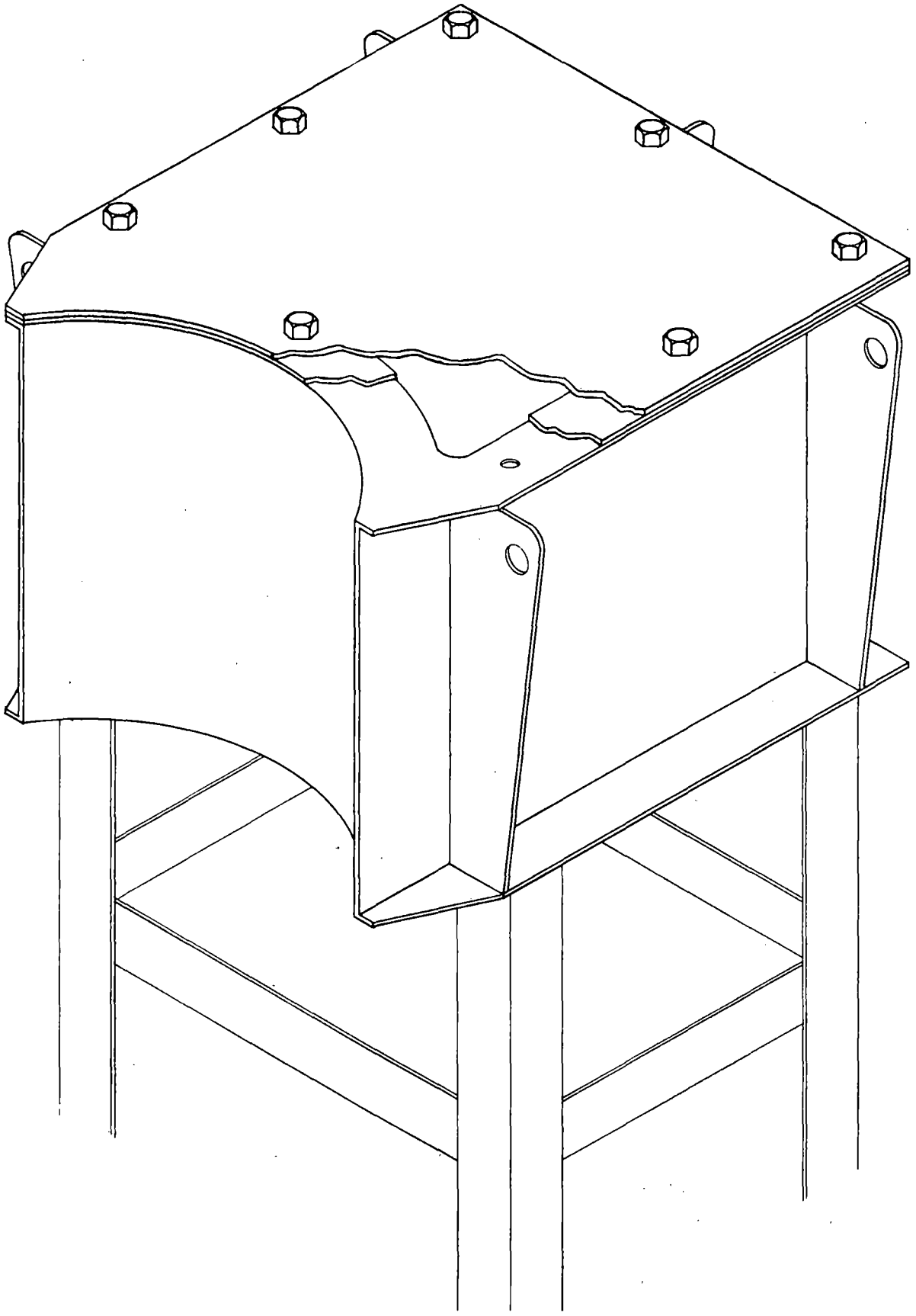

FIGURE 16. TYPICAL IRRADIATION BOX DESIGN

VII. INSTRUMENTS AND CONTROLS

The reactor instrumentation is divided into three broad categories: nuclear, annunciator and alarm, and auxiliary process.

The nuclear instrumentation provides the neutron flux information which is the primary basis for operator actions. Expected ranges of detection are shown in Figure 17. Outputs of the nuclear channels are also inputs to the annunciator and alarm instrumentation.

The annunciator and alarm instrumentation provides for automatic scrams when reactor flux is too high or increasing too rapidly, or when various other parameters are unsatisfactory. In some cases, only an annunciation is given, to call the operator's attention to parameters which are important to reactor operation but do not require an immediate scram.

The process instrumentation for this reactor is very simple, consisting primarily of pool water temperature, purity, level, and water flow detection.

The instrumentation requiring operator observation and actions during reactor operation is located in a low-silhouette, three-panel desk console. Certain power supplies and process chassis will be located in a separate instrumentation rack placed near the control console in the control room.

A. NUCLEAR INSTRUMENTATION

Four channels of neutron-measuring instruments are used during the transition from source to full-power operation. Figure 18 is a block diagram of the four nuclear channels.

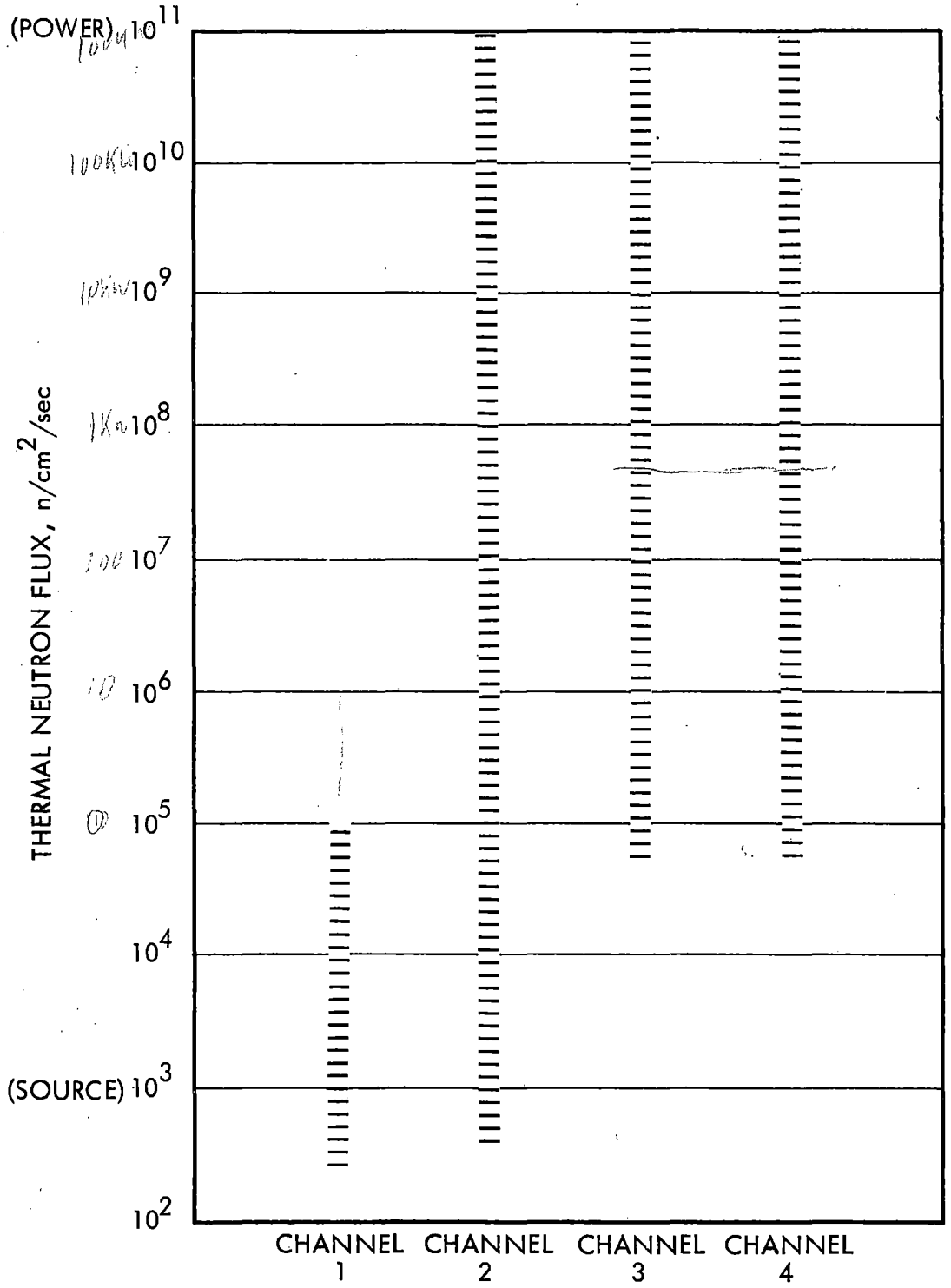

FIGURE 17. EXPECTED OPERATING RANGES OF NEUTRON DETECTORS

85.39-64-1924

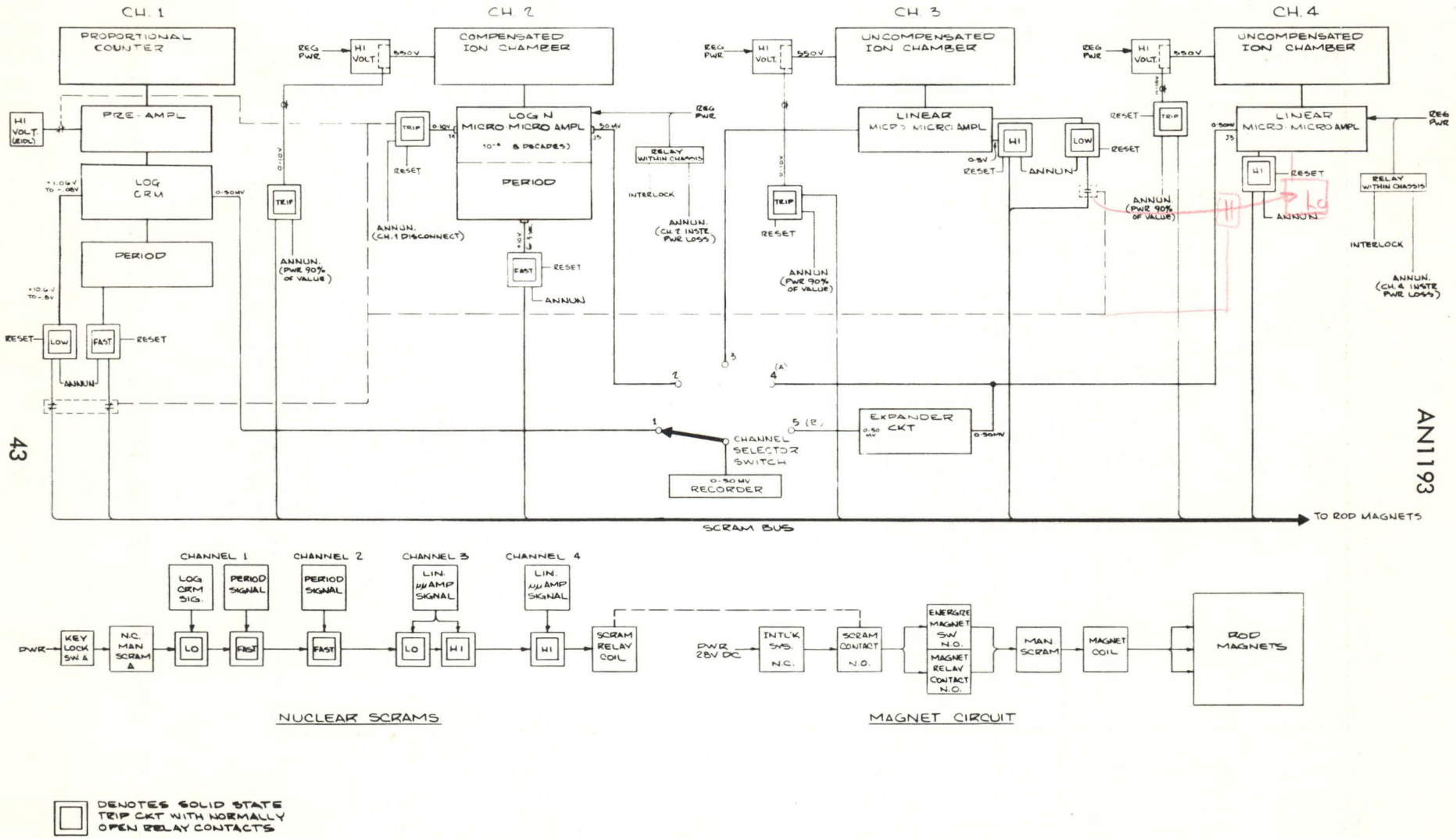

FIGURE 18. BLOCK DIAGRAM OF NUCLEAR INSTRUMENTATION

1. Startup, Channel 1

The detector for this channel is a proportional counter incorporating boron-10 as the neutron-sensitive material. Its purpose is to ensure the presence of a source before startup and to provide a neutron count on which to base multiplication as the safety rod is withdrawn. The detector output pulses are amplified and then rate-averaged by a six-decade log count ratemeter (10^1-10^7 cpm). The count ratemeter output is amplified and used to drive a period circuit. This period circuit and alarm is operative until a switchover is made automatically to Channel 2 at an intermediate power. A solid state relay on Channel 2, similar to the scram trip circuits, initiates the action. At this point the high voltage for the Channel 1 detector is removed and the detector shorted. The period scram on Channel 1 and a lower level alarm requiring presence of a source before startup are disabled by the same trip circuit.

2. Intermediate, Channel 2

A compensated ion chamber serves as the detector for the intermediate channel. The current is measured by a seven-decade log micromicroammeter, with the meter output driving a period and alarm circuit. The primary functions of this channel are to provide an automatic period protection while power is increasing and for use in neutron multiplication calculations. The period alarm is operative from switchover through full power operation.

3. Control, Channel 3

Channel 3 is a linear micromicroammeter coupled to an uncompensated ion chamber detector. Since it has both upper and lower alarms (lower alarm inoperative until automatically switched in by Channel 2), the operator must switch ranges as power increases. In this manner, an upper-level alarm protection is available within approximately 1/3 decade of actual power. Thus, if the period circuit were to fail to shut the reactor down on a fast period, the upper alarm would serve as a backup for all periods too fast for operator control.

4. Safety, Channel 4

This channel is identical to Channel 3 with the exception that Channel 4 has no lower alarm contacts. Its alarm would normally be set

for approximately 120% of full permissible power and its switch setting would be limited to the power range.

B. ANNUNCIATOR AND ALARM SYSTEMS

All annunciators and alarms are combined within two chassis. The indicators, scram reset switches, lamp test and horn-acknowledge switch are on the front panel for convenient operator control. The semi-conductor trip cards and associated relays are mounted at the rear of the console behind locked doors.

The trip cards and relays are mounted separately so that removal of a trip card will automatically scram the reactor by releasing the relays, all of which are energized during normal operation. This assures fail-safe conditions for not only trip card removal, but electronic power supply and power line failure as well.

The bistable trip cards are designed to give an output of either 12 volts or 0 volts. Depending upon the type of normal input, i.e., continual signal or no signal, the relays are kept energized by proper choice of the output connection.

The reactor is scrammed by interrupting the power to the magnets which hold the rods. All trips remain in the tripped condition until they are manually reset after the scram condition has been cleared. A block diagram of the scram bus and trip circuits is shown in Figure 18.

1. Scram Bus

The following trip channels are provided:

a) Period and low level - Channel 1
b) Period, power supply low, instrument power - Channel 2
c) Upper and lower limits, power supply low - Channel 3
d) Upper limit, power supply low, instrument power. - Channel 4
e) Manual scram (automatic reset, no trip card required)

2. Interlocks

Two additional conditions for reactor operation must be met in addition to clearing the scram bus. The pool water level and earthquake or seismic shock interlocks must be made up to apply rod magnet power. Loss of pool water or a seismic shock during operation will scram the reactor. (Additional interlock information is given below under Control Function).

3. Annunciator Signals

Several parameters other than interlocks and scrams are of interest to the operator. Accordingly, labeled lights are provided on the annunciator for the following:

a) Area monitor (on reactor room wall)
b) Water radioactivity
c) Crane bridge location
d) Water flow
e) Water holding tank full
f) Air flow on air monitor

4. Control Function

The control rods are controlled by nine lighted pushbuttons. The buttons are arranged in three vertical rows, one row for each rod drive. One light indicates the down limit, a second indicates the up limit, and the third light is a split indicator, one half for magnet contact, the other half for magnet current. When lighted, the double pushbuttons indicate magnet current on and magnet contact with the rod armatures. When the double pushbuttons are depressed, the magnet current ON lights will be extinguished. If a drive is above the down limit, the rod will fall back into the core and the contact light will be extinguished until the automatic magnet-drive-down control lowers the magnet so that it makes contact with the rod again. Releasing the button will close the magnet circuit, and magnet current will be reset.

The UP and DN pushbuttons remove the short circuit across a motor phase-shifting capacitor and apply power to the motor in the correct phase to drive it either up or down. Several interlocks in the UP pushbutton circuit make this circuit inoperative under certain conditions. The lower level scram provision of Channel 1 removes magnet power so that the rods cannot be raised in the absence of a set minimum source count.

In order to prevent more than one rod being raised at a time, the UP switches are arranged so that when one is activated, it activates the interlock signal to control all other rods, preventing their movement.

Indication of the shim and control rod positions is by means of two servo motor-driven registers.

C. AUXILIARY INSTRUMENTS

Continuous indication of pool water temperature and conductivity is provided for reference use. Interpretation of this information is required during reactor operation.

An area monitor with alarms is located on the wall of the reactor room.

VIII. SHIELDING

Shielding for the AGNIR will consist, vertically, of a minimum of 17 ft of water above the top of the core, and laterally of water plus the soil and concrete around the sides of the sunken reactor tank. The dose rate at the bridge above the tank will be less than 15 mr/hr. There will be no appreciable radiation elsewhere in the building.

IX. ROUTINE REACTOR EQUIPMENT MAINTENANCE

The only items requiring routine maintenance will be:

1) Demineralizer and pump

2) Control rod drives

3) Heat exchanger and pump

4) Instrumentation

Resins in the demineralizer will be replaced when required. Although the activity level is expected to be low, expedient shielding will be available if required. The pump will be readily accessible.

All components of the control rod drives which require maintenance are located on the reactor bridge and are readily accessible. Any work done on the rod drives will be performed in accordance with written procedures and under direct supervision of responsible personnel (see Section XI).

A low activity level is anticipated in the heat exchanger, so that direct maintenance will be permissible. Thus, routine maintenance can readily be performed on both the pump and heat exchanger.

All electronic instrumentation will be checked and recalibrated at least semiannually according to established procedures.

X. INITIAL TESTS AND OPERATING PROCEDURES

A. PRE-OPERATIONAL TESTS AND CHECKOUTS

Before the initial loading of fuel elements, all mechanical and electrical systems will be tested for proper operation. In particular, the control rod drive mechanisms will be checked to ensure:

1) Proper drive speed
2) Proper scram action
3) Repeatability of position indication
4) Proper operation of limit switches and sequence interlocks
5) Absence of instrument noise resulting from control rod action

Also, the neutron flux instrumentation channels will be tested by using a neutron source to determine their operability and approximate calibration. Where possible, scram will be initiated by means of the source. The water instrumentation, including flow, radiation, conductivity and temperature, will be calibrated. The earthquake interlock will be tested. Finally, the water conductivity will be brought down to an acceptable level and the water will be circulated until it is at temperature equilibrium before the initial critical loading is begun. A detailed pre-operational testing report will be written and approved by the reactor supervisor and the cognizant design engineers, certifying that the reactor meets proper safety standards and design intentions.

B. INITIAL LOADING AND CRITICALITY TESTS

The criticality tests will be conducted according to a detailed procedure which will be approved by the AGN Reactor Safeguards Committee and submitted to the USAEC at the time the request is made to convert the

construction permit to a facility license. This procedure will be based on successive measurements of the inverse subcritical multiplications of a neutron source by the reactor core, as measured on the reactor flux instruments and on additional neutron pulse-counting channels. Throughout the procedure, each addition of fuel will be limited to one-half or less of the fuel required to reach the extrapolated critical point, until the worth of the increment becomes less than the allowed available excess reactivity. No fuel elements will be introduced into the pool until they are to be loaded into the core. The initial critical configuration will be built up by loading elements into water-filled spaces in the most nearly circular geometry, with all available graphite reflector elements used to build up a reflector around the expected minimum core configuration. It is not anticipated that any hazard will be associated with this procedure, because of the great similarity of this core to existing cores.

C. ZERO AND LOW POWER PHYSICS TESTS

After the initial critical configuration has been established, the control rods will be calibrated. The entire regulating rod and the accessible portion of the shim rod will be calibrated by supercritical period measurements. The safety rod and the remainder of the shim control rod will be calibrated by the rod drop technique, thus establishing the shutdown margin. Next, the temperature coefficient of reactivity will be measured at various temperatures throughout a nominal range. This procedure will be followed by a preliminary power calibration by means of irradiation of gold foils. Lastly, the worth of substitutions of fuel, water, and graphite will be measured at various locations and the worth of the glory hole will be determined. During this testing, the power will be about 100 w.

After these basic measurements have been completed, the critical configuration will be established for the core. Checks will be made to determine if the control rod worth, power calibration, or temperature coefficient have changed significantly from the original values. The worth of empty and flooded experimental chambers will be measured.

D. OPERATING PROCEDURES

All reactor operations will be conducted in accordance with detailed, written procedures which will be submitted to the AGN Reactor Safe-

guards Committee and to the USAEC. This document will cover pre-operational checkout, operations, standard operating limitations, and procedures for non-standard or emergency conditions. Detailed logs will be maintained and notations made on the strip chart recorder in accordance with these operating procedures. Logs will also be maintained of all irradiations and experiments conducted in the reactor.

XI. ADMINISTRATIVE AND PROCEDURAL SAFEGUARDS

A. ORGANIZATION AND RESPONSIBILITY

The General Manager of Aerojet-General Nucleonics is ultimately responsible for ensuring that all reactor operations are conducted safely and in full compliance with applicable regulations of the United States Atomic Energy Commission. Advising him are the AGN Reactor Safeguards Committee, the Radiological Safety Committee, and the Legal Supervisor. The Radiological Safety Officer is responsible to the General Manager for compliance with state and federal radiation regulations, and for enforcing proper operational controls with regard to radiation protection.

The Reactor Supervisor for the AGNIR will be responsible to the General Manager for the safe and proper condition of all nuclear facilities under his jurisdiction and for their safe operation. He will also be responsible for ensuring compliance with state and federal regulations concerning the operation of reactor facilities, and particularly with the provisions of all applicable facility licenses. He will supervise any approved modifications made to the facility. The Reactor Administrator will be responsible to the Reactor Supervisor for performance of routine maintenance, for scheduling of routine operations, and for maintenance of records. Operation will be conducted by Senior Operators and Operators, who will be responsible to the Reactor Supervisor. The duties and responsibilities of all of these persons will be documented in detail in the written procedures which will be submitted to the US Atomic Energy Commission for approval when a facility license is requested.

B. ADMINISTRATIVE CONTROL AND PROCEDURES

Administrative control of AGNIR facility operations will be maintained through procedures such as the following:

1) Access to the reactor building and facility area will be limited to authorized persons.

2) Performance of maintenance and janitorial work will be controlled by special work permits.

3) Possession of reactor keys will be limited to the Senior Operators, one of whom must be present during startup.

4) Reactor operation will require 1) the presence of two persons, at least one of whom is a licensed operator, 2) the availability of a Senior Operator, and 3) the authorization of the Reactor Administrator or Reactor Supervisor.

5) All modifications to the reactor and all non-routine operations must be approved by the Reactor Supervisor, who will obtain the approval of the Reactor Safeguards Committee and, when required, license amendments from the USAEC.

6) All licensed operators will be required to read thoroughly the operating procedures manual and all reactor operations memoranda, and will be required to attend periodic briefing sessions.

7) The AGN Health and Safety Department will conduct periodic radiation surveys and safety inspections.

C. REVIEW AND AUTHORIZATION OF TESTS AND EXPERIMENTS

The AGNIR operating procedures will detail the requirements for review and authorization of tests and experiments. In general, a request for authorization will be initiated by submitting to the Reactor Supervisor a written description of the experiment planned. The Reactor Supervisor may:

1) Approve the experiment

2) Request a hazards analysis

3) Seek review by the Reactor Safeguards Committee

4) Prepare for submission to the USAEC an application for license amendment

This decision will depend on the nature of the experiments and the provisions of the facility license. Written approvals from the Reactor Supervisor will constitute authorization to the reactor operators and senior operators for conduct of the experiments.

D. TRAINING

Operator training will be conducted as required under the direction of the Reactor Supervisor. The amount of training given, both at the reactor and in the classroom, will depend on the skill and prior training of the trainees. Before competence is attested for an AEC operator license application, the trainee must pass written and operating examinations of a standard at least comparable to that of the AEC examination. In addition, all licensed operators will be required to operate the reactor periodically and to attend periodic briefings in order to maintain their proficiency.

XII. HAZARDS

A. HAZARDS ASSOCIATED WITH NORMAL OPERATION

1. Normal Radiation Exposure

When the reactor is operating at full power (250 kw), the radiation level at the surface of the pool will not exceed 50 mr/hr. Since the reactor will be set into the ground, the surrounding concrete and soil will act as shielding in the radial direction. On the bridge and at the edge of the pool, the radiation level will be less than 15 mr/hr. There will be no appreciable radiation level elsewhere in the building.

2. Exposure During Fuel Handling

Fuel handling will be held to a minimum after the reactor has been brought to power. A storage facility for fuel elements will be provided on the wall of the tank, 6 ft above the floor. [redacted] Thus, it will not normally be necessary to remove irradiated elements from the tank. However, for occasions when it does become necessary to remove elements, a special cask will be provided which will limit the dose received by the persons performing the work to the applicable standards.

3. Irradiation Level Above Storage Holes

Storage of hot materials will be limited so that radiation levels on top of the storage hole plugs will not exceed 2.5 mr/hr, which is within the standard 40-hr week exposure limit.

4. Argon Activity

Calculations of the activity resulting from activation of argon dissolved in the reactor pool water are presented in Appendix E. No problem in personnel protection is anticipated from this source.

5. Spillage of Radioactive Material

Spillage of activated material is possible with this system, since the reactor will be used for research. However, AGN is thoroughly versed in the emergency procedures to be followed in such an event, so that no undue hazard is foreseen.

B. HAZARDS ASSOCIATED WITH ABNORMAL OPERATION

The hazards associated with abnormal operations can be divided into the following five accidents.

1) Start-up accident
2) Uncontrolled rod withdrawal
3) Step insertion accident
4) Loading accident
5) Poison experiment removal accident
6) Loss of coolant and shield water accident

1. The Startup Accident

In this accident it is postulated that the reactor is subcritical and the control rod is withdrawn at the maximum rate of 12 in./min. Assuming that the rod is active only over the active 14 in. of the fuel element, and further assuming that the peak worth of the blade will be about 1.6 times the average worth, the maximum ramp insertion rate will be 0.058% Δk/k per sec. Since the maximum reactivity available in the reactor to be inserted at this rate is 2.25% Δk/k, this accident will produce a much lower peak power than would result if the entire available excess were inserted instantly. This case is described in Section 3 below.

2. Uncontrolled Rod Withdrawal

Removal of all rods simultaneously would result in a maximum possible insertion rate of 0.13% Δk/k per sec. This could only be caused by sabotage of the reactor interlock system. Since, under the reactor operating

conditions, the total reactivity available would still be less than 2.25% Δk/k, the resulting power rise and temperature rise in the reactor will be less than the 2.25% Δk/k step insertion. This case is described in Section 3 below.

3. The Step Insertion Accident

In this accident, it is assumed that the entire 2.25%Δk/k available is suddenly inserted into the core. However, a reactor having the same core as AGNIR has been safely pulsed many times with 2.25% Δk/k insertions.* The resulting power excursions attained a peak power of 1000 Mw on a reactor period of 4.0 msec with a total energy release during the burst of approximately 16 Mw-sec. The maximum measured fuel temperature for this pulse was less than 500°C. Curves of the transient power level and fuel temperature resulting from such an insertion of reactivity are shown in Figure 19. This reactivity insertion does no harm to the reactor itself, nor does it create any hazard for personnel.

4. The Loading Accident

In a core of the AGNIR type, 0.70% Δk/k (or one dollar) is required to increase the steady state power by 100 kw.** This large amount of reactivity insertion is necessary to overcome the large negative temperature coefficient. Further, the reactivity of the most reactive fuel element is worth 1.05% Δk/k (or 1.5 dollars). Therefore, if one were to load single elements (once criticality is approached) at 5-minute intervals, one could load continuously until there is an obvious production of heat in the reactor. It is assumed that power equilibrium is attained within 5 minutes of the power addition. Thus, under no conditions would more than 150 kw be added to the system at one time. Even if elements were continuously added at the above rate, no serious problems would occur.

* Hazards Report for the 250 kw TRIGA Mark II Reactor, GA 2025, August 1961

** Hazards Analysis for the TRIGA Mark II Training and Research Reactor to be Installed at the University of Illinois, Urbana, Illinois, NP-8299, 1959.

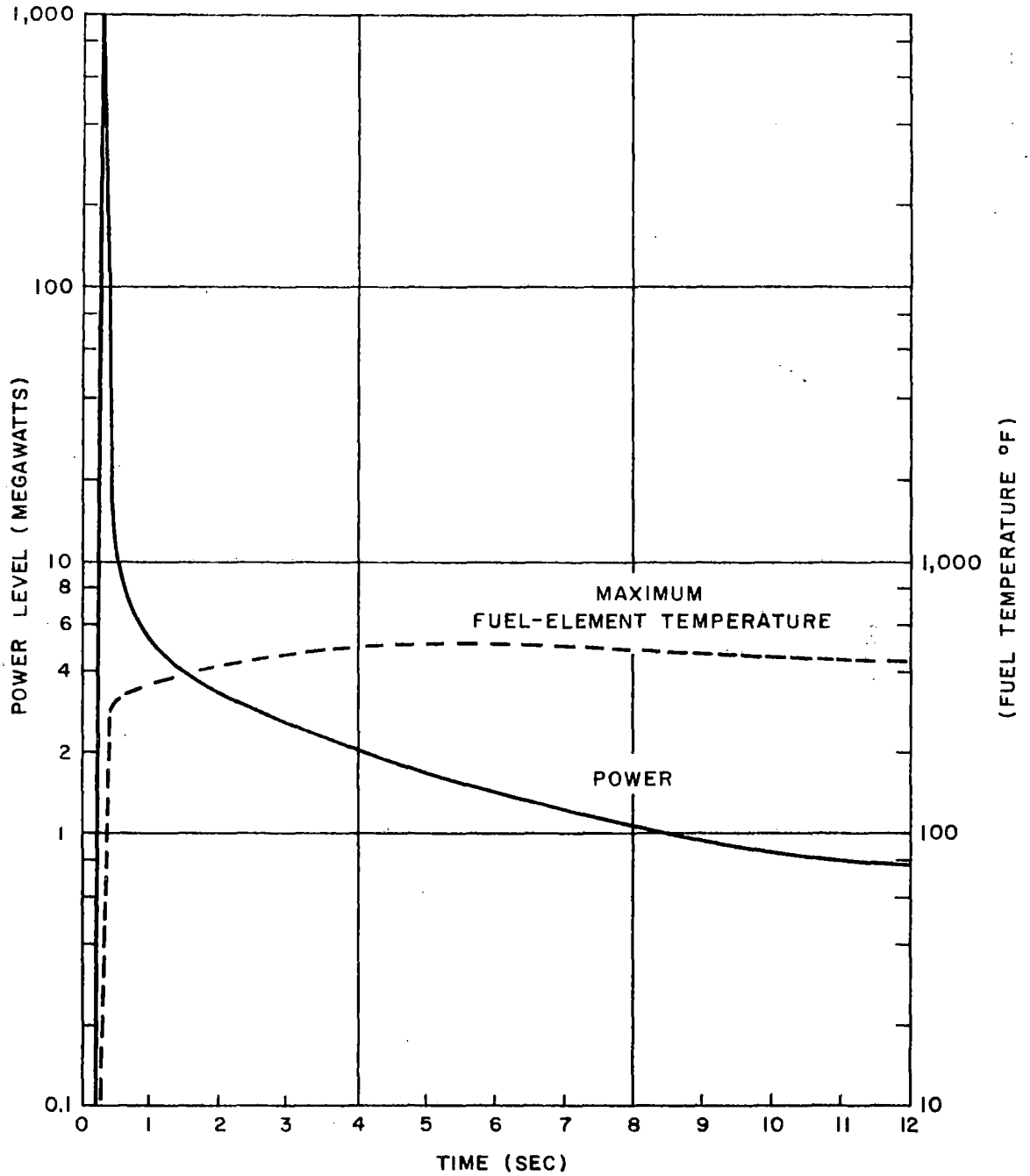

FIGURE 19. TRANSIENT POWER AND FUEL TEMPERATURE AS FUNCTIONS OF TIME AFTER 2.25% $\triangle k/k$ (3.00 DOLLAR) REACTIVITY INSERTION

85.39-64-1925

5. Poison Experiment Removal Accident

In this accident, it is postulated that an experiment located in the glory tube is instantaneously removed from the core. Since all experiments in the glory hole are limited to a total worth of 0.70% $\Delta k/k$, the accident would result in a much lower peak power than that from an insertion of 2.25% excess, as described in Section 3 above.

6. Loss of Coolant Accident

The reactor tank will be fabricated from aluminum. It will be reinforced with a minimum of 12 in. of concrete, which will strengthen the tank and protect it from damage. In addition, the ground in which the tank sits supports the concrete.

It is conceivable that some sharp object might fall into the tank and damage it. If this were to occur, a slow leak might result. The water level scram would then scram the reactor. Since the flow would be slow, it would be possible to add make-up water to maintain water level until the core was unloaded. It is difficult to conceive of any accident which might result in either a rapid or an instantaneous loss of the entire coolant.

Even though the possibility of the loss of shielding water is believed to be exceedingly remote, a calculation has been performed to evaluate the radiological hazard associated with this type of accident. For the condition when the reactor has been operating for a long period of time at 250 kw prior to losing all of the shielding water, the radiation dose rates at two different locations are listed below. The first location (direct radiation) is 18 ft above the unshielded reactor core, at the top of the core tank. The second is near the tank, but away from the opening. This location is shielded from the direct radiation by the concrete surrounding the tank and the earth shield, but is subject to the scattered radiation. The conservative assumption is made that there is a thick concrete ceiling 9 ft above the top of the reactor tank which will maximize the reflected radiation dose. Normal roof structures would give considerably less back-scattering. Time is measured from the conclusion of a 250-kw operation. Dose rates assume no water in the tank.

Time	Direct Radiation, r/hr	Scattered Radiation, r/hr
10 sec	2.7×10^4	15
1 day	1.4×10^3	0.8
1 week	9.3×10^2	0.5
1 month	4.5×10^2	0.2

The above data show that if an individual did not expose himself to the core directly, he could work for approximately 90 minutes at the top of the reactor tank after one day without being exposed to radiation in excess of approximately 1.25 rem. This would permit more than sufficient time to view the interior of the tank with a mirror and to make emergency repairs.

For persons outside the building, the radiation from the unshielded core would be collimated upward by the core tank and therefore would not give rise to a public hazard.

Calculations have been made to determine the temperature rise in a central TRIGA fuel element if the cooling water is lost instantaneously. The calculations (presented in Appendix D) were made in a very conservative manner in order to give an upper-limit estimate of the fuel-cladding temperature.

The calculations show that the maximum fuel-element temperature reached after an instantaneous and complete loss of water would be less than 650°C. If a more realistic calculation were made, taking into account all of the heat-removal mechanisms available, the maximum temperature reached would be very much lower than the above value.

On the basis of the considerations discussed above, it can be concluded that:

1) The probability of a total loss of water from the tank is extremely small.

2) The concrete and water around the reactor tank provide adequate protection for personnel near-by in the event of the loss of all of the water from the tank.

3) The maximum fuel temperature would be less than the melting point of the cladding (660°C) and consequently the loss of water would not damage the core.

C. RADIOACTIVE CONTAMINATION OF SHIELDING WATER

Contaminant material susceptible to neutron irradiation in the shield water is maintained at low levels by the demineralizing system. The hazards associated with a failure of the fuel-element cladding and consequent fission-product contamination of the water have been calculated and studied experimentally as described in Appendix C. The results show that in the improbable event of a cladding failure, the water activity may reach a maximum level of 1.2 $\mu c/cm^3$; however, the activity will decay to a level of approximately 10^{-4} $\mu c/cm^3$ 24 hours after the cladding failure. The water may be decontaminated by using the demineralizer or by dilution. Manufacturing inspection and quality control assure that the possibility of a cladding failure is extremely small.

Three mechanisms (recoil, diffusion, and dissolution) govern the release of fission products from a fuel element. The most important of these mechanisms is the fission-product recoil from near the surface of the fuel. This mechanism, therefore, is considered in the calculation of the fission-product release after a fuel-element failure shown in Appendix C. The dissolution rate of unclad fuel in water has also been studied experimentally by General Atomic and was found to be small.

D. MAXIMUM CREDIBLE ACCIDENT

The maximum credible accident which can occur with this reactor system is thought to be the occurrence of a defect in the cladding of a fuel element either prior to or simultaneously with an accidental sudden insertion of all the available excess reactivity (2.25% $\Delta k/k$).

It is concluded that a cladding failure, even the failure of the cladding of several fuel elements, would not constitute an undue hazard to the operating crew or the general public. Should an accident occur, it is possible that small amounts of radioactive noble gases would be dispersed from the reactor pool into the air of the reactor building, and these would decay into particulate matter.

According to the Heating, Ventilating, and Air-Conditioning Guide,* the number of air changes in a building without a ventilating system varies from 0.5 to 2 air changes per hour under average conditions. Based on this, it can be assumed that most of the fission-product gases would leak out of the building within 1 hr. The fission-product gases are mainly xenon and krypton, with an average total activity in the building of 9.2 curies, as calculated and discussed in Appendix C. The average concentration of xenon and krypton in the reactor-building air will be $4.5 \times 10^{-3} \mu c/cm^3$. If it is assumed that the fission-product gases leak out of one side of the building only, a person present for 1 hr near that side of the building could receive an integrated dose of 60 mr, due to the decay of the fission-product gases. If it is assumed that the fission-product gases escape from the building at a lower rate than previously postulated, the integrated dose received by a person would be approximately the same as before, due to the longer decay period for the fission-product gases before they leave the building. If the building ventilation system is operating during the release of fission-product gases, the integrated dose received by a person near the building would be less than 60 mr for a 1-hr period, due to air dilution. Assuming that a fuel-element failure occurred once each year, the concentration of the fission-product gases leaving the building, averaged over a 1-yr period, would be $5 \times 10^{-7} \mu c/cm^3$, and this concentration would be very much decreased by fresh-air dilution after traveling a short distance from the building.

An example of the activity caused by a cladding failure is provided by an incident that occurred during operation of the prototype TRIGA at San Diego.** During transient tests undertaken to verify TRIGA's operational safety, an early-model fuel element suffered a cladding failure following the step insertion of 2.85% $\Delta k/k$ (3.90 dollars). The results are summarized below:

1) The activity in the pool water reached a maximum of $0.2 \mu c/ml$. It decayed very rapidly and was measured as $5 \times 10^{-5} \mu c/ml$ 24 hr after the cladding failure.

* Heating, Ventilating, and Air-Conditioning Guide, American Society of Heating and Ventilating Engineers, New York, 1953, p. 223.

** Hazards Report for the 250 kw TRIGA Mark II Reactor, GA 2025, August 1961.

2) The activity in the air of the reactor room reached about ten times the MPC for fission products and decayed very rapidly. The maximum exposure to operating personnel was less than 1 mr.

3) The noble gases were not collected on the filter samples used, but it may be inferred from the nature of the particulates observed that only the noble-gas fission products escape from the TRIGA pool in significant proportions when a fuel cladding fails.

The preceding discussion shows that no significant hazard to the public would result from such an accident.

APPENDIX A

METEOROLOGY

Climatological data for the San Ramon area have been drawn mainly from three sources: the 80-year record of the U. S. Weather Bureau climatological station at Livermore; the 10-year (1934-1943) record of hourly weather observations made for the Weather Bureau by the Civil Aeronautics Administration (CAA) station at the Livermore Sky Ranch Airport, west of Livermore; the 18-month record (February 1945-August 1946) from the Livermore Naval Air Station, which is now the site of the University of California Radiation Laboratory; and the results of a two-month study (June and July, 1961) at AGN, San Ramon. In addition, primarily to get upper air data, records for nearby Oakland and San Francisco have been consulted.

Average data on the surface wind direction and speed, temperature, humidity, rainfall, winds aloft, atmospheric stability conditions, and other pertinent meteorological information are presented below.

A. WINDS

1. Livermore Wind Data

a. Surface Winds

Figures A-1 through A-4 are surface wind roses giving various annual and seasonal joint frequency distributions of wind direction and speed at Livermore. The percentage frequency of occurrence of a wind from any direction is represented by the total length of a compound bar extending from the center of the rose toward the direction from which the wind

is blowing. Percentage frequencies of certain ranges of wind speed are indicated by breaks in the bar, according to the code on each figure. The percentage frequency of calms is entered in the center of each rose.

Figure A-1 shows annual wind roses for both the Livermore CAA and the Navy stations. Each of these roses shows a primary direction maximum in the southwest quadrant and a secondary maximum in the northeast, although the most frequent directions at the CAA station are W and NE, whereas the Navy station directions are SW and N. The Navy station also has a higher frequency of calms. These roses show quite clearly the channeling effect of San Ramon and Livermore Valleys on surface wind. It will also be observed that winds greater than 31 miles per hour are rare. Percentages of less than one-half of one percent do not appear on the roses. In this connection, Table A-1 below gives the fastest miles of wind ever recorded for each direction, at nearby Oakland, California. For strong winds such as these, the Oakland record should represent conditions at San Ramon amply well. The fastest wind mile, recorded in February 1938, was 67 mph, a southwest wind.

TABLE A-1

FASTEST MILE OF WIND RECORDED AT OAKLAND, CALIFORNIA

Month	Speed	Dir.	Year
J	50	N	1948
F	67	SW	1938
M	45	SSE	1948*
A	41	SSE	1948
M	38	W	1949
J	44	W	1939
J	33	W	1939
A	34	W	1939
S	39	W	1939
O	43	W	1938*
N	45	W	1947
D	63	NE	1943

* Also recorded on later dates

It is not possible to make any definite statement about the reality of the differences between the wind roses for the CAA and the Navy stations. However, it is reasonable to speculate that a longer

record at the Navy station would more closely resemble the CAA station's record, since there is no evident reason to suspect any systematic difference. Accordingly, the remainder of the wind roses are based on the longer, more significant record of the CAA station.

Figure A-2 gives annual seasonal wind roses for the day-time hours, 0800 to 1830 LST (local standard time). The comparatively low expectancy of calms during the day-time is clearly shown. The annual rose locates the overall wind speed maximum for Livermore; it is associated with a southwest wind direction, the most probable day-time direction. Notice also the pronounced west wind maximum during the summer half-year (April through September) and the northeast wind maximum during the remainder of the year. The overall double maximum of the annual roses is seen to be associated with two oppositely directed seasonal regimes. During the summer especially, the San Joaquin Valley, and to almost the same degree the San Ramon and Livermore Valleys, are heated through the day. A large temperature contrast develops between the air in the valleys and the relatively cool maritime air of the San Francisco Bay region. The colder air then rushes into the San Joaquin Valley. The route followed by much of this air is across the San Pablo Bay and Suisun Bay areas, but some of it comes through the narrow, straight connecting valleys past the towns of Walnut Creek, Danville, and San Ramon to the Livermore Valley. This air, probably with additional air which spills over the lower parts of the ridges between the Livermore Valley and the Bay Area, crosses the Livermore Valley from west to east and flows over Altamont Pass. This phenomenon occurs almost daily, with considerable regularity, during the late spring and summer. During fall and winter, in contrast, the temperature gradient is in the opposite direction; and the flow from east to west through the Altamont Pass produces a northeast wind frequency maximum, although this is less pronounced than is the summertime effect.

The situation during the night is shown in Figure A-3. The main difference between these wind roses and the day-time ones is the higher frequency of calms and the lower frequency of winds above 18 mph. The locations of the direction maxima are much the same.

Figure A-4 has been prepared in order to give some information on the wind structure during periods of precipitation, to help assess the washout problem. On all these roses a definite shift of the direction frequency maximum into the southwest will be noticed. Otherwise, they are similar in structure to the other roses.

b. Winds Aloft

Pilot balloon runs are made four times daily at Oakland, California; and observations for about three years have been examined to obtain the frequency of winds aloft at the 500 and 750 meter levels. Table A-2 shows the seasonal variation of wind direction frequency at 750 m. The most striking difference between the winds at this level and those at the surface is the fact that maximum direction frequency is in the west-northwest and northwest rather than in the west.

TABLE A-2

PERCENTAGE FREQUENCY WIND DIRECTION,
750 METERS MSL, AT OAKLAND, CALIFORNIA

	Winter	Spring	Summer	Fall
N	9.9	7.8	3.2	7.7
NNE	13.2	7.0	2.5	10.6
NE	9.2	3.9	1.7	8.3
ENE	4.5	1.7	0.7	4.6
E	4.4	1.4	0.5	3.9
ESE	4.2	1.2	0.2	2.5
SE	4.5	1.1	0.5	2.6
SSE	5.0	2.0	0.6	2.4
S	5.4	3.4	2.4	3.9
SSW	5.0	4.1	5.6	4.6
SW	3.7	5.8	7.8	5.0
WSW	4.0	7.2	10.9	5.2
WNW	5.7	14.9	21.3	8.7
NW	6.7	14.5	14.2	9.5
NNW	6.4	8.6	5.3	7.0
Calm	3.7	4.5	5.2	6.8

Table A-3, the percentage frequency of various wind speed classes at 500 and 750 m, shows that there is not any great change in conditions with height.

TABLE A-3

PERCENTAGE FREQUENCY OF 500 AND 750 METER MSL WINDS BY SPEED CLASS AND SEASON

	Wind Speed, Miles Per Hour				
	0-1	2-7	8-14	15-21	>21
	500 Meters MSL				
Winter	5.2	71.4	21.8	1.4	0.2
Spring	15.3	65.9	18.6	0.2	- -
Summer	5.6	84.9	9.3	0.2	- -
Fall	8.1	78.3	12.6	1.0	< 0.1
	750 Meters MSL				
Winter	3.7	62.8	29.6	3.7	0.2
Spring	4.5	69.4	24.6	1.3	0.2
Summer	5.2	79.9	14.8	0.3	- -
Fall	6.8	73.5	18.2	1.4	0.1

2. San Ramon Wind Data (Limited Study)

Figures A-5 through A-9 are wind roses showing the joint frequency distribution of wind direction and speed for Aerojet-General Nucleonics' San Ramon site. The wind roses show percentage frequency distribution of the wind from the surface layer of the atmosphere to an altitude of 2000 ft. The percentage frequency of occurrence of a wind from any direction is represented by the total length of the compound bar extending from the center of the wind rose toward the direction from which the wind is blowing. Percentage frequencies of a certain group of wind speeds are indicated by discontinuity in the bar according to the code in the lower left-hand corner of the figure. The percentage frequency of calms has been entered in the center of each wind rose.

The wind roses in Figures A-5, A-6, and A-7 depict the wind flow for a mean layer wind 500 ft in depth. The winds used in the compilation of Figures A-5, A-6, and A-7 were the average winds observed during the first 30 seconds after the release of a 100-gram pilot balloon. The average time of release for the morning runs was 0630 and 1833 for the afternoon runs. Both the morning and later afternoon observations were combined to show the percentage frequencies represented by Figure A-5. Figure A-5 clearly shows

the dominating influence of the higher velocity winds attributed to the afternoon sea breeze regime. The predominantly southwest flow may be attributed to the orientation of the site in relation to the mouth of Crow Canyon. The blocking effect of the Las Trampas Ridge reduces the west wind component normally associated with the sea breeze circulation that is found farther away from restricting ridges. The path of least resistance for the eastward moving air is channeled through Crow Canyon. The air then tends to diverge as it leaves the canyon mouth. The apparent movement of air across the site is then from the southwest as the wind backs away from its original trajectory. The sea breeze which is a common summer afternoon phenomenon is believed to nearly always act in this fashion at the San Ramon site.

The reciprocal effect to the sea breeze is the countercurrent called land breeze, the land breeze being predominantly a night-time wind. While Figures A-6 and A-7 clearly show the day-time development of the sea breeze, a land breeze development is not evident. This may be from a lack of data, but the local topography is felt to play the determining role. The location of the San Ramon site in the land breeze regime is on the windward side of the Las Trampas Ridge. Any land breeze effect that might develop would be terminated by the blocking action of the Las Trampas Ridge.

The channeling effect which produces higher velocity winds near the surface is not evident at 1000 ft, as shown in Figure A-8. While the predominance of the sea breeze effect may be seen in Figure A-8, characterized by the high frequency of wind from the west through southwest, the higher wind speeds observed in Figure 1 are not evident. This is believed to be caused by a more even horizontal flow of air over the Las Trampas Ridge followed by vertical divergence over the site.

The wind rose for 2000 ft is shown in Figure A-9. Although there is not an obvious prevailing direction, the differences between Figures A-5, A-8, and A-9 show a basic veering of the wind as a function of height. Since the 2000 ft level is nearing the top of the planetary boundary layer, the frictional effects of the surface are less, and the wind flow tends to correspond to the average isobars.

The orientation of the isobars during the summer months is influenced by two major factors. First, a weak thermal low-pressure area is

usually observed over southern Nevada with a thermal trough extending toward the northwest over the Sierra Nevada. This results in a northwest-southeast orientation of the surface isobars. The second factor is the sub-tropical, semi-permanent high located in the Eastern Pacific which allows a northwest to southeast movement of air at the geostrophic level.

B. PRECIPITATION

The average annual precipitation at San Ramon is about 15 in., varying between about 7 and 25 in. for very dry and very wet years, respectively. Expected monthly and seasonal precipitation amounts are presented in Table A-4, and precipitation extremes in Table A-5. Most of the precipitation (virtually all of which is rainfall) occurs during the winter months in connection with Pacific storms, which occasionally bring enough rain to cause water to stand in some fields. Negligible amounts of solid precipitation (snow, sleet, or hail) occur, since the surface temperature is below freezing only about one percent of the time.

TABLE A-4

EXPECTED MONTHLY AVERAGE PRECIPITATION, INCHES

J	F	M	A	M	J
2.97 (3.49)*	2.47 (3.34)	2.24 (2.52)	1.03 (1.27)	0.51 (0.57)	0.12 (0.17)

J	A	S	O	N	D
0.01 (0.01)	0.02 (0.03)	0.27 (0.08)	0.68 (0.87)	1.51 (1.50)	2.72** (3.34)

Winter	Spring	Summer	Fall	Annual
8.16	3.78	0.15	2.46	14.55

Average Snowfall

J	F	M	A	M	J	J	A	S	O	N	D
0.1	T(1)	T	0	0	0	0	0	0	0	0	0.1(2)

* Figures in parentheses are rainfall amounts for Oakland, California
** Based on 80-year record
(1) T = trace
(2) Based on 52-year record

TABLE A-5

PRECIPITATION EXTREMES, INCHES

Month	Maximum Monthly	Minimum Monthly	Maximum in 24 Hours
J	12.60	0.22	0.20
F	6.23	0.08	-
M	8.85	0.15	-
A	6.51	0	0.25
M	2.66	0	-
J	1.73	0	-
J	0.27	0	-
A	0.73	0	-
S	5.72	0	3.97
O	2.52	0	0.93
N	7.23	0	3.05
D	11.69*	0.17*	2.60**

* Based on 60-year record
** Based on 53-year record

No data on the occurrence of thunderstorms at San Ramon are available, but at Oakland, which Table A-4 shows to have a similar rainfall regime, thunderstorms are rare, occurring on the average only one day a year, in January. The frequency of days with 0.01 in. or more precipitation, and of days on which heavy fog occurred, is shown in Table A-6. The rather uniform monthly distribution of fog days stands in contrast to the seasonal variation of precipitation; and it may be inferred that the wintertime fogs are associated with the general seasonal storminess, but that the summertime precipitation consequently can be attributed partly to traces accompanying the stratus, and partly to occasional summertime showers, these being of no special severity.

TABLE A-6

AVERAGE FREQUENCY OF CERTAIN METEOROLOGICAL PHENOMENA

	Average Number of Days												
	J	F	M	A	M	J	J	A	S	O	N	D	Annual
Precipitation ≥ 0.01 in.	11	10	9	5	3	1	t	t	1	3	6	10	59
Heavy fog*	4	2	1	2	2	2	2	3	2	2	2	3	27

t = less than 1/2 day
* visibility < 1/4 mile

C. TEMPERATURE

1. Surface Dry Bulb Temperature

The expected annual average temperature is 59°F. The expected average monthly temperatures, together with average maximum, minimum, and extremes, are presented in Table A-7. The most frequent temperature will lie in the range from 40-70°F, and in fact this range should include about 75% of all observed temperatures.

TABLE A-7

EXPECTED TEMPERATURES, °F

	J	F	M	A	M	J	J	A	S	O	N	D
Average*	48	51	54	57	61	66	71	72	68	63	55	49
Av. Maximum**	57	61	65	71	76	82	88	87	85	77	67	58
Av. Minimum**	37	39	41	44	47	51	54	53	52	47	41	37
Highest***	77	80	88	95	108	111	113	112	115	100	93	78
Lowest***	19	23	27	30	32	38	41	40	35	29	25	20

* Based on 79-year record
** Based on 44-year record
*** Based on 54-year record

Table A-8 contains the percentage frequency of occurrence of temperatures in various ranges. It is based on the ten-year record of the CAA station, and annual frequencies for the Navy station are included for comparison. Evidently, the temperatures at the two stations are directly comparable.

TABLE A-8

EXPECTED AVERAGE PERCENTAGE FREQUENCY
OF INDICATED TEMPERATURE RANGE

Temperature Range, °F	Annual	J-F-M	A-M-J	J-A-S	O-N-D
90	2 (2)		2	6	0.5
80-89	5 (5)		5	12	2
70-79	9 (9)	1	13	19	5
60-69	18 (19)	8	24	25	16
50-59	36 (38)	37	40	35	35
40-49	22 (22)	38	15	3	29
30-39	7 (4)	15	1		12
30	1 (0.5)	1			1

Based on ten-year record; figures in parenthese show comparison with Livermore Navy Station.

The temperature climate is essentially moderate. Table A-9 gives the percentage of the time that the temperature will be above or below a specified temperature. It shows, for example, that during January, February, and March temperatures below 32°F should be expected about 2% of the time. Temperatures above 90° and 100°F are similarly rare. Sometimes it is necessary to burn orchard heaters in the winter, and summer afternoons are likely to be uncomfortably hot. It was, for example, never cooler than 32°F between 1200 and 1800 LST during the winter months; and seldom warmer than 70°F between 2200 and 0900 LST during the summer, over the ten-year period of the CAA station's record.

2. Wet-Bulb Temperatures

The wet-bulb temperature is the lowest temperature to which the ambient air can be cooled by evaporation, and as such is important from the standpoint of the design of evaporative cooling towers. Table A-10 gives the percentage frequency of the time that the wet-bulb temperature can be expected to exceed a specified value, annually and by seasons. For example, during the period April, May, and June, the wet-bulb temperature will be at or below 60°F 85% of the time, and it will rise to 70°F only about 1% of the time.

TABLE A-9

EXPECTED PERCENTAGE FREQUENCY OF HOURS THAT TEMPERATURES WILL BE ABOVE OR BELOW A SPECIFIED TEMPERATURE

Temperature, °F	Annual	J-F-M	A-M-J	J-A-S	O-N-D
100	** (**)	0	**	*	0
90	2 (2)	0	1	5	1
80	6 (7)	0	6	16	2
70	14 (15)	1	17	35	6
60	31 (32)	7	40	58	20
50	67 (69)	40	79	96	54
40	8 (4)	16	1	0	13
32	1 (**)	2	**	0	2
20	** (0)	**	0	0	0

0.1% * $\leq$ 0.5%
** $\leq$ 0.1%

Based on ten-year record; figures in parenthese show comparison with Livermore Navy Station.

TABLE A-10

EXPECTED PERCENTAGE FREQUENCY OF TIME THAT WET-BULB TEMPERATURES WILL EXCEED A SPECIFIED VALUE

Temperature, °F	Annual	J-F-M	A-M-J	J-A-S	O-N-D
80					
70	**		1	1	
65	2 (*)	*	10	9	1
60	13 (*)	**	15	34	5
50	56 (13)	22	66	92	42
40	89 (72)	74	98	99	81
30	99 (99)	97	100	100	98
20	100 (100)	100			100
Max.	79 (63)	65	77	79	69

* $\leq$ 0.1%
** $\leq$ 0.5%

Based on ten years of record; figures in parenthesis are for Navy Station at Livermore.

The ten-year record of the CAA station has been used in compiling Table A-10, and again the short record of the Navy Station is included for comparison. Here there seems to be a significant difference in the two locations, the wet-bulb temperatures at the Navy Station being appreciably lower. Once again, there is nothing to indicate a real difference persisting for a longer period of time, and in any event the practical importance is not great.

3. Marine Stratum and Inversion

Twenty-two temperature soundings were taken at the Aerojet-General Nucleonics San Ramon site during June and July, 1961, with a transistorized temperature-sensitive radiosonde. The purpose of obtaining the temperature soundings was to investigate the marine stratum and associated inversion.

The basic summer circulation over the western coastal sections of California above the planetary boundary layer is from the northwest. This northwest flow, as mentioned earlier, is due to the relative positions of the sub-tropical, semi-permanent high cell located in the Eastern Pacific and the thermal low centered in the southern Nevada area. Due to frictional out-flow from the high cell and the acquired anticyclonic curvature around the high cell, the air flow subsides. This subsidence causes the air to be warmed dynamically. The movement of the air over warmer water also modifies the air from below. The result is a cool, moist layer of air near the Earth's surface called the marine stratum, which is topped by a layer of warm air called the subsidence inversion.

Neiburger in 1944 found the inversion base over the Los Angeles basin showed one general characteristic, whether the station was located inland or near the coast. The general characteristic was that the base of the temperature inversion rose in height during the day followed by a height fall late in the day. The inversion rise during the early daylight hours is probably the result of vertical mixing associated with the first insolation reaching the Earth's surface. It was noted in Neiburger's work, however, that stations very close to the coast reported a more direct decline in the inversion layer as the sea breeze regime began. It may be observed in Figure A-10 that the mean inversion base for the San Ramon area lowered

only 71 ft during the daylight hours. It should be noted from Table A-11 that Oakland's mean inversion base for the same average period lowered 715 ft during the day. While there are no observations available for stations farther inland, it is believed that the inversion base would rise, then lower to a height several hundred feet above the height of the base that would have been representative in the early morning.

The base of the inversion near the San Ramon site does not show clearly either of these characteristics. It is, therefore, believed to be in a transition zone between definite coastal and definite inland inversion oscillation characteristics.

TABLE A-11

MEAN INVERSION DATA

	Mean Inversion Top, ft		Mean Inversion Base, ft		Mean Inversion, °C	
	a.m.	p.m.	a.m.	p.m.	a.m.	p.m.
Oakland	3080	2640	1215	570	11.6	5.2
San Ramon	2970	2190	1088	1017	10.3	3.4

The lowering of mean inversion top from the a.m. profile to the p.m. profile is observed from Figure A-10. This lowering is probably caused by horizontal divergence within the inversion layer that is taking place farther inland during the day. The warming of the marine stratum due to insolation was relatively greater than any advection processes that occurred above the inversion layer. This results in a reduction of the relative strength of the inversion from a ΔT of 10.3°C in the morning to 3.4°C in the afternoon. Insolation and surface heating increased the surface superadiabatic lapse rate from 3.43°C per 1000 ft for the morning mean to 8.65°C per 1000 ft in the afternoon.

Of the 11 days that temperature soundings were taken, 6 days showed a definite inversion layer in the afternoon. Figure A-11 shows a day when the inversion was observed in the afternoon. The day-time change closely followed the mean shown in Figure A-10. The dashed line on the right was the actual temperature sounding taken at 1830 the same day. The three solid lines show the anticipated profile change at the hours of 0800, 1000, and 1400.

On the remaining 5 days, an inversion was not discernible in the afternoon. Figure A-12 shows one of these days. When the synoptic situation on any given day allows the flow in the lowest levels to be of continental origin, it is usually warmer than the sea surface, and the subsidence inversion is effectively lowered. Figure A-12 shows a day, June 30, 1961, on which the subsidence inversion is on the ground, and an inversion base aloft is absent all day. The dashed profile on the left is an actual sounding taken at 0610, and the dashed profile on the right is an actual sounding taken at 1735. The four solid lines represent the anticipated temperature profile change from the actual morning profile taken at 0610 through the hours of 0800, 1000, 1200 and 1400 to the actual afternoon profile taken at 1735. It should be noted that the only time that the surface lapse rate becomes subadiabatic (i.e., less than 2.99°C per 1000 ft) is when the subsidence inversion base is on the ground with the sea breeze associated with the marine stratum being completely absent. Surface lapse rates in the marine stratum are rarely less than the dry adiabatic lapse rate. More frequently, the surface lapse rate will be 3.5°C per 1000 ft, or more, for a mean depth of about 500 ft. The surface lapse rates in the marine stratum are expected to approach the adiabatic lapse rate at San Ramon around midnight or in the early morning hours before sunrise. The subsidence inversion on the ground at sunrise is an indication of an afternoon maximum temperature above normal because it denotes the absence of the marine stratum and its associated sea breeze.

4. Atmospheric Stability

Although few radiosonde records are available for the San Ramon area there seems to be no obstacle to making fairly accurate, generalized estimates of the low level atmospheric stability there, based on accepted meteorological principles.

For the purpose of estimating the frequency of inversion below 1500 ft, ceiling frequencies should provide an indication, not of the actual frequency of inversions, since this is certain to be greater than the frequency of low cloud occurrence, but of the location of the maximum inversion frequency. Low level inversions are most frequent during the night and during the summer half year. Low cloud layers, in fact, occur a little

more than 10% of the time during the summer night-time hours; during the day they occur only 4% of the time. During the remainder of the year, on the other hand, ceilings below 1500 ft are about equally probable; day and night ceilings below 1500 ft occur slightly less than 10% of the time. The summer maximum of low cloudiness is associated with the well-known nocturnal stratus regime of the area.

The diurnal march of stability conditions in the low layers is expected to be normal at San Ramon. In general, unstable conditions will predominate during the day, and isothermal and inversion conditions at night. Because of the somewhat high frequency of low stratus during the summer nights, more frequent isothermal, or even unstable, conditions beneath the cloud base can be anticipated than would be found if the nights were all clear.

ANNUAL WIND ROSES FOR LIVERMORE CAA AND NAVY STATIONS

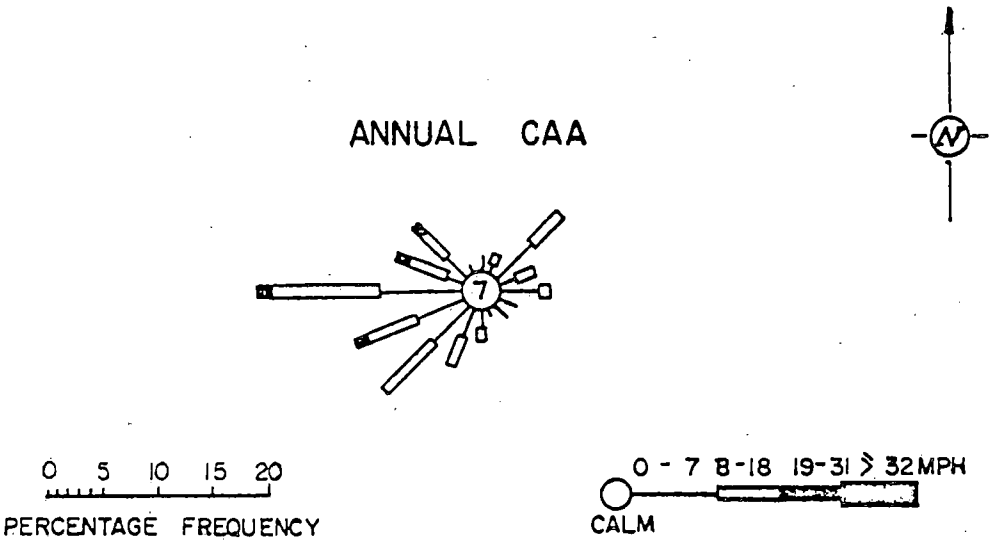

FIGURE A-1

ANNUAL AND SEASONAL WIND ROSES FOR DAYLIGHT 0800—1830 LST, AT LIVERMORE

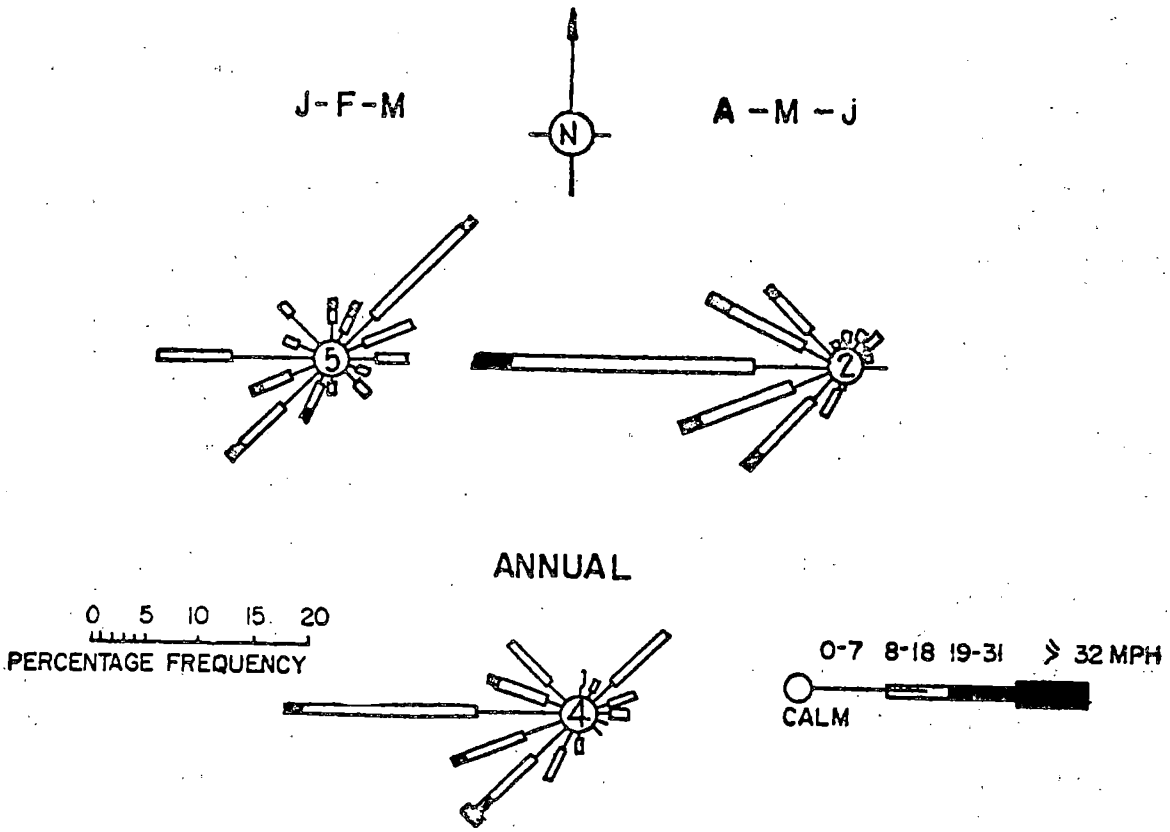

FIGURE A-2

ANNUAL AND SEASONAL WIND ROSES FOR NIGHT HOURS 1900-0730 LST, AT LIVERMORE

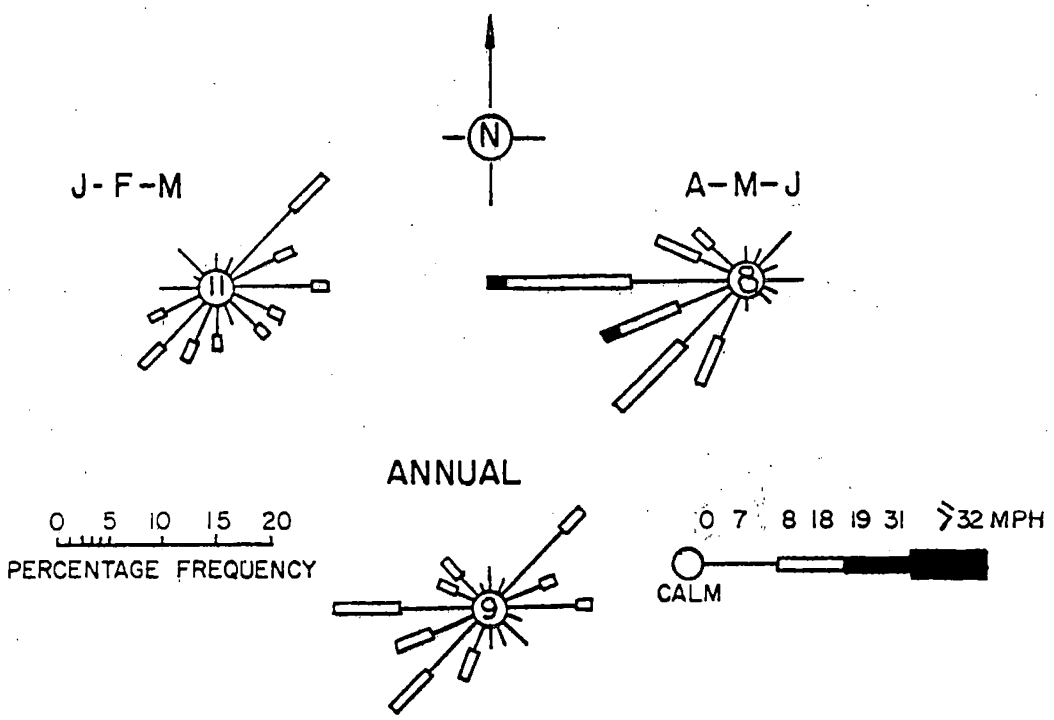

FIGURE A-3

ANNUAL AND SEASONAL WIND ROSES DURING PERIODS OF PRECIPITATION, AT LIVERMORE

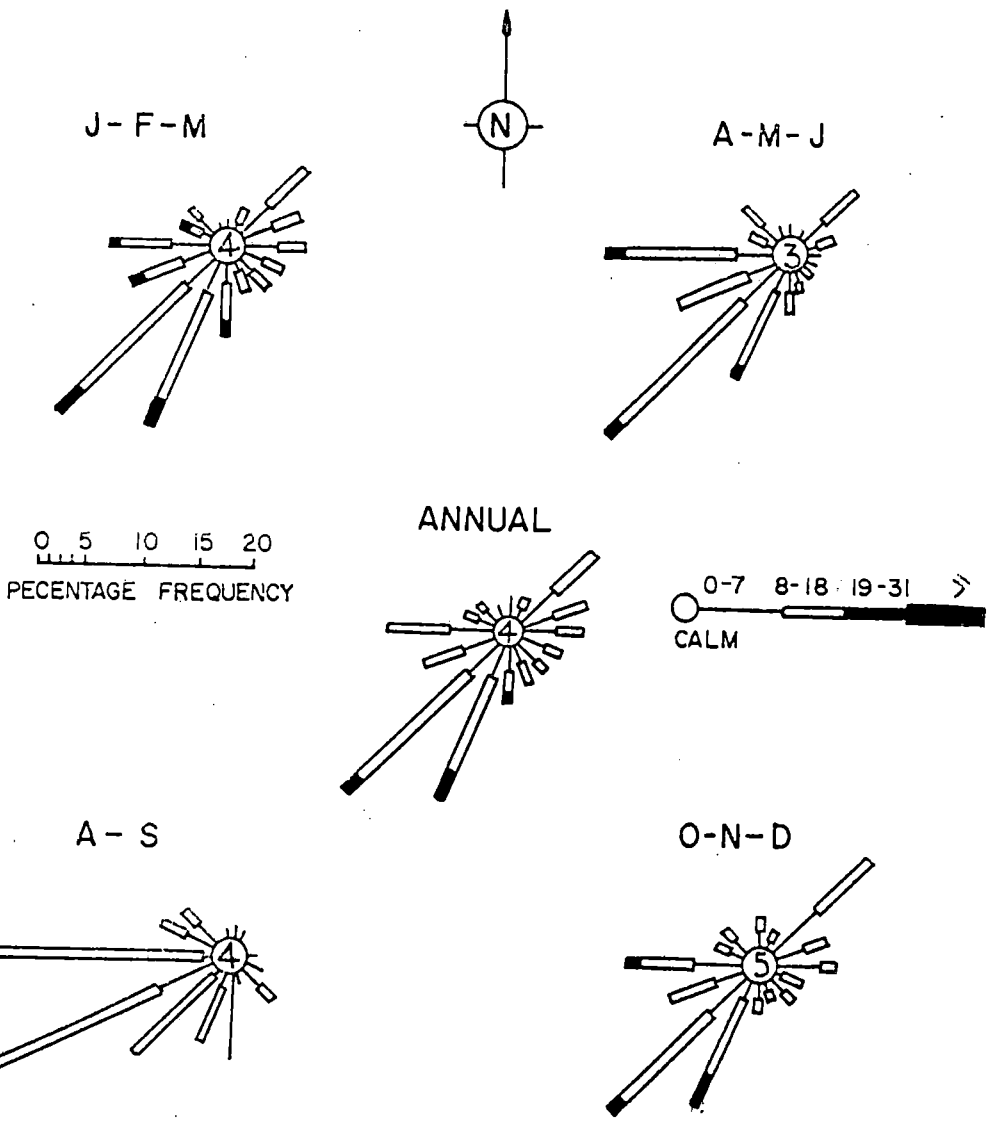

FIGURE A-4

MEAN LAYER
WIND

SFC TO 500'
Combined a.m. & p.m.
18 OBS
June - July 1961

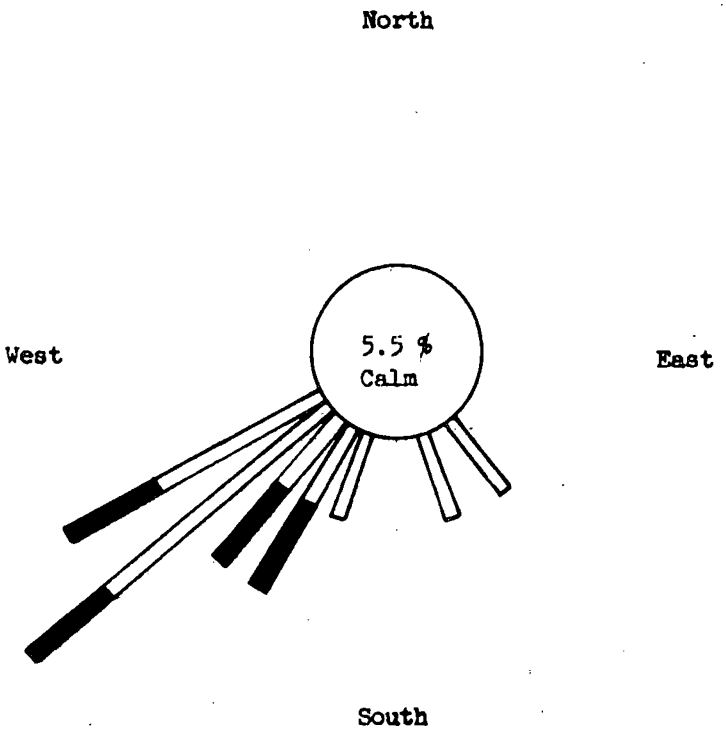

Figure A-5

MEAN LAYER
WIND

SFC TO 500'

9 a.m. OBS
June - July 1961

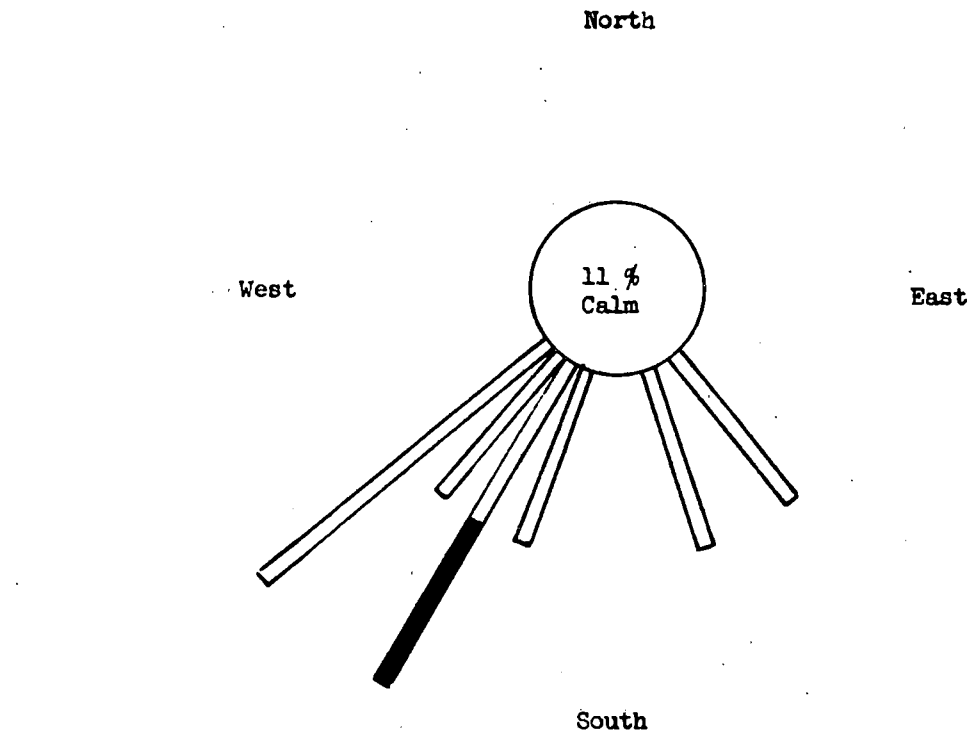

Figure A-6

MEAN LAYER
WIND

SFC TO 500'

9 p.m. OBS
June - July 1961

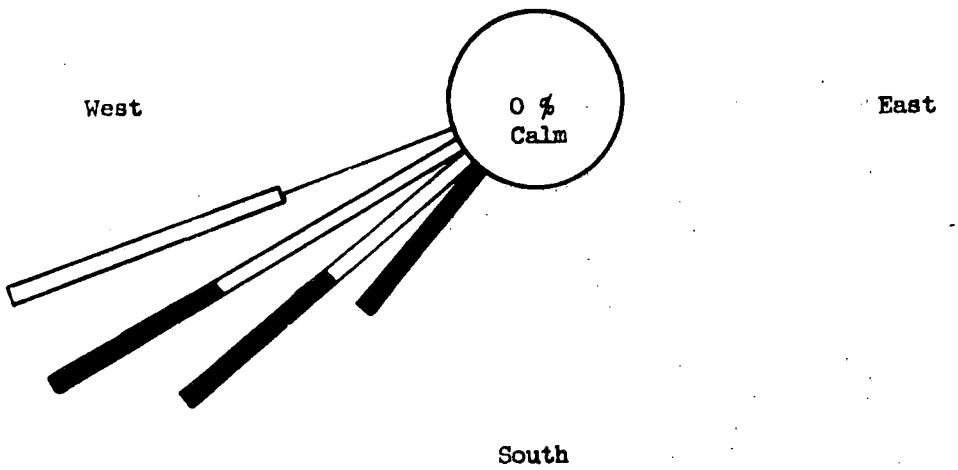

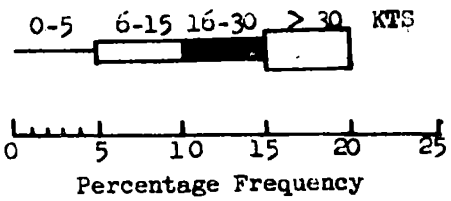

Figure A-7

1000' WIND
Combined a.m. & p.m.
18 OBS
June - July 1961

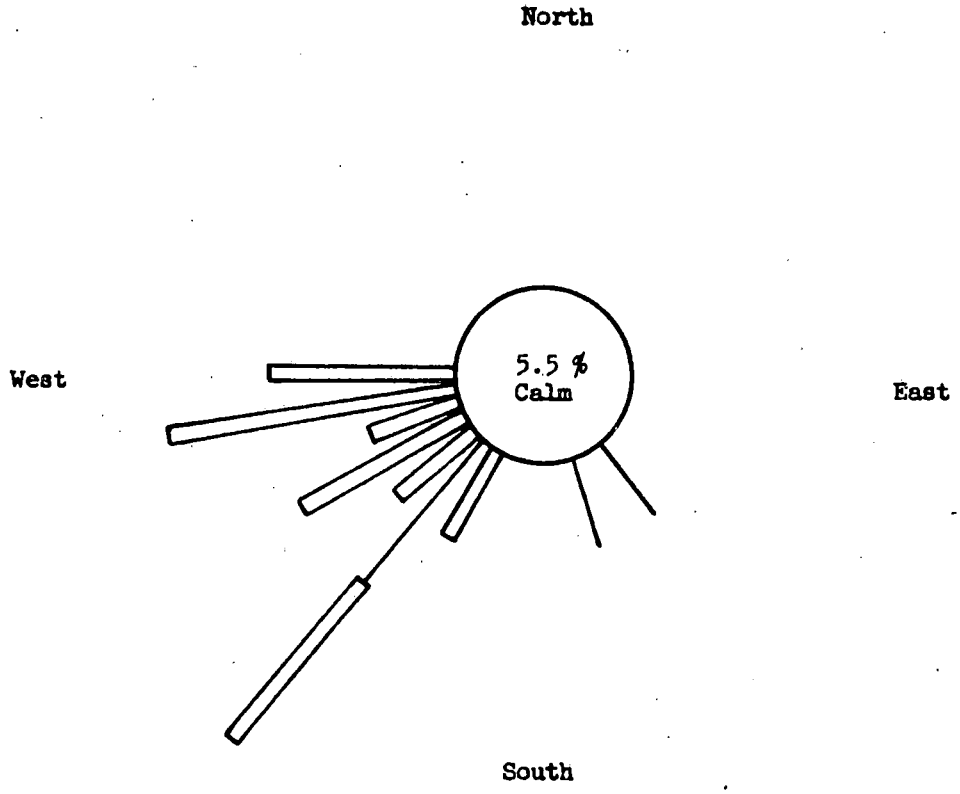

Figure A-8

2000' WIND
Combined a.m. & p.m.
18 OBS
June - July 1961

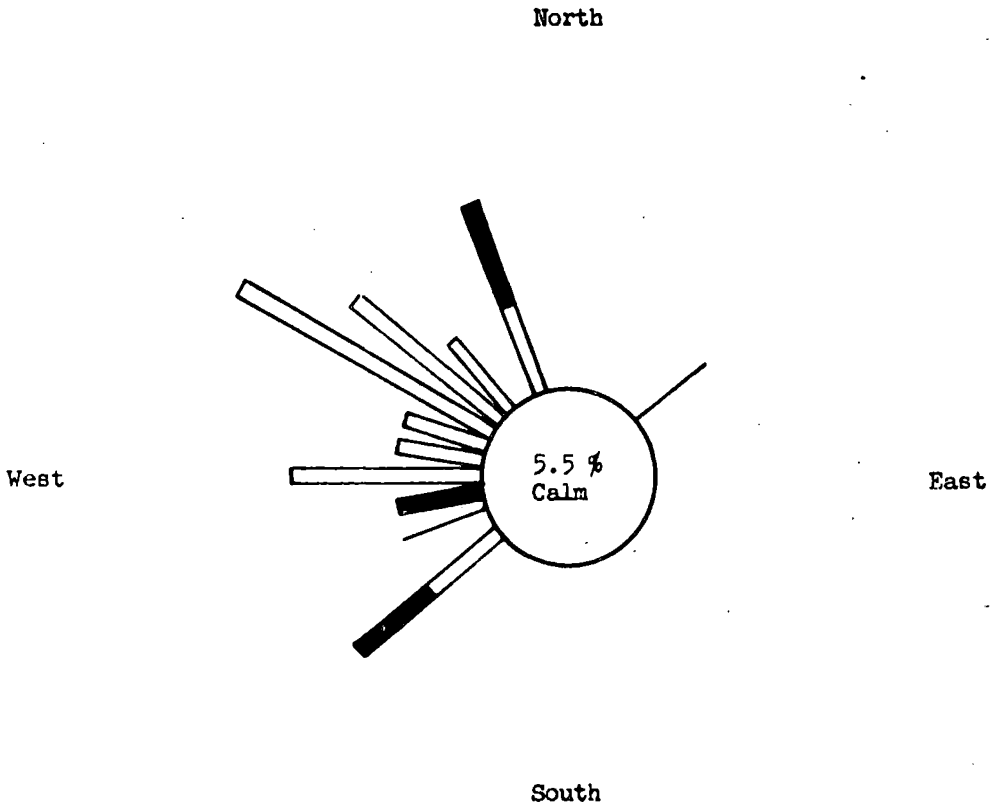

Figure A-9

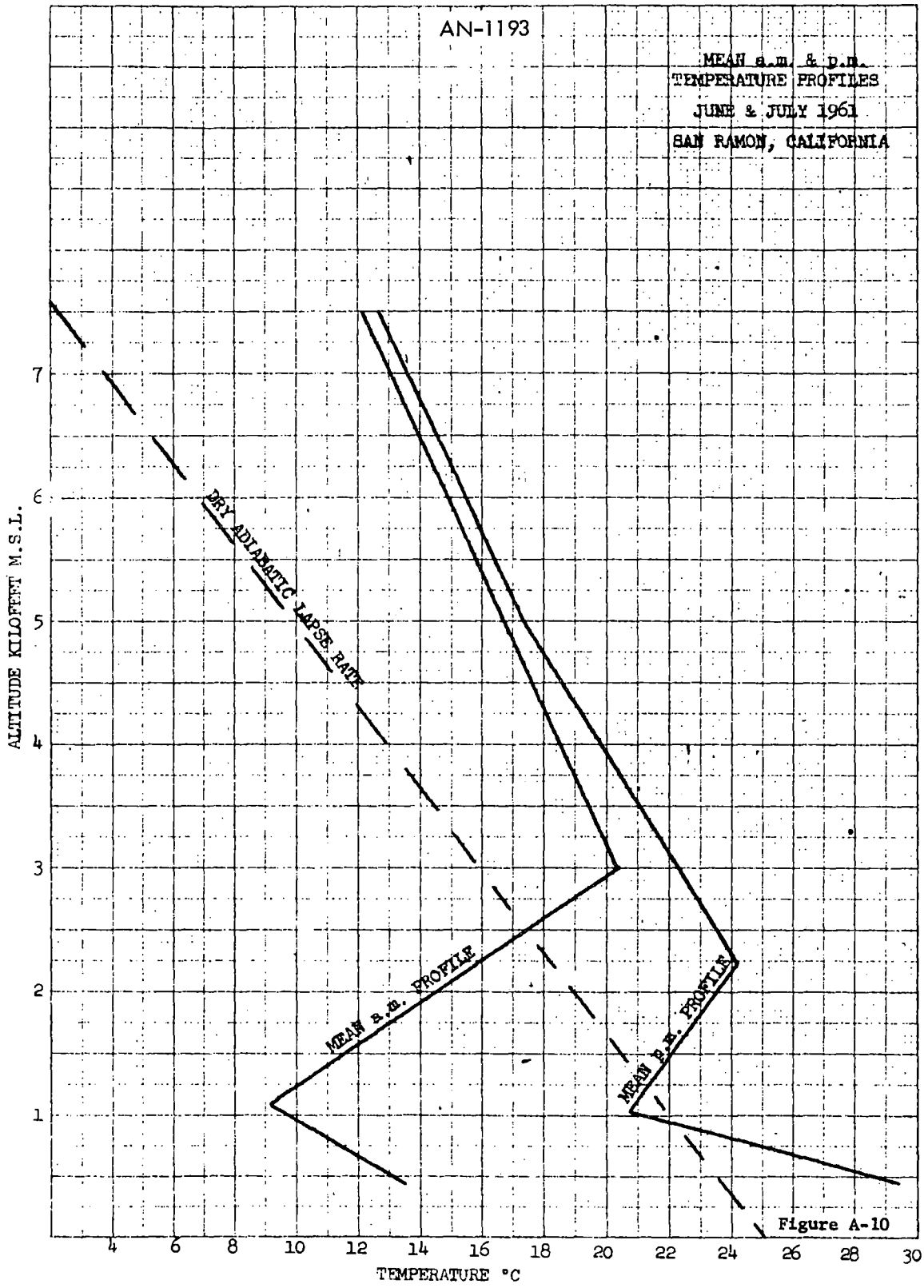
AN-1193
MEAN a.m. & p.m.
TEMPERATURE PROFILES
JUNE & JULY 1961
SAN RAMON, CALIFORNIA
DRY ADIABATIC LAPSE RATE
MEAN a.m. PROFILE
MEAN p.m. PROFILE
ALTITUDE KILOFEET M.S.L.
1
2
3
4
5
6
7
4
6
8
10
12
14
16
18
20
22
24
26
28
30
TEMPERATURE °C

Figure A-10

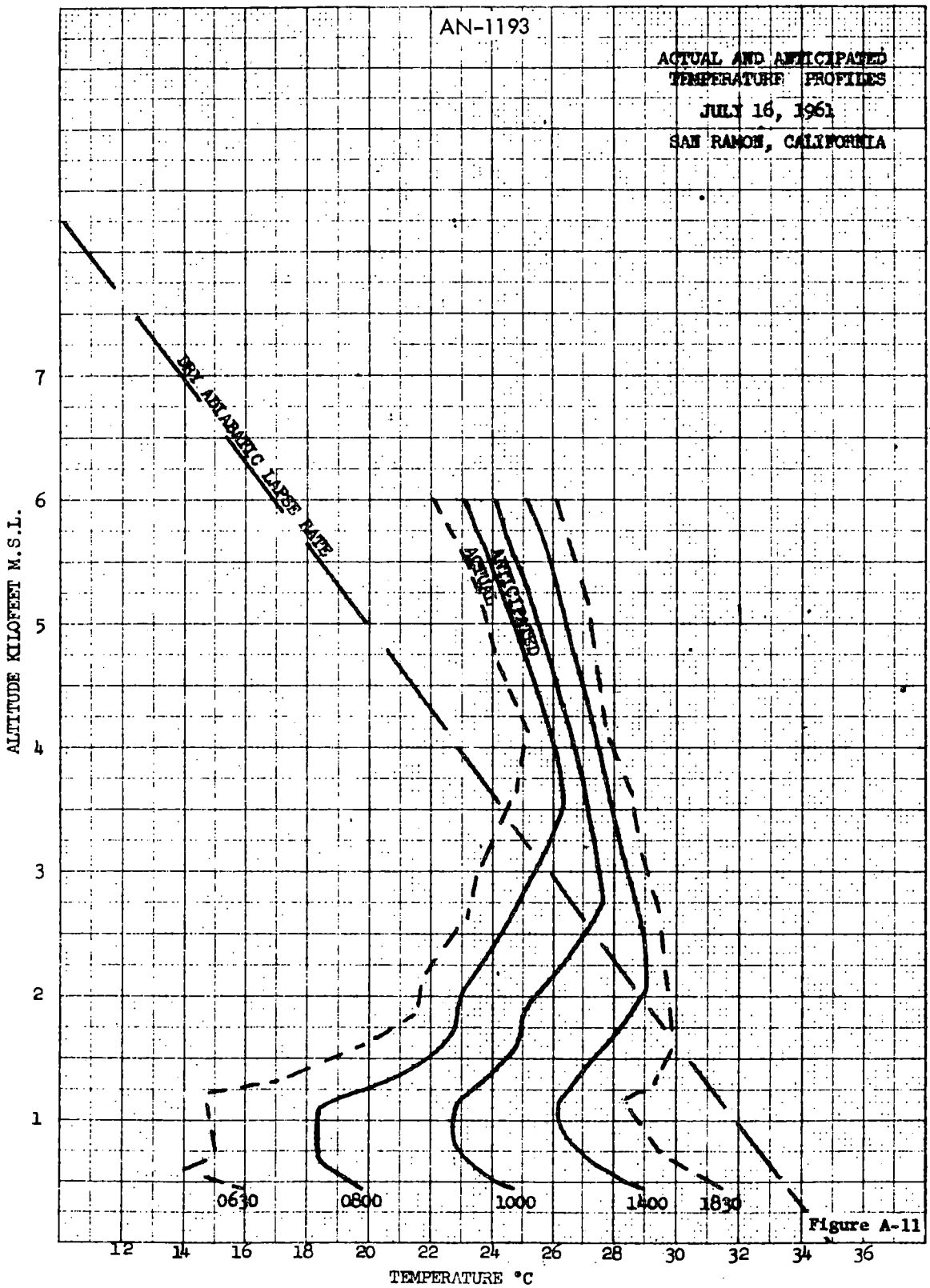
AN-1193
ACTUAL AND ANTICIPATED TEMPERATURE PROFILES
JULY 16, 1961
SAN RAMON, CALIFORNIA
DRY ADIABATIC LAPSE RATE
ANTICIPATED
ACTUAL
0630
0800
1000
1400
1830
ALTITUDE KILOFEET M.S.L.
1
2
3
4
5
6
7
12
14
16
18
20
22
24
26
28
30
32
34
36
TEMPERATURE °C

Figure A-11

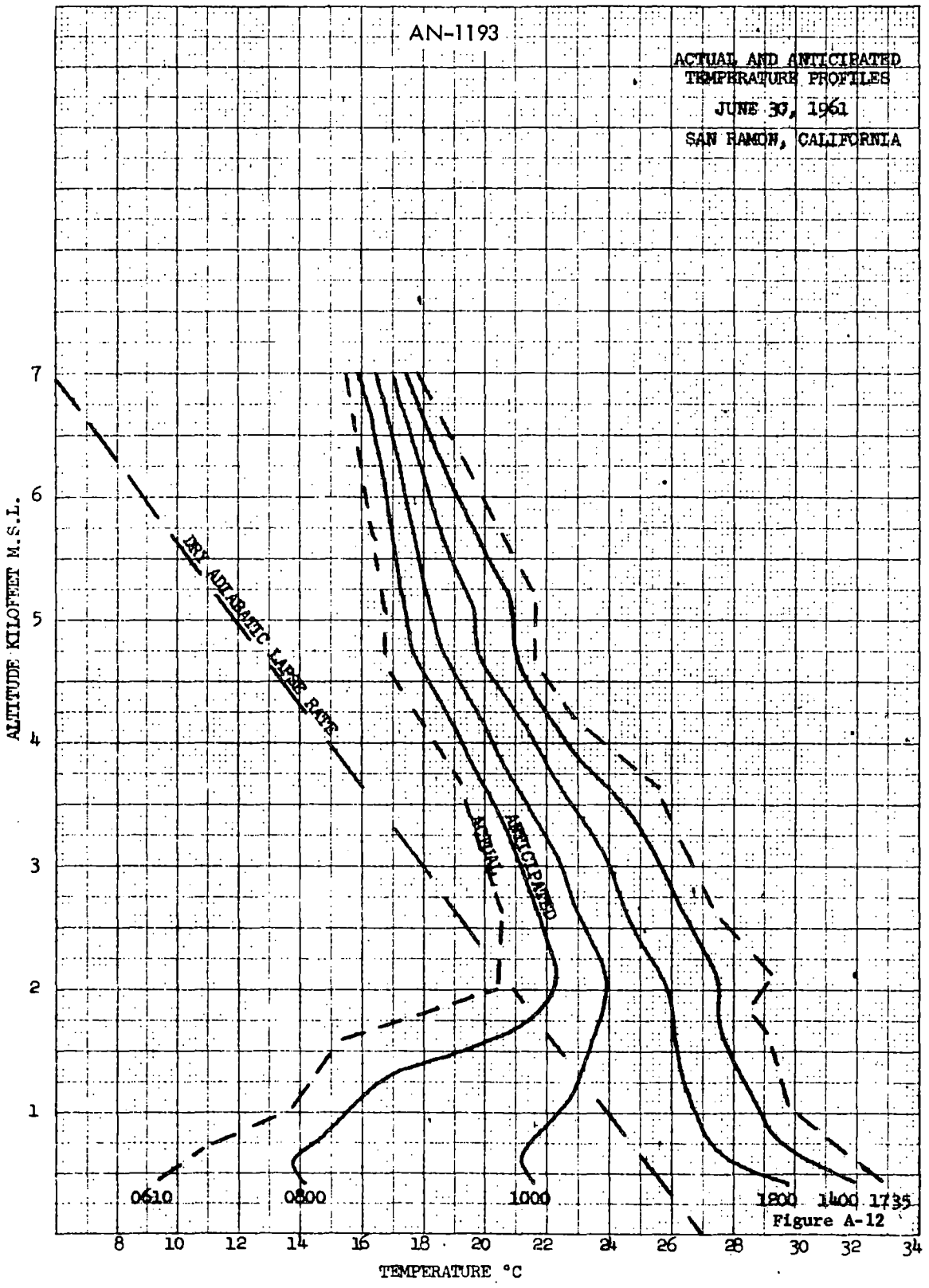
AN-1193
ACTUAL AND ANTICIPATED TEMPERATURE PROFILES
JUNE 30, 1961
SAN RAMON, CALIFORNIA
ALTITUDE KILOFEET M.S.L.
7
6
5
4
3
2
1
DRY ADIABATIC LAPSE RATE
ACTUAL
ANTICIPATED
0610
0800
1000
1200
1400
1735
8
10
12
14
16
18
20
22
24
26
28
30
32
34
TEMPERATURE °C

Figure A-12

APPENDIX B

SEISMIC CHARACTERISTICS OF SAN RAMON, CALIFORNIA

Jack F. Evernden*

An evaluation of the seismicity of a given area is based upon a study of the earthquake occurrences and the correlation of these earthquakes with known or inferred faults. The attempt is made to define the presently active faults and to establish the relation of these faults to the area under inspection.

In order to appreciate the latter remarks, the technique followed in the location of epicenters must be made clear (the epicenter of an earthquake is the point on the surface of the ground vertically above the inferred position of the earthquake focus). First, one must have a set of travel-time curves. These have been derived from seismic studies and are quite accurate. One must have a group of recording stations essentially surrounding the area of study. This desideratum is not always realized and the plotted epicenters in the eastern portion of the area of study suffer from this lack (recording stations are at Berkeley, San Francisco, Palo Alto, and Mt. Hamilton). Small quakes in this eastern area may be impossible to locate due to lack of control. Thus, the blank area along the central portion of the Riggs Canyon Fault may be more a function of this difficulty than of lack of earthquakes. Finally, a simplifying assumption used in these locations has been that all foci were at the surface. It is realized that they were at varying depths but, with lack of detailed control, the inaccuracy of the above assumption will only become evident when the epicenter locations over an extended period of time show a persistent divergence from

---

* Professor of Geology, University of California, Berkeley, California

established faultlines. Actually, only in the case of recording stations close to the epicenter will this assumption of zero depth lead to poor epicenters for quakes with focal depths of 15-25 kilometers. Thus the eastern epicenters will not be affected by this assumption, but the western ones may be.

The larger faults in the area of study are indicated on the sketch map, Figure B-1. A brief discussion follows:

1. Sunol Fault

This is a major fault. It is the easternmost member of the system of essentially parallel strike-slip faults that characterize and control the geology of the Bay Area. The other two major members of this system are the Hayward and San Andreas Faults. The Sunol Fault extends through Amador Valley, San Ramon Valley, to and beyond Walnut Creek, ultimately crossing Carquinez Straits. Structural discontinuity along it is evident (i.e., termination of folds and faults against it on both sides). Stratigraphic relationships along it confirm its gross effect upon the geology of the area. Vickery cites evidence to show that there have been 13 miles of lateral movement on the fault since the lower Pliocene (approximately ten million years). Evidence along the fault indicates an associated vertical movement of a few thousand feet.

The position of this fault at San Ramon cannot be exactly defined. It is probably close to the highway along the western side of San Ramon Valley.

2. Riggs Canyon Fault

This fault is of basically different character. It is associated with the Mt. Diablo piercement anticline and is the result of overturning of the west limb of that incline with resultant thrusting from east to west. An accurate estimate of the magnitude of displacement along this fault cannot be made. It is important in that it marks the western limit of this strong anticlinal piercement fold.

3. Hayward Fault

This is the major fault of the East Bay region. It has very obvious structural, stratigraphic, and topographic characteristics. It is the only fault east of the San Andreas Fault along which there has been surface displacement during historical times (1836, 1868).

4. Tesla Fault

No evidence of the fault exists in the valley due to extensive alluvium, but it must continue to an intersection with the Sunol Fault. Both thrust and strike-slip movement have occurred along this fault where it is observable to the east. It appears tectonically related to the Sunol rather than to the Riggs Canyon Fault.

5. Williams Fault

It is similar in nature to the Tesla Fault but of smaller magnitude.

6. Bolinger Fault

This thrust fault of comparatively small magnitude is not indicated on the map; it is not a continuation of the Tesla Fault.

There are additional faults between the Sunol and Hayward Fault but these have no apparent bearing upon the present report.

The correlation of fault pattern and epicenter locations appears to be as follows:

1. Hayward Fault

Most of the epicenters on the map are directly associated with the Hayward Fault. It is to be noted that the general line of epicenters diverges eastward from the surface trace of the Hayward Fault south of Berkeley, this divergence attaining a magnitude of 6-7 miles at the south end of San Francisco Bay. This divergence strongly suggest faulty epicenters. Recent studies, making use of additional stations now available, indicate that the divergence of these old epicenters from the Hayward Fault is probably due to significant depth

of the foci and proximity to Mt. Hamilton. Thus, the indicated epicenter locations in this area are not a true picture of the earthquake foci positions, and low seismic activity in the south portion of the Hayward Fault is incorrect. The divergence in the central portion of the fault is also thought to be a function of depth.

2. Sunol Fault

A corollary of the conclusion above is that the apparently high seismic activity of the southern portion of the Sunol Fault is also incorrect. If this concentration of epicenters is correlated with the Hayward rather than the Sunol Fault, the seismic activity of the latter fault appears to be of a definitely lower order than that of the Hayward. There are virtually no epicenters along the northern part of the Sunol Fault and very few along its central part. There is no evidence of recent surface movements along this fault such as are prevalent along the Hayward Fault. Recognizing that it probably is still geologically active, it appears at this moment in geological time to be largely inactive. This does not signify total absence of earthquakes, but it does imply no earthquakes of sufficient magnitude to do real structural damage.

3. Mt. Diablo Piercement Anticline

There is a marked grouping of comparatively small earthquakes along the trend of this anticline. The western limit of this grouping seems to show a very strong correlation with Riggs Canyon Fault. The agreement of the epicenters with this fault-line is surprisingly good in light of the basically poor control available for the location of these epicenters. The departure of many of the epicenters to the east of the Riggs Canyon Fault is probably real, since the anticline encompasses this entire area and probably is faulted on its eastern side. Thus, the Mt. Diablo anticline must be considered to be an active seismic source. However, no earthquake of any appreciable magnitude has occurred within this area during historical time, and none is expected.

4. Tesla Fault

The line of epicenters east and northeast of Pleasanton may be associated with this fault. The swarm of earthquakes felt in Livermore in the second quarter of 1943 and some earlier reports (1861, maybe 1903) suggest seismic activity of limited amount along this line.

5. Williams and Bolinger Faults

The former may have some activity. There is great uncertainty due to the previously noted inconsistency in the epicenter locations in this general area. The Bolinger Fault can be considered inactive.

It must be remembered that probably any one of these faults (excepting Bolinger) may be the site of an earthquake destructive to chimneys, some brick buildings, etc. The major damage, seismically speaking, however, comes from proximity to the Hayward Fault. As both San Ramon and Pleasanton are within 10 miles of the Hayward Fault, it would be prudent to build according to accepted earthquake-resistance standards of construction.

Some observations relative to probable foundation conditions should be made. These comments are based solely on field evidence and are not to be construed as being authoritative from an engineering point of view. San Ramon Valley appears to have only a very few feet of alluvium in it. South of Danville, San Ramon Creek has cut a channel of 15-25 feet depth. Rock outcrops extend to within three or four feet of the surface in this channel. All observed roadcuts in this portion of the valley cut through rock rather than alluvium. In addition, the proposed construction site is virtually at the point of drainage reversal in San Ramon Valley. The occurrence of firm foundation material within a very few feet of the surface seems certain.

Conclusions: The proposed construction site is in proximity to the Sunol Fault, a fault of limited activity at this time. The exact position of the fault in the vicinity of San Ramon is uncertain, but is probably 2000 feet west of the site. Large earthquakes and actual fault displacements are not to be expected along this line of faulting.

The following publications discuss the geology of the San Ramon area:

1. Tectonics of the Mt. Diablo and Coalinga Areas -- Middle Coast Ranges of California, B. L. Clark, Geological Society of America Bulletin, Vol. 46, no. 7, 1025-1078. (1935)

2. Geology of Mt. Diablo and Vicinity, J. A. Taff, Geological Society of America Bulletin, Vol. 46, no. 7, 1079-1100. (1935)

3. Geology of Las Trampas Ridge, C. K. Ham; California, Division of Mines, Special Report 22. (1952)

4. Geology of the San Francisco Bay Counties, N. L. Taliaferro; California, Division of Mines, Bulletin 154, 117-150. (1951)

5. Geologic Map of the San Francisco Bay Region, O. E. Bowen, Jr., and R. A. Crippen, Jr.; California, Division of Mines, Bulletin 154, 161-174. (1951)

6. The Structural Dynamics of the Livermore Region, F. P. Vickery, Journal of Geology, 33, 608-828. (1933)

Epicenters Located Within Indicated Area

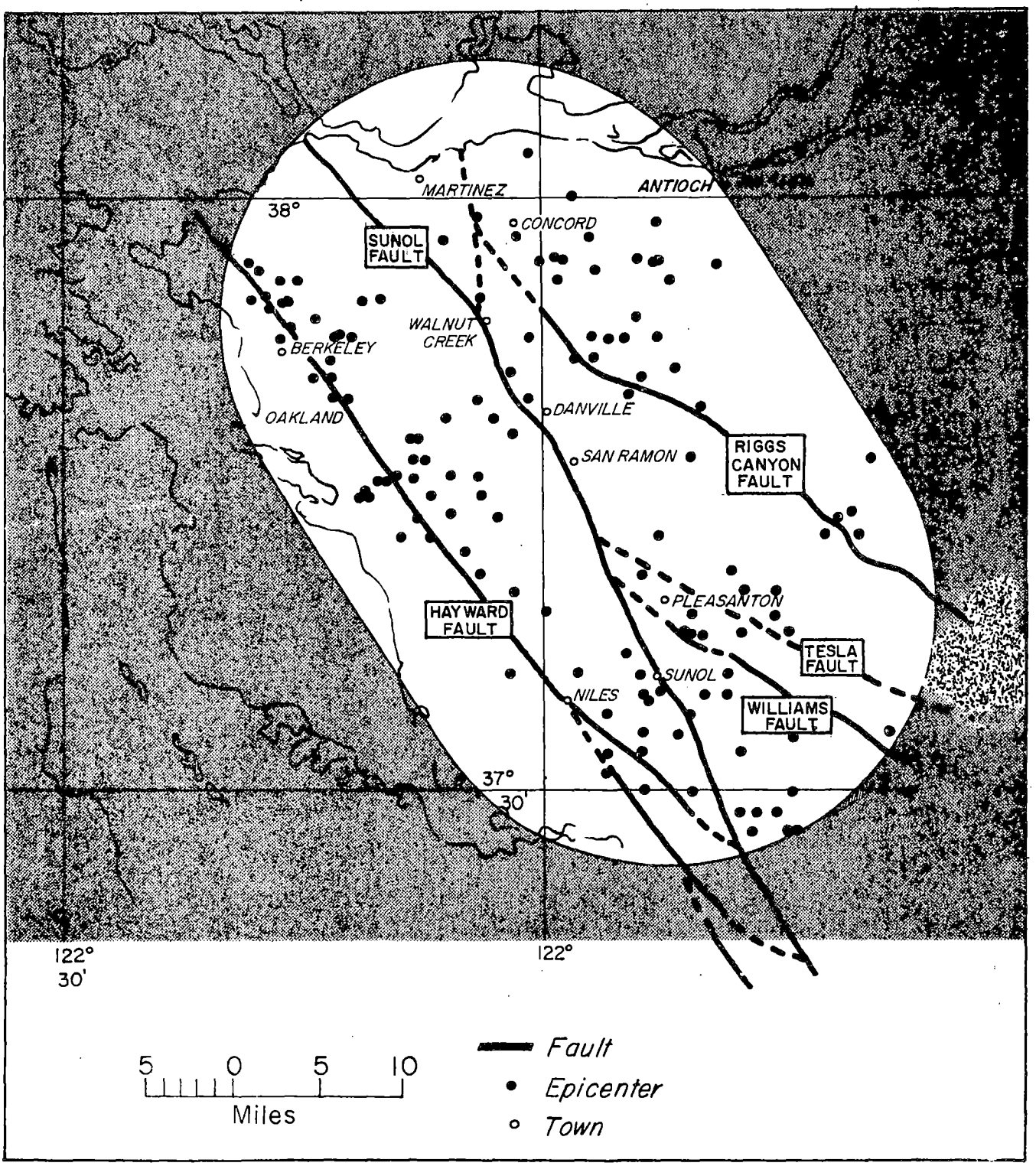

FIGURE B-1

APPENDIX C

CALCULATED MAXIMUM FISSION-PRODUCT RELEASE AFTER A FUEL ELEMENT FAILURE

Calculations and a related experiment have been made to determine theoretically the maximum concentration of fission products that might be present in the reactor-room air following a fuel element cladding filure.

The calculations are based on the fact that, as the reactor operates, fission products will be built up in the uranium-zirconium hydride fuel mixture until an equilibrium concentration is reached for each nuclide, dependent on 1) the total energy release in the reactor, 2) the decay process for each nuclide, and 3) the yield of the species from fission. Of the various fission products produced in the fuel material, only certain nuclides will migrate into the gap between the fuel material and the fuel element cladding. These nuclides are the iodines, the xenons, and the kryptons, and their decay products.

CALCULATION OF GASEOUS FISSION PRODUCTS

In the event of a rupture of the fuel element cladding, the fission products released to the water in the reactor tank will be limited to all or a portion of those fission products that have collected in the gap between the fuel material and the aluminum cladding. A portion of these fission products will then go into the air above the water, this fraction depending on the solubility of the species in water.

The quantity of gaseous fission products produced in the fuel element was determined by Blomeke and Todd.* The amounts of krypton, xenon, and iodine produced in a typical element after infinite operation at 250 kw are given in Table C-1. These data are based on a loading of [redacted] of U^{235} per element where $N_{25}o$ is the initial number of U^{235} nuclei (9.2×10^{22}) and N_s is the number of nuclei of the isotopes in the fuel element, and on an average flux of 4×10^{12} thermal neutrons/cm^2-sec.

The sum of all the activities of the gaseous fission products in an element after it has reached equilibrium at 250 kw, therefore, is 5120 curies.

EXPERIMENTAL DETERMINATION OF FISSION PRODUCTS IN GAP

In order to determine the actual percentage of fission product gases which escape from the fuel material and collect in the air gap between the cladding and the fuel material, the following experiment was conducted in the TRIGA reactor at General Atomic. A fuel element was fabricated with a sealed tube which vented the gap to a charcoal-filled cold trap at the surface of the reactor tank. All of the fission product gases which accumulated in the gap were then collected in the liquid air-cooled charcoal trap by purging the system with helium, and the trap was then analyzed. This measured amount of radioactive noble gases enabled the determination of the fraction of the fission products which diffused through the uranium-zirconium hydride material into the gap.

In the experiment, a total of 210 kw-hr of reactor operation occurred in 1 hr. The test element was exposed to an average thermal flux of 2.1×10^{12} neutrons/cm^2-sec during this time, and the Xe^{133} that collected in the gap in this period of operation was determined to be 78 microcuries. Through determination of the Xe^{133} that finds its way into the gap during the exposure of the element to a known amount of reactor flux, the percentage of Xe^{133} and consequently of all other fission-product gases that collect in the gap can be determined.

*J.O. Blomeke and Mary F. Todd, Uranium-235 Fission-product Production as a Function of Thermal Neutron Flux, Irradiation Time, and Decay Time, Pt. 1, Vol. 1, Oak Ridge National Laboratory, Report ORNL-2127, 1957.

TABLE C-1

GASEOUS FISSION PRODUCTS PRODUCED IN FUEL ELEMENT

Isotope	$N_s/N_{25}{}^o$	N_s	Decay Constant (sec^{-1})	Activity (curies)
Kr^{83m}	1.1×10^{-7}	1.0×10^{16}	1.0×10^{-4}	28
Kr^{85m}	7.8×10^{-7}	7.2×10^{16}	4.4×10^{-5}	85
Kr^{85}	3.0×10^{-3}	2.8×10^{20}	2.2×10^{-9}	16
Kr^{87}	3.2×10^{-7}	2.9×10^{16}	1.5×10^{-4}	119
Kr^{88}	1.2×10^{-6}	1.1×10^{17}	7.0×10^{-5}	208
Kr^{89}	2.0×10^{-8}	1.8×10^{15}	3.6×10^{-3}	179
Kr^{90}	5.8×10^{-9}	5.3×10^{14}	2.1×10^{-2}	303
Kr^{92}	2.7×10^{-10}	2.5×10^{13}	2.3×10^{-1}	155
I^{130}	1.6×10^{-6}	1.5×10^{17}	1.5×10^{-5}	59.6
I^{131}	7.0×10^{-5}	6.4×10^{18}	1.0×10^{-6}	174
Xe^{131m}	1.0×10^{-6}	7.2×10^{16}	6.7×10^{-7}	1.7
I^{132}	1.3×10^{-6}	1.2×10^{17}	8.0×10^{-5}	259
I^{133}	1.6×10^{-5}	1.5×10^{18}	9.3×10^{-6}	371
Xe^{133m}	1.0×10^{-6}	9.2×10^{16}	3.5×10^{-6}	8.7
Xe^{133}	1.0×10^{-4}	9.2×10^{18}	1.5×10^{-6}	373
I^{134}	8.0×10^{-7}	7.4×10^{16}	2.2×10^{-4}	438
I^{135}	4.7×10^{-6}	4.3×10^{17}	2.9×10^{-5}	339
Xe^{135m}	5.7×10^{-8}	5.2×10^{15}	7.4×10^{-4}	105
Xe^{135}	4.8×10^{-6}	4.4×10^{17}	2.1×10^{-5}	251
I^{136}	8.8×10^{-9}	8.1×10^{14}	8.1×10^{-3}	178
Xe^{137}	4.6×10^{-8}	4.2×10^{15}	3.0×10^{-3}	351
I^{138}	6.7×10^{-10}	6.2×10^{13}	1.2×10^{-1}	200
Xe^{138}	1.9×10^{-7}	1.8×10^{16}	6.8×10^{-4}	327
I^{139}	1.6×10^{-10}	1.5×10^{13}	2.6×10^{-1}	104
Xe^{139}	6.5×10^{-9}	6.0×10^{14}	1.7×10^{-2}	274
Xe^{140}	2.0×10^{-9}	1.8×10^{14}	4.3×10^{-2}	214

During the experiment, Xe^{133} was produced in the fuel element from the chain:

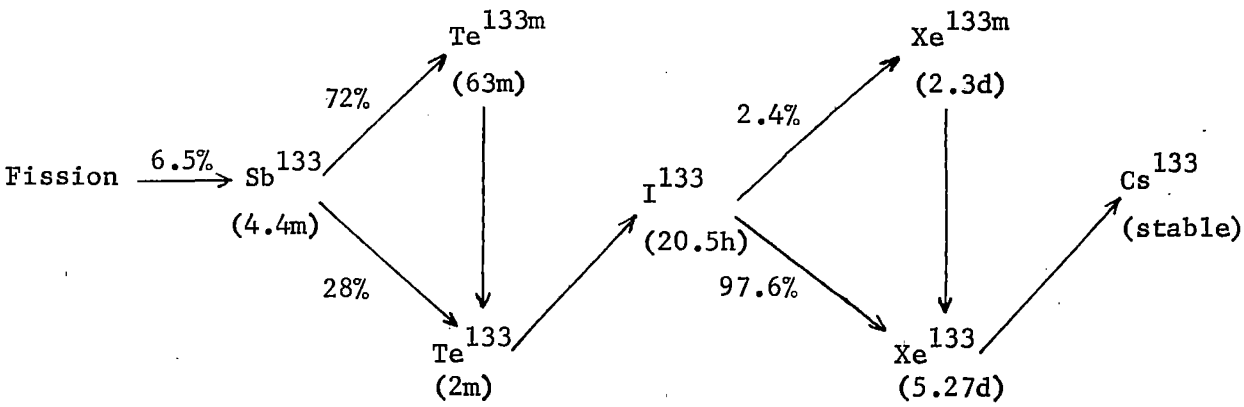

The activity of Xe^{133} present in the element at the end of 1 hr at 2.1×10^{12} neutrons/cm^2-sec was determined from the work of Bolles and Ballou.* In this work, the number of Xe^{133} nuclei present after the fission of 10,000 U^{235} nuclei is given as a function of time. Integrating these data over a time of 1 hr gives 0.49×10^{-3} Xe^{133} nuclei present per fission. In the 1-hr experiment, the number of fissions that occur is

$$\text{Number of fissions} = 9.4 \times 10^{22} \frac{U^{235}\ \text{atoms}}{\text{element}} \times 5.83 \times 10^{-22} \frac{cm^2}{U^{235}\ \text{atom}}$$

$$\times 2.1 \times 10^{12} \frac{\text{neutrons}}{cm^2\text{-sec}} \times 3.6 \times 10^{3}\ \text{sec}$$

$$= 4.15 \times 10^{17}.$$

Thus, the number of Xe^{133} nuclei is $0.49 \times 10^{-3} \times 4.06 \times 10^{17}$, or 2.03×10^{14} nuclei. This gives a total available Xe^{133} activity of

$$A = \frac{1.52 \times 10^{-6} \times 2.03 \times 10^{14}}{3.7 \times 10^{4}}\ \mu c = 8.18 \times 10^{3}\ \mu c.$$

*R. C. Bolles and N. E. Ballou, Calculated Activities and Abundances of U^{235} Fission Products, USNRDL-456, August 30, 1956.

As was indicated previously, the amount of Xe^{133} that was collected in the gap at the end of 1 hr was 78 microcuries. The percentage of the total inventory of Xe^{133} that escaped to the gap between fuel and cladding, therefore, can be calculated as follows:

$$\frac{Xe^{133} \text{ measured in gap}}{Xe^{133} \text{ totals available}} = \frac{78\ \mu c}{8.18 \times 10^{3}\ \mu c} = 0.96\%$$

As shown in Table C-1, at 250 kw the total quantity of all fission product gases in a TRIGA fuel element at equilibrium is 5,120 curies. For the purposes of this calculation, it is assumed that the fractions of the iodine, krypton, and xenon isotopes produced that collect in the gap between fuel and cladding are the same as that determined for Xe^{133}. Thus, the total gaseous activity in the gap is calculated to be 49.2 curies.

Therefore, the maximum amount of fission products that could be released in the event of a cladding failure is

Iodines	23.1 c
Xenons	16.6 c
Kryptons	9.5 c
Total fission products	49.2 c

The volume of water in the AGNIR reactor tank is approximately 4.9×10^{7} cm^3. For purposes of this calculation, it is assumed that the total 49.2 curies of gaseous fission products in the gap escapes into the water. However, when these fission products (the iodines, kryptons, and xenons) are released from the fuel element into the water, the iodines will be dissolved in the water. Since the kryptons and xenons are quite insoluble in water, it has been assumed for purposes of this analysis that a major portion of these isotopes will escape into the reactor-room atmosphere. Based on the assumption that xenon and krypton follow Henry's law, it is estimated that 95% of the xenon and 98% of the krypton will escape into the air and that all of the iodines will remain in the water. Therefore, the activity in the water will be

$$A_{water}\ \frac{\mu c}{cm^3} = \frac{23.1 + 0.05 \times 16.6 + 0.02 \times 9.5}{4.9 \times 10^{7}\ cm^3} \times 10^{6}\ \mu c = \frac{24.1 \times 10^{6}\ \mu c}{4.9 \times 10^{7}\ cm^3}$$

$$= 0.5\ \mu c/cm^3,$$

and the activity in the air will be

$$A_{air}\ \frac{\mu c}{cm^3} = \frac{0.95A\ (xenon)\ (\mu c) + 0.98A\ (krypton)\ (\mu c)}{volume\ of\ air\ (cm^3)}$$

$$= \frac{0.95 \times 16.6 + 0.98 \times 9.5}{1.57 \times 10^9\ cm^3} \times 10^6\ \mu c = \frac{24.7 \times 10^6\ \mu c}{1.57 \times 10^9\ cm^3}$$

$$= 1.57 \times 10^{-2}\ \mu c/cm^3.$$

Since krypton and xenon are inert gases, the hazard presented by their being in the air is from the dose a person in the room would receive from their decay. To estimate this dose, it is assumed that each decay of a krypton or xenon nucleus results in the emission of a 0.5-Mev gamma photon. Then the dose rate at the center of a hemispherical volume of 55,413 ft^3 (equivalent radius = 23.6 ft) is

$$D = \frac{1.57 \times 10^{-8}\ c/cm^3 \times 3.7 \times 10^{10}\ photons/sec\text{-}c(1 - e^{-8 \times 10^{-5} \times 23.6 \times 30.5})}{2 \times 8 \times 10^{-5}\ cm^{-1} \times 1.085 \times 10^6\ photons/cm^2\text{-}sec/rad/hr}$$

$$= 3.35\ (1 - e^{-0.0578}) = 0.189\ rad/hr = 189\ mr/hr,$$

where the attenuation coefficient for air is taken as $8 \times 10^{-5}\ cm^{-1}$ and the flux-to-dose conversion factor is 1.085×10^6.

To estimate an integrated dose to a person remaining in the reactor room for 1 hr after a rupture, the xenon and krypton activities in the room were averaged over 1 hr. This average is 9.2 curies, or an average concentration of $5.8 \times 10^{-3}\ \mu c/cm^3$.

If we assume that each disintegration is accompanied by a 0.5-Mev photon and that the room can be approximated by a hemisphere of equivalent volume, then by proportion, using the above initial dose value, the average dose rate will be

$$D = \frac{5.8 \times 10^{-9}\ c/cm^3}{1.57 \times 10^{-8}\ c/cm^3} \times 189\ mr/hr = 70\ mr/hr.$$

It can thus be observed that, even on the basis of the conservative assumptions made herein, a person could remain in the reactor room for about 1.4 hours after a fuel element cladding failure without exceeding the

permissible radiation dose limit of 100 mr/week. Standard operating procedures for the facility will require prompt evacuation of the reactor room by the operating personnel on indication of airborne radioactivity in the reactor room.

According to the Heating, Ventilating, and Air-Conditioning Guide,* the number of air changes in a building without a ventilation system varies from 0.5 to 2 air changes per hour under average conditions. Based on this, it can be assumed that most of the fission-product gases leak out of the reactor building within 1 hr. With an average total activity in the building of 9.2 curies, as calculated above, the average concentration of xenon and krypton in the reactor-building air will be 5.8×10^{-3} $\mu c/cm^3$. If it is assumed that the fission product gases leak out of one side of the building only, a person present for 1 hr near that side of the building would receive a maximum dose rate of 70 mr, due to the decay of the fission-product gases equal to that received by a person in the building for one hour.

If it is assumed that the fission product gases escaped from the building at a lower rate that previously postulated, the integrated dose received by a person would be approximately the same as before, owing to the longer decay period for the fission product gases before leaving the building. If the building ventilation system were operating during the release of fission product gases, the integrated dose received by a person near the building would be less than 70 mr because of air dilution.

Assuming that a fuel-element failure occurred once each year, the concentration of the fission-product gases leaving the building, averaged over a 1-yr period, would be

$$A_{air} = \frac{5.8 \times 10^{-3} \mu c/cm^3 \times 1 \text{ hr}}{8765.8 \text{ hr/yr}} = 6.61 \times 10^{-7} \mu c/cm^3,$$

and this concentration would be very much decreased by fresh-air dilution after traveling a short distance away from the building.

*Heating, Ventilating, and Air-Conditioning Guide, American Society of Heating and Ventilating Engineers, New York, 1953, p. 223.

APPENDIX D

LOSS-OF-COOLANT CALCULATIONS

INTRODUCTION

The instantaneous, total loss of cooling water is considered to be extremely unlikely; however, calculations have been made to determine the temperature rise in a central fuel element if such a loss of coolant should occur. Results of these very conservative calculations indicate that the maximum fuel temperature would be less than 650°C. More realistic calculations, taking advantage of all applicable heat removal mechanisms, would undoubtedly indicate maximum temperatures well below the melting point of the aluminum cladding.

BASIS OF CALCULATION

The calculation was made in a very conservative manner, in order to give an upper-limit estimate of the fuel-cladding temperature, and was based on the following assumptions:

1) No account was taken of any heat-removal mechanism other than natural convection flow of air through the core.

2) No heat would be removed until the fuel-element cladding had reached a temperature sufficient to transfer heat at a rate equal to the power production in the fuel elements.

3) The specific heat of the element would include only the uranium-zirconium hydride section.

4) No account was taken of the heat capacity of the graphite and end-fittings of the fuel element.

5) The reactor had been running continuously at 250 kw for an infinite time prior to water loss.

6) The cooling water would be lost instantaneously, with no water droplets remaining on the cladding.

7) The water would be lost completely from the core.

8) The "stack" height for producing the driving force would be only the length of the core.

HEAT REMOVAL

The heat-removal rate by natural convection of air between three central elements was determined. The flow channel considered was bounded by a B-ring element and two C-ring elements. The flow area in the channel was 0.327 $in.^2$, and the length of the channel was 2 ft. Holes of 0.625-in. ID were placed in the center regions of the bottom grid plate to provide coolant flow through the center of the core. Actually, most of the cooling flow came from the large annular openings above the lower grid plate. One of these holes was placed at the bottom of the channel considered. Flow out of the top of the channel was through the top grid-plate holes through which the elements are loaded. These holes were obstructed by the spacers used to center the elements. The effective flow area through the top grid plate was approximately 0.5 $in.^2$.

To find the weight flow of air through the channel, the driving pressure was equated to the pressure loss in the channel. The entrance and exit losses were neglected. The driving pressure is given by

$$P_d = (\rho_o - \rho_a)L, \qquad \text{(D-1)}$$

where ρ_o is the ambient air density (in lb/ft^3), ρ_a is the average density of the air in the channel, and L is the length of the channel (in feet). The frictional pressure loss in the channel is given by

$$P_f = \frac{2L\,\mu w}{g\,R_H^2 A\,\rho_a}, \qquad \text{(D-2)}$$

where μ is the viscosity of the air (in lb/ft-sec); w is the air weight flow (in lb/sec); g is 32.2 ft/sec^2; R_H is the "hydraulic radius," which is the channel flow area divided by the wetted perimeter (in feet); and A is the channel flow area (in ft^2).

As the density and viscosity of the air are functions of the air temperature, the weight flow was determined for a range of average air temperatures in the channel. For this weight flow, the heat-removal rate required to raise the average air temperature to the given value is

$$q_{required} = 2(T_a - T_o)\, c_p w, \qquad \text{(D-3)}$$

where T_o is the ambient air temperature (75°F) and c_p is the specific heat of air (0.25 Btu/lb-°F).

The rate at which heat can be removed from a central channel for a given average air temperature in the channel is shown in Fig. D-1, curve 1.

The decay power after shutdown of a 250-kw reactor is shown in Fig. D-2; these data are from the work of Stehn and Clancy.* Figure D-3 shows the integration of the decay power over shutdown time from 100 to 100,000 sec. The integrated power is then used to determine temperature rise in a central element as a function of shutdown time, by

$$T_s = \frac{2E}{C}, \qquad \text{(D-4)}$$

where E is the integrated decay power released in the reactor, C is the heat capacity of the fuel in the reactor (30 kw-sec/°F), and the factor 2 is an assumed ratio of the power in the central element to the average power. It is further assumed that at the time of shutdown, the element temperature is 300°F. The element temperature as a function of time after shutdown, assuming no heat loss, is also shown in Fig. D-3.

The surface temperature of the fuel-element cladding was taken to be the temperature of the element. Based on this value, the average air temperature in the channel that would exist if the decay power at a given time after shutdown were transferred to the air in the channel can be calculated. This air temperature is given by

$$T_a = T_s - \frac{q}{hA_s}, \qquad \text{(D-5)}$$

*J. R. Stehn and E. F. Clancy, "Fission Product Radioactivity and Heat Generation," published in the Proceedings of the Second United Nations International Conference on the Peaceful Uses of Atomic Energy, Geneva, September 1-13, 1958, Paper No. 1071

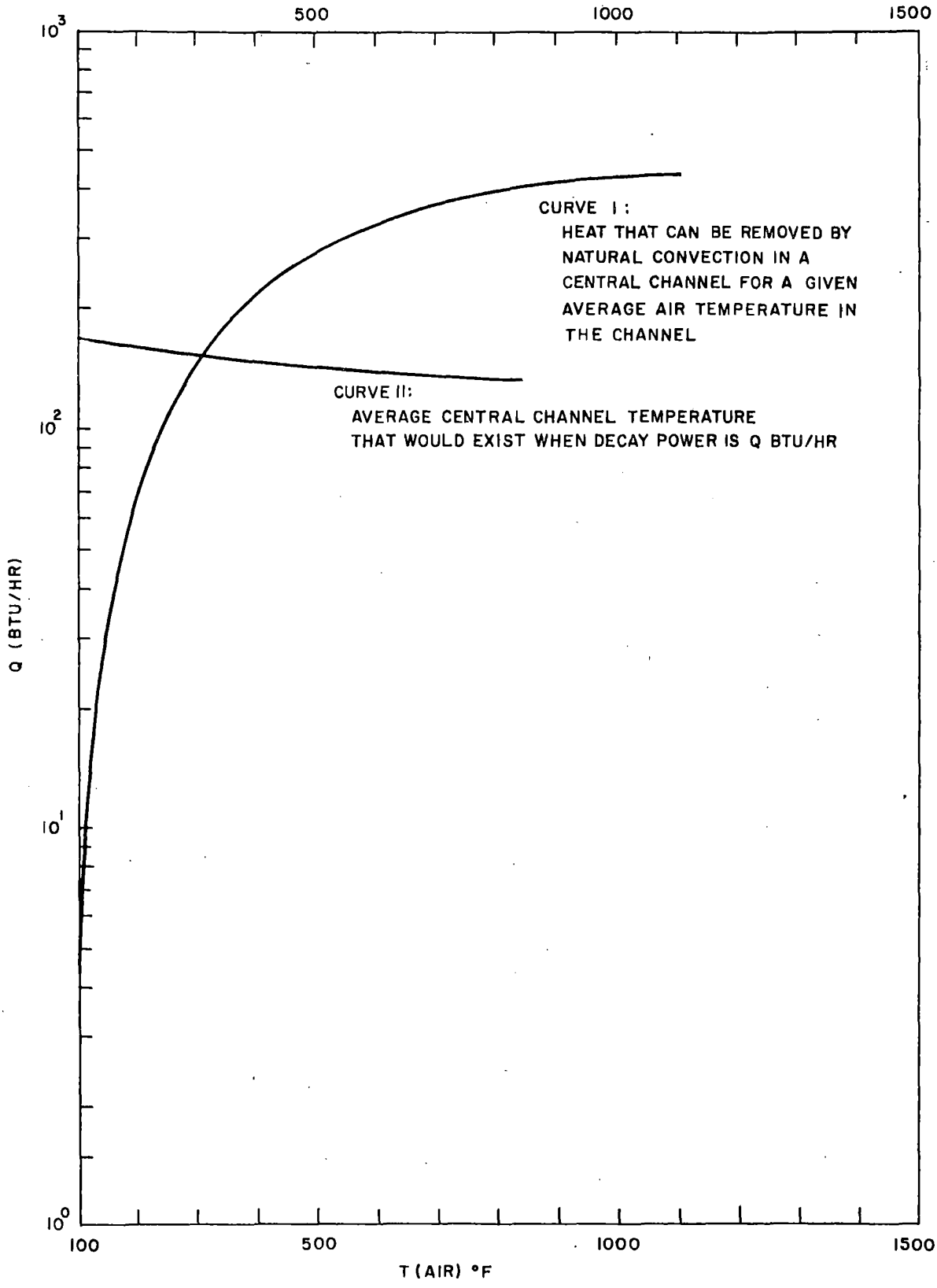

FIGURE D-1. RATE OF HEAT REMOVAL FROM CENTRAL CHANNEL AND AVERAGE CENTRAL-CHANNEL TEMPERATURE

85.39-64-1911

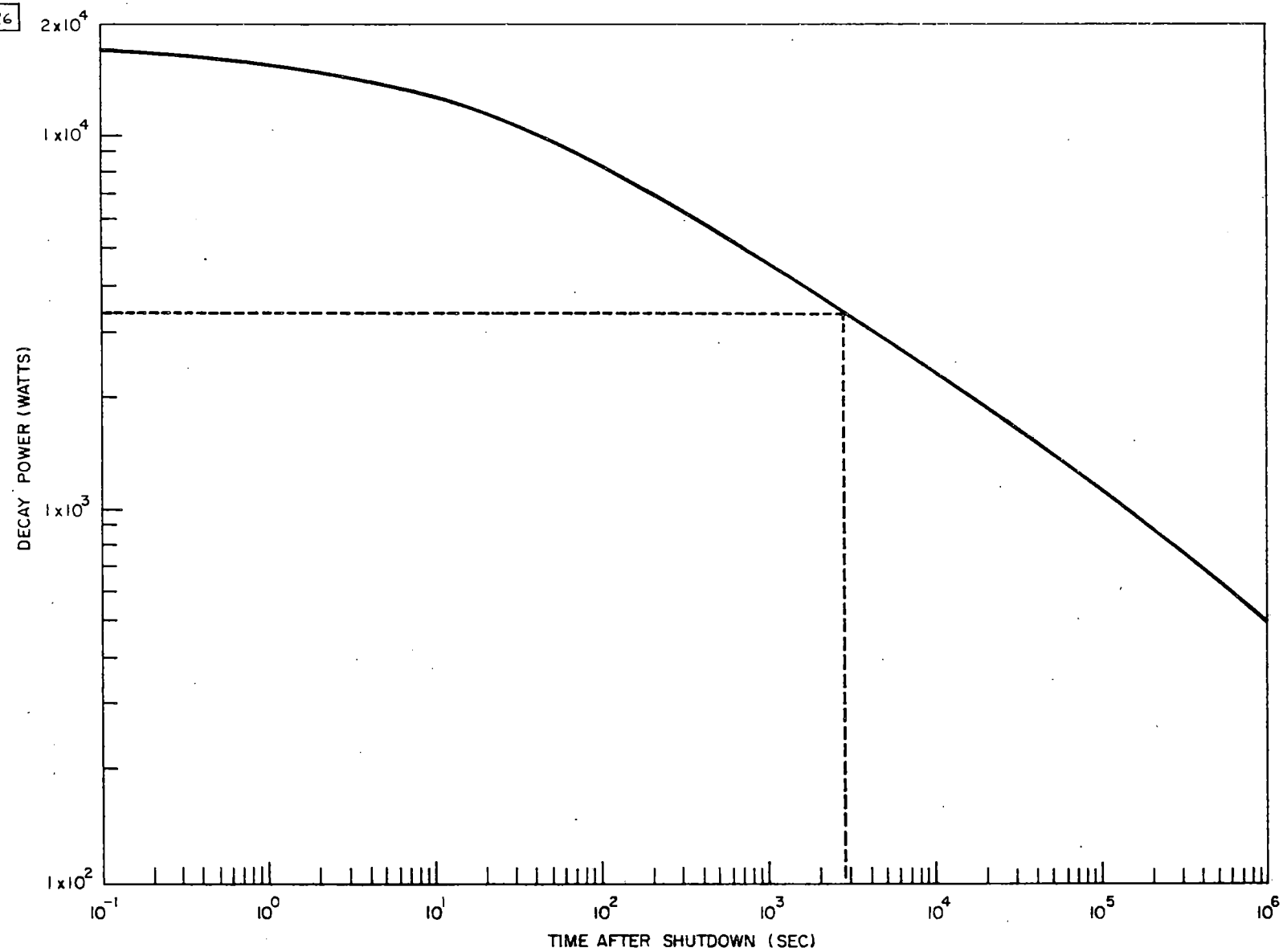

FIGURE D-2. DECAY POWER AFTER INFINITE OPERATION AT 250 kw VERSUS TIME AFTER SHUTDOWN

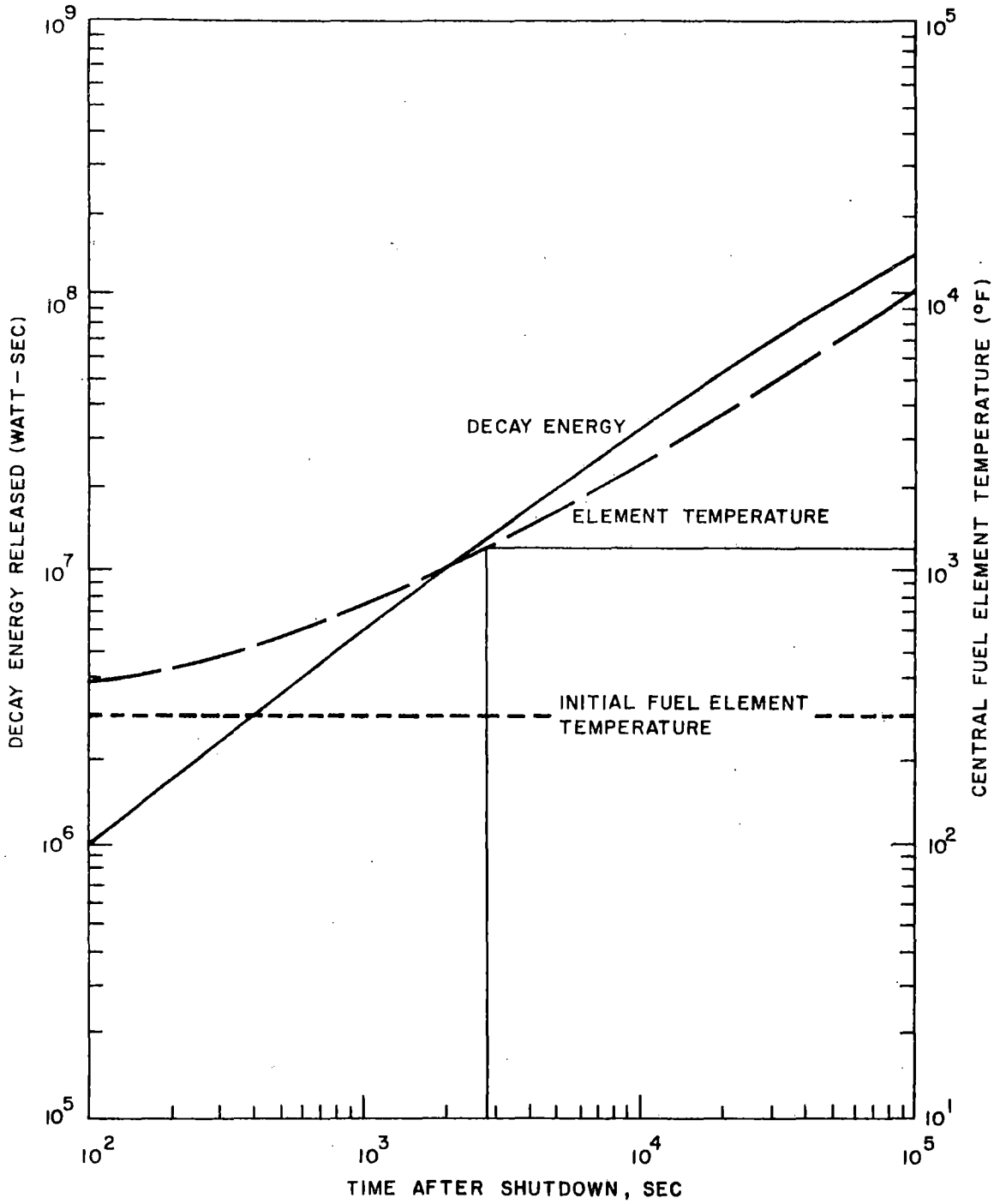

FIGURE D-3. DECAY ENERGY RELEASED AND CENTRAL FUEL ELEMENT TEMPERATURE VERSUS TIME AFTER SHUTDOWN

85.30-64-1014

where T_s is the element surface temperature at a given time after shutdown, q is the decay heat production rate in the central element at the same time after shutdown, A_s is the surface area of the element in the channel, and h is the heat-transfer film coefficient. The heat-transfer film coefficient was conservatively estimated to be 1 Btu/hr-ft^2-^{o}F), from data in the Chemical Engineer's Handbook.*

The average air temperature that would exist if the heat produced were transferred to the air in the channel is plotted in Fig. D-1, curve 2. The point at which curve 1 and curve 2 intersect defines the equilibrium conditions in the channel; that is, the point at which all the heat produced in the element would be transferred to the air. Thus, the element temperature would not increase beyond this point, where the decay power in the central element is 154 Btu/hr and the average air temperature is 312^{o}F.

From Fig. D-2, we see that 2,800 sec is the time after shutdown at which the decay power has decreased to 154 Btu/hr x 0.293 watts/(Btu/hr) x 75 elements/core, which equals 3,380 watts. As may be seen in Fig. D-3, the element temperature at 2,800 sec after shutdown is 1200^{o}F.

DISCUSSION OF RESULTS

These calculations were made using conservative assumptions, as listed earlier. To substantiate the conclusion that the maximum fuel-element temperature will be less than 1200^{o}F, the following discussion of these assumptions is presented.

First, account has not been taken of any heat-removal mechanism other than natural convection of air through the core. Other mechanisms, however, will play a part, principally conduction to the grid plates and to other structural members of the assembly.

It was assumed that the water would be lost instantaneously and completely from the core. Even if the water were lost by some inconceivable disaster that opened the bottom of the tank, it would still take a finite time for the out-rushing water to pass through the core. During this time, afterheat would be removed. It should be noted here that loss of water in the core will shut it down.

*J. H. Perry (ed.), Chemical Engineer's Handbook, McGraw-Hill Book Company, Inc., New York, 1950, pp. 471-472.

Several other assumptions, conservative but with less effect on the results than those above, were made. One of these was that the reactor had been running continuously for an infinite time prior to the water loss. This certainly will never be the case; however, it is possible that the reactor may be operated for several days continuously. In such a case, the decay power would approach the infinite operation limit, especially during the first hour or so after shutdown.

Another assumption of importance is the value of the peak/average power ratio. The number used is an overestimate of the order of 20%. Similarly, a high value was chosen for the initial fuel temperature.

The driving force on the air passing up through the core was calculated, assuming that only the air in the core is hotter than ambient. However, the air above the core will be above the ambient temperature, creating an effective "stack" above the core. This means that the weight flow of air through the core will be somewhat greater than that calculated; consequently, more heat can be removed by the air.

It was assumed that no heat would be removed by the air while the fuel-element temperature was rising to its peak value. Actually, the air would be cooling the element even as the element temperature rose. This cooling would be small, however.

It may be noted that the only pressure losses considered were those due to friction encountered in the flow through the channel. There will also be entrance and exit losses in the grid plates; however, at the flow velocities being dealt with, these losses are so small that they have been ignored.

APPENDIX E

ARGON ACTIVATION IN REACTOR WATER

The argon activity in the reactor pool water results from the argon dissolved in water. To evaluate the activation of argon in the reactor pool, the following reasoning and assumptions were used.

The amount of argon which is dissolved in water is calculated, assuming that argon follows Henry's law. If the water temperature is taken to be $70^{\circ}F$, then the corresponding water vapor pressure is 26 mm Hg. The partial pressure of air is then 760 - 26 = 734 mm Hg. The argon content of air is 0.94% by volume, and hence the partial pressure of argon is $734 \times (9.4 \times 10^{-3}) = 7$ mm Hg.

The saturated concentration of argon in water, according to Henry's law, is

$$X = \frac{P}{K} \quad , \tag{E-1}$$

where X is the mole fraction of argon in water, P is the partial pressure of argon above water, and K is Henry's constant, 2.84×10^{7} at $70^{\circ}F$. Thus, $X = 2.46 \times 10^{-7}$ mole A^{40} per mole of $(H_2O + A^{40})$, or $X = 1.367 \times 10^{-8}$ mole A^{40} per 1 cm^3 H_2O.

Argon-41 production, assuming saturated conditions and an irradiation time t, is given by

$$N_1 = \frac{\overline{\phi}_n \Sigma_a \left(1 - e^{-\lambda t}\right)}{\lambda} \quad , \tag{E-2}$$

where

N_1 = atomic density of A^{41} (atoms of A^{41} per cm^3),
$\bar{\phi}_n$ = average neutron flux (neutrons/cm^2-sec),
Σ_a = macroscopic absorption cross section of A^{40} (cm^{-1}),
λ = decay constant for A^{41} (sec^{-1}).

A corresponding activity for small values of λt is

$$A_1 = \bar{\phi} \lambda t \Sigma_a \quad . \tag{E-3}$$

The average thermal flux in the reactor core is estimated to be 4×10^{12} neutrons/cm^2-sec. The circulation of water in the core occurs mainly through natural convection, and it is estimated that it changes completely in 4 sec. Since the core holds 2.4×10^4 cm^3 of water, the rate of flow of water through the core is 0.6×10^4 cm^3/sec. Substituting appropriate values for Σ_a and taking irradiation time as 4 sec results in

$$A_1 = 7.4 \text{ disintegrations/cm}^3\text{-sec}. \tag{E-4}$$

The total activity from the core is thus

$$Q_0 = 1.2 \ \mu\text{c/sec}. \tag{E-5}$$

The travel time of A^{41} from the core to the water surface, a distance of 17 ft, is about 45 sec. Applying the decay law, A^{41} activity reaching the surface is

$$Q = 1.19 \ \mu\text{c/sec}. \tag{E-6}$$

Under saturated, steady-state conditions, the maximum rate at which A^{41} can escape from the water surface will be 1.19 μc/sec, and an equivalent amount of A^{40} will dissolve in water in place of A^{41}. In reality, a much smaller fraction of A^{41} will escape from the water. At increased water temperature, the partial pressure of water vapor will increase and the amount of dissolved A^{40} will decrease.

The radioactive argon escaping from the reactor pool will dissipate in the air of the reactor room. Assuming that the leak rate from the room is small and therefore that the A^{41} is evenly distributed throughout the entire room, the concentration of A^{41} in the air may be obtained by considering the material balance of A^{41} (in μc/sec).

Letting Q be the production rate, P the exhaust rate, and D the decay rate, the accumulation rate will be

$$A = Q - P - D. \qquad \text{(E-7)}$$

If the reactor is operated for a long time, equilibrium conditions in the air may be assumed. The accumulation rate, then, is equal to zero. Hence,

$$Q - D = P.$$

From Eq. E-2, $Q = 1.19$ μc/sec.

The <u>average</u> decay rate may be expressed as

$$D = Q - \frac{1}{\theta}\int_0^{\theta} Qe^{-\lambda t}\, dt \ \mu\text{c/sec}, \qquad \text{(E-8)}$$

where θ is the time in which decay occurs and is the average time of residence of an atom of A^{41} in the reactor room before it is vented to the atmosphere. Assuming the air in the building is replaced once an hour,

$$\theta = \frac{55{,}413 \text{ ft}^3}{15 \text{ ft}^3/\text{sec}} = 3.69 \times 10^3 \text{ sec}. \qquad \text{(E-9)}$$

Integrating Eq. E-8 and substituting in Eq. E-9 yields

$$P = Q\,\frac{1 - e^{-\lambda\theta}}{\lambda\theta} \ \mu\text{c/sec}. \qquad \text{(E-10)}$$

Substituting for λ and θ yields

$$P = 0.987 \ \mu\text{c/sec}.$$

Since equilibrium conditions are assumed, the same concentration of A^{41} will exist in the air of the reactor room as in the exhausted air. Concentration in the exhausted air is

$$0.987/(15)(2.832 \times 10^4) = 2.3 \times 10^{-6} \ \mu\text{c/cm}^3.$$

This is approximately the maximum permissible occupational tolerance level of 2×10^{-6} μc/cm^3 for a 40-hr week which is recommended by the U.S. Federal Register. Moreover, it is an upper limit, since actually a much smaller amount of A^{41} than 1.19 μc/sec will escape into the air.

AEROJET-GENERAL NUCLEONICS